ANKARA YILDIRIM BEYAZIT UNIVERSITY

GRADUATE SCHOOL OF NATURAL AND APPLIED SCIENCES

GROWTH AND CHARACTERIZATION OF TITANIUM DIOXIDE THIN FILMS BY SOL-GEL SPIN COATING AND DIP COATING METHODS

M.Sc. Thesis by

Samet UYSAL

Department of Materials Engineering

July, 2023

ANKARA

GROWTH AND CHARACTERIZATION OF TITANIUM DIOXIDE THIN FILMS BY SOL-GEL SPIN COATING AND DIP COATING METHODS

A Thesis Submitted to

The Graduate School of Natural and Applied Science of

Ankara Yıldırım Beyazıt University

In Partial Fulfillment of the Requirements for the Degree of Master of Science in Materials Engineering, Department of Materials Engineering

by

Samet UYSAL

July, 2023

ANKARA

M.Sc. THESIS EXAMINATION RESULT FORM

We have read the thesis entitled **"GROWTH AND CHARACTERIZATION OF TITANIUM DIOXIDE THIN FILMS BY SOL-GEL SPIN COATING AND DIP COATING METHODS"** completed by **Samet UYSAL** under supervision of **Prof. Dr. Aytunç ATEŞ** and we certify that in our opinion it is fully adequate, in scope and in quality, as a thesis for the degree of Master of Science.

Prof. Dr. Aytunç ATEŞ

_____

(Supervisor)

Asst. Prof. Begüm ÜNVEROĞLU ABDİOĞLU

_____

(Jury member)

Assoc. Prof. Dr. Irmak KARADUMAN ER

_____

(Jury member)

Prof. Dr. Sadettin ORHAN

_____

(Director)

Graduate School of Natural and Applied Science

ETHICAL DECLARATION

I hereby declare that, in this thesis which has been prepared in accordance with the Thesis Writing Manual of Graduate School of Natural and Applied Sciences,

- All data, information and documents are obtained in the framework of academic and ethical rules,
- All information, documents and assessments are presented in accordance with scientific ethics and morals,
- All the materials that have been utilized are fully cited and referenced,
- No change has been made on the utilized materials
- All the works presented are original,

and in any contrary case of above statements, I accept to renounce all my legal rights.

Date: **Signature: ……**

Name & Surname: ……..

ACKNOWLEDGEMENTS

I would like to express my deepest gratitude to my supervisor Prof. Dr. Aytunç ATEŞ who contributed in making this project possible with his valuable guidance, support and advice. I am grateful to him for sharing his knowledges and experiences with me from the beginning to the end of this project. It has been a pleasure for me to work with him.

I am thankful to R.A. Semih Ağca for their cooperation for the XRD and SEM measurements.

I would like to thank Ankara Yıldırım Beyazıt University Scientific Research activities, which financially supported my thesis with the Project code FYL-2022-2427.

Finally, I would like to thank my family for their support and understanding.

July, 2023 **Samet UYSAL**

GROWTH AND CHARACTERIZATION OF TITANIUM DIOXIDE THIN FILMS BY SOL-GEL SPIN COATING AND DIP COATING METHODS

ABSTRACT

Titanium dioxide is an advantageous metal oxide semiconductor material for solar cell applications such as photovoltaic and photocatalytic applications owing to its outstanding optoelectronic properties with good chemical stability. Researchers conducted studies to investigate and improve the characteristics of titanium dioxide thin films. In this study, titanium dioxide thin films were grown by sol-gel spin coating and sol-gel dip coating methods on glass substrate. The properties of the titanium dioxide thin films were investigated as a function of the aging time, layer number, and dipping time effect. For this purpose, the aging time, layer number and the dipping time changed as 1, 7, 14, 21, 28 and 56 days, 3, 5 and 10 layers and 5, 10 and 20 seconds, respectively. Besides that, to investigate the influence of annealing temperature on the thin film properties, the films were annealed at 300 °C, 400 °C, 500 °C, 600 °C, and 700 °C. According to the characterization results, all the titanium dioxide thin films were succesfully grown by Sol-Gel method. As-grown thin films and layers annealed at 300 °C were in amorphous form. The samples annealed at 400 °C and above were formed into a tetragonal anatase structure. The crystallization was increased in films annealed at 400 °C for both coating methods. Films by sol-gel dip coating contain isolated nano-sphere features according to top-down scanning electron microscopy images. Optical measurements showed that absorption thresholds shifted with changes in growth parameters. The bandgap values were calculated in the range between 2.97 – 3.63 electronvolt for all titanium dioxide thin films. The refractive index, dielectric constant, static dielectric constant, and porosity were improved with increasing annealing temperature. As a results it is found that the aging day, number of layers, dipping time and annealing temperature affected the structural, surface and optical properties of the titanium dioxide thin films.

Keywords: Titanium dioxide, thin films, sol-gel, spin coating, dip coating, characterization

TİTANYUM DİOKSİT İNCE FİLMLERİN SOL-JEL DÖNDÜRMELİ KAPLAMA VE DALDIRMALI KAPLAMA YÖNTEMİ İLE BÜYÜTÜLMESİ VE KARAKTERİZASYONU

ÖZET

Titanyum dioksit, iyi kimyasal stabiliteye sahip olağanüstü optoelektronik özellikleri sayesinde fotovoltaik ve fotokatalitik uygulamalar gibi güneş pili uygulamaları için avantajlı bir metal oksit yarı iletken malzemedir. Araştırmacılar, titanyum dioksit ince filmlerin özelliklerini araştırmak ve geliştirmek için çalışmalar yaptılar. Bu çalışmada, titanyum dioksit ince filmler, cam alttaş üzerinde sol-jel döndürmeli kaplama ve sol-jel daldırmalı kaplama yöntemleriyle büyütüldü. Titanyum dioksit ince filmlerin özellikleri, yaşlanma süresi, katman sayısı ve daldırma süresi etkisinin bir fonksiyonu olarak incelenmiştir. Bu amaçla titanyum dioksit çözeltisinin yaşlandırma süresi, katman sayısı ve daldırma süresi sırasıyla 1, 7, 14, 21, 28 ve 56 gün, 3, 5 ve 10 kat ve 5, 10 ve 20 saniye olarak değiştirilmiştir. Öte yandan tavlamanın ince film özellikleri üzerindeki etkisini araştırmak için filmler 300 ^{0}C, 400 ^{0}C, 500 ^{0}C, 600 ^{0}C and 700 ^{0}C'de tavlanmıştır. Karakterizasyon sonuçlarına göre tüm titanyum dioksit ince filmler sol-jel yöntemi (döndürmeli kaplama ve daldırmalı kaplama) ile başarıyla büyütüldü. Büyütülmüş ince filmler ve 300 °C'de tavlanmış katmanlar amorf formdaydı. 400 °C ve üzerinde tavlanan numuneler tetragonal anataz yapısı oluşturdu. Her iki kaplama yönteminde de 400 °C'de tavlanan filmlerde kristalleşme artmıştır. Sol-jel daldırma kaplamalı filmler, taramalı elektron mikroskobu görüntülerine göre izole edilmiş nano küre özellikleri içerir. Optik ölçümler, absorpsiyon eşiklerinin büyüme parametrelerindeki değişikliklerle değiştiğini gösterdi. Tüm titanyum dioksit ince filmler için bant aralığı değerleri 2,97 – 3,63 elektronvolt aralığında hesaplanmıştır. Artan tavlama sıcaklığı ile kırılma indeksi, dielektrik sabiti, statik dielektrik sabiti ve gözeneklilik iyileştirildi. Sonuç olarak yaşlandırma günü, katman sayısı, daldırma süresi ve tavlama sıcaklığının titanyum dioksit ince filmin yapısal, yüzey ve optik özelliklerini etkilediği tespit edilmiştir.

Anahtar kelimeler: Titanyum dioksit, ince film, sol-jel, döndürmeli kaplama, daldırmalı kaplama, karakterizasyon

CONTENTS

NOMENCLATURE

List of Abbreviations

AES	Auger Electron Spectroscopy
AFM	Atomic Force Microscope
BM	Burstein-Moss
CB	Conduction Band
CMOS	Complementary Metal-Oxide-Semiconductor
CO_2	Carbon Dioxide
CVD	Chemical Vapour Deposition
EDAX	Energy Dispersive X-Ray Spectroscopy
FESEM	Field Emission Scanning Electron Microscope
FWHM	Full Width Half Maximum
MIS	Metal Insulator Semiconductor
MISFET	Metal Insulator Semiconductor Field Effect Transistor
NO_x	Nitrogen Oxide
RF	Radio Frequency
SEM	Scanning Electron Microscope
SGSC	Sol-Gel Spin Coating
SGDC	Sol-Gel Dip Coating
SILAR	Successive Ionic Layer Adsorption and Reaction
TGA	Thermal Gravimetric Analyses
TiO_2	Titanium Dioxide
TTIP	Titanium Tetra Isopropoxide
UV-VIS	UltraViolet-Visible Spectroscopy
UV	UltraViolet
VB	Valance Band
XPS	X-Ray Photoelectron Spectroscopy
XRD	X-Ray Diffraction

List of Symbols

Å	Angstrom
λ	Wavelenght
^0C	Deggree Centigrade

h	Hour
nm	Nanometer
2θ	Diffraction Angle
d	Distance Between Atomic Layers
D	Crystallite size
β	FWHM
δ	Dislocation Density
ε	Microstrain
α	Absorbance Coefficient
t	Thickness
hv	Incident Photon Energy
n	Refractive Index
ε_∞	Dielectric Constant
ε_0	Static Dielectric Constant
σ	Optical Conductivity

LIST OF TABLES

LIST OF FIGURES

CHAPTER 1

INTRODUCTION

Semiconductor materials are solid-state materials that lies between a conductor and an insulator in terms of electrical conductivity. Semiconductor thin films constitute an indispensable part of constantly evolving technology. Semiconductor materials exhibit versatile uses due to their superior optical and electrical properties. The thin-film coating in the semiconductor industry determines the application and performance of the semiconductor. The coating of a semiconductor can be made of conductive metals or non-conductive metal oxides, depending on the kind of semiconductor. Metal oxides, which are of great importance in semiconductor technology, are used in many areas such as gas sensors, transistors, solar cells, photovoltaic devices, information storage devices and photocatalytic applications with their unique properties [1].

1.1 Titanium dioxide (TiO_2)

Titanium dioxide (TiO_2), also known as titania, is a organic compound with properties such as high dielectric constant, wide band gap, high refractive index, excellent mechanical durability, good chemical stability. TiO_2 is a metal oxide semiconductor material that is most commonly used in applications such as photocatalytic, photovoltaic, electrochromic devices, hydrogen storage, sensing due to its superior properties [2].

The first studies of the preparation of TiO_2 as a thin films were made by Matthews (1986). In his study, he investigated the passage of photocatalytic oxidation in aqueous solution through the flow reactor of TiO2 thin films under UV light and observed a significant decrease on the flow rate and reached the effect on the flow rate and solution concentration of the products [3].

1.1.1 Crystal Structure and Properties of TiO_2

TiO_2, one of the IV-VI group binary compound semiconductors, is formed by the combination of the titanium atom in the group IV and the oxygen atom in the group

VI of the periodic table. Titanium is an element with atomic number 22 and atomic weight 47.9. It is one of the transition elements and its electronic configuration is $1s^2$ $2s^2$ $2p^6$ $3s^2$ $3p^6$ $4s^2$ $3d^2$. There are three different main crystal structures of titanium dioxide, these are; rutile, anatase and brookite [4]. The lattice structure of the anataze, rutil and brookite phase and phase diagram are shown in Figure 1.1.

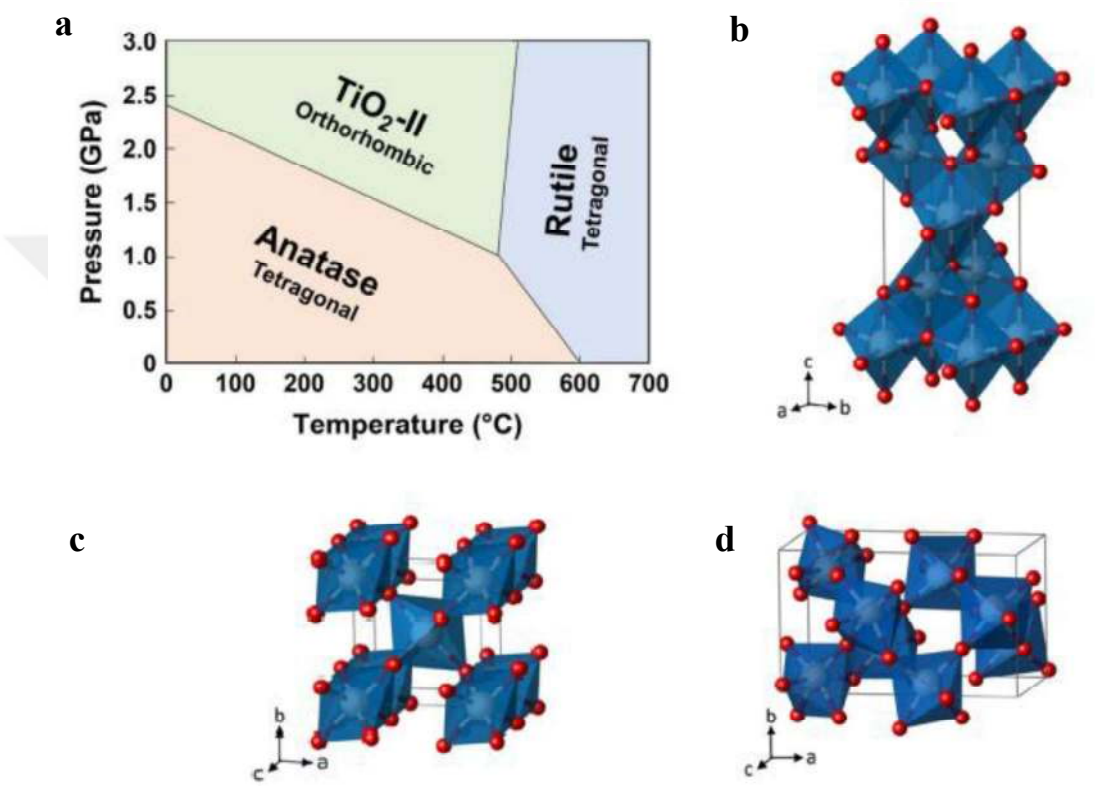

Figure 1.1 The phase diagram of TiO_2 (a) [5] and lattice structure of the rutil (b) anatase (c) and brookite phase (d) [1].

Anatase and rutile structure are defined by the arrangement of TiO_6 octahedra chains. In both structures, each Ti^{+4} ion is surrounded by an octahedron of 6 O^{-2} ions. An oxygen atom bonds with 3 titanium atoms, so it belongs to three octahedra. Anatase and rutile are both tetragonal and brookite is orthorhombic. The anatase and rutile structure contain 12 and 6 atoms per unit cell, respectively. While the distance between Ti-Ti is shorter in anatase structure than in rutile structure, the distance between O-Ti-O is longer than in rutile structure [6]. Of the 6 bonds a Ti atom with oxygen atoms, two are longer. In both structures, there are two different bond angles between Ti-O

and O-Ti-O. The number of octahedra neighbors in the anatase structure is less than the number of neighbors in the rutile structure. In anatase structure, each octahedron has 8 neighborhoods on 4 sides and 4 corners, while rutile structure has 10 neighborhoods on 2 sides and 8 corners [7]. The crystal parameters for the three phases are summarized in Table 1.1.

Table 1.1 The crystal properties of TiO_2 [8].

Phase	**Anatase**	**Rutile**	**Brookite**
Crystal structure	Tetragonal	Tetragonal	Orthorhombic
Lattice constant (Å)	α=3.784 c=9.515	α=4.5936 c=2.9587	α=9.184 b=5.447 c=5.145
Space group	$I4_1/amd$	$P4_2/mnm$	Pbca
Molecule/cell	4	2	8
Volume/molecule ($Å^3$)	34.061	31.2160	32.172
Density (g/cm^3)	3.79	4.13	3.99
Ti-O bond lenght (Å)	1.937(4) 1.965(2)	1.949(4) 1.980(2)	1.87~2.04
O-Ti-O bond angle	77.7° 92.6°	81.2° 90.0°	77.0°~105°

This difference in the lattice structure causes different mass densities and electronic band structure between the two phases of TiO_2. This difference explains why the anatase phase is more active than the rutile phase [9].

During annealing, there is a first-order phase transition from the metastable anatase and brookite phase to the stable rutile phase. Multiple phase transitions occur as anatase → rutile, anatase → brookite → rutile, brookite → rutile, and brookite → anatase → rutile. According to Elbushra et al. (2018), experimental conditions during transition depend on properties such as annealing temperature, size of substrate, type of substrate [10]. The transition of titanium dioxide from an amorphous phase to anatase occurs at a temperature of around 300°C [11]. Of the three polymorphic

structures of TiO_2, the most thermodynamically stable phase is rutile [12]. The lattice energies of the other crystal phases are close to each other and they become stable over long periods of time. Above 700 °C, a monotropic change from the anatase phase to rutile phase takes place. Rutile phase is the hardest phase compared to other polymorphic structures because it has the the most tightly packed and highest density [13]. Some properties of anatase and rutile phases are shown in Table 1.2.

Table 1.2 Properties of Anatase and Rutile Structure of TiO_2 [14-16].

Phase	Anatase	Rutile
Melting point (^{0}C)	1825	1825
Boiling point (^{0}C)	2500 ~ 3000	2500 ~ 3000
Light absorption (nm)	$\lambda \leq 385$	$\lambda \leq 415$
Band-gap (eV)	~ 3.0	~ 3.2
Refractive index	2.55	2.75
Dielectric constant	31	114
Hardness (Mohs)	5.5 – 6.0	6.0 – 6.5
Bulk modulus (GPa)	183	206
Solubility in H_2O	Insoluble	Insoluble
Solubility in HF	Soluble	Insoluble

1.1.2 Application of TiO_2

The pigments in the form of anatase, which is very active, are used in paints because they calcify very quickly when exposed to moisture/humudity and sunlight. The anatase crystalline phase is advantageous for photoelectrochemical energy conversion. The rutile form is less photoactive and a higher refractive index will give higher opacity. It is known that the light absorption and refractive index of TiO_2 increase under UV light, which reduces the viscosity and surface tension [17].

This phenomenon, which absorbs light and transfers its energy to another object, is called photocatalysis. Photocatalyst is called semiconductor materials that create a strong oxidizing environment on the surface with the effect of UV light. TiO_2 is the most widely used semiconductor material as a photocatalyst. By using the TiO_2 electrode, the water was separated into its components by Fujishima et al. (1969) and

it was demonstrated that the cyanide in the water could be separated with its use by Frank and Bard (1977). Then, TiO_2 has been used in solving environmental problems caused by organic wastes [18-20].

As a semiconductor it has a wide band gap, high dielectric constant, high transmittance in the visible region of the spectrum, and a large refractive index, so it has a different range of uses from many other semiconductors [21]. Its high dielectric constant makes TiO_2 a good candidate for complementary metal/oxide/semiconductor (CMOS), metal/insulator/semiconductor (MIS) and field effect (MISFET) transistor applications [22]. Due to their attractive properties, TiO_2 nanoparticles have found vast array of applications such as in gas sensor [23], solar energy [24], self cleaning [25], cancer therapy [26], food [27], healthcare and cosmetic products [28].

According to Hsu and Sheu (2004), air pollution is enhanced by environmental pollutants such as nitrogen oxides (NOx) and sulfur oxides emitted by many sources. TiO_2 removes these environmental pollutants from the air and can decompose them into less harmful CO_2 gas [29].

1.2 Thin Film Growth Methods

Thin film term; It includes film layers that are deposited on surfaces from a few micrometers to nanometers in thickness by various coating methods. Thin film; defines a new structure between the bulk state and molecular state of the material. Thin films can exhibit very different physical properties from the bulk state of the material [30,31]. Thin film coating methods can generally be grouped physical and chemical method [32].

Nanostructured TiO_2 thin films have been grown by several methods like radio frequency (RF) sputtering [34], ultrasonic spray pyrolsis [35], hydrothermal [36], solvothermal [37], chemical vapour deposition (CVD) [38], electrochemical [39], successive ionic layer adsorption and reaction (SILAR) [40], sol-gel [41]. The main methods and techniques used to prepare thin films are given in Figure 1.2.

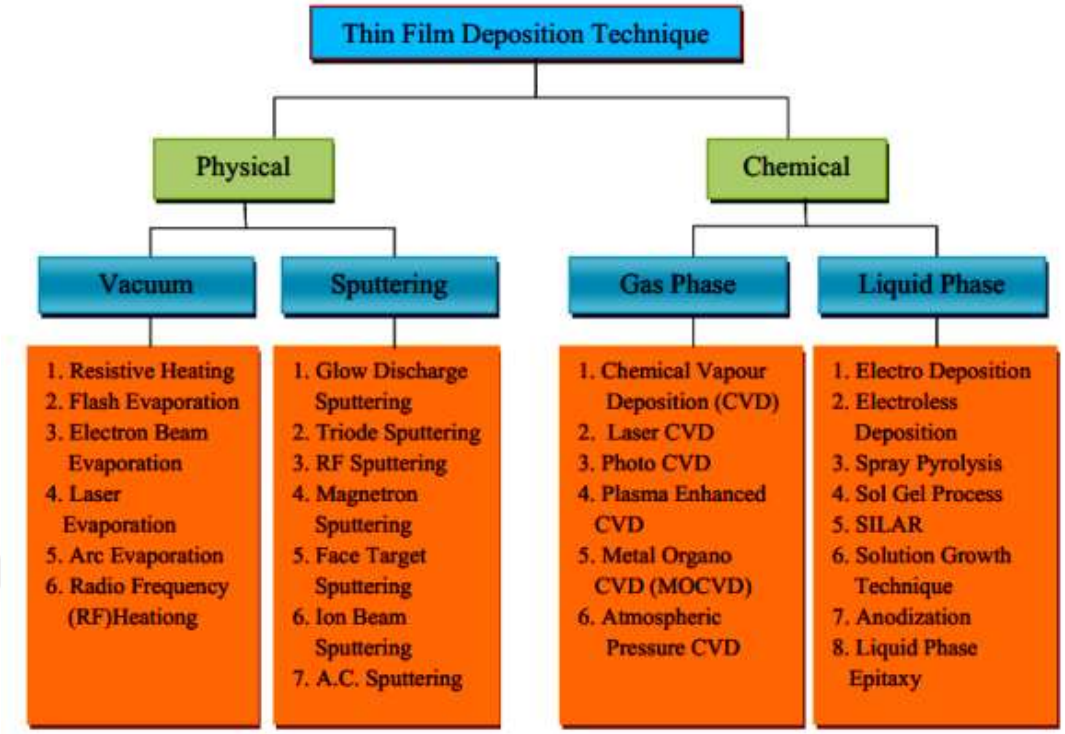

Figure 1.2 Classification of thin film deposition techniques [33]

1.3 Sol-Gel Method

Sol-gel technology, whose existence dates back to the mid-1800s, provides a versatile approach to the synthesis of inorganic polymers and organic-inorganic hybrid materials [42]. The first sol-gel was prepared by Ebelmen (1846) with metal alkoxide ($SiCl_4$) and alcohol. This prepared compound gelled under atmospheric conditions [43]. Geffcken realized that this method could be used to prepare oxide films [44]. In the 1970s, the formation of monolithic inorganic gels at low temperatures without the use of high-temperature melting and transforming them into glasses brought the interest back to the agenda [45].

Sol-gel process, also called soft chemistry, is based on the preparation of a solid material from solution at lower temperatures than traditional preparation methods, using a sol or gel as the intermediate stage. Through this process, homogeneous inorganic oxide materials with desired properties (hardness, optical transparency, porosity and chemical resistance, etc.) can be obtained at room temperature without

the need for the high melting temperature required for conversion to inorganic glasses. The ability of the sol-gel process to take place in exceptionally mild conditions (often at room temperature) and the availability of products in a variety of shapes, sizes and formats has allowed this technology to find increasing applications in various scientific and engineering fields [46,47].

The most important advantage of the sol-gel process is that the microstructure of the material can be adjusted by parameters such as the type of catalyst, type of solvent, temperature of the reaction. By using the sol-gel method, it is possible to produce metal oxide-based materials such as SiO_2, TiO_2, ZrO_2, GeO_2, SnO_2, Al_2O_3, V_2O_5 at much lower temperatures. These oxide-based materials can be produced as monolithic materials in various shapes and sizes, as thin films of different thicknesses ranging from nm to microns, or as powders [48].

1.3.1 Overview of Sol-Gel Method

The steps and end products of the sol-gel process are shown in Figure 1.3. The sol-gel process can be shortly defined as the preparation of the sol, the gelation of the sol and the removal of the solvent, and the preparation of ceramic and glass materials. The sol is different from solution. The solution is a single phase system. Sol is the suspension of solid particles in liquid. If solids remain dispersed in liquids, this system is called sol. The effect of intermolecular Van Der Waals and electrical repulsive forces is greater than the gravitational force. Therefore, the materials that forming of the sol do not precipitate to the bottom. The gel structure is a phase seen after the sol. Gel structure is a visco-elastic material with submicrometric interconnected pores [45,50,51]. Not all sols transform into gels. An important condition for gel formation is bonding between the smallest solvent particles and solute particles [30]. With the drying of the sol, the liquids and solvents in the system are removed and a solid phase with high porosity is formed. The amount of porosity of the solids is high. As a result, they have large surface area and correspondingly high surface free energy. Because of their high surface free energy, these solids can be annealed at much lower temperatures than would be expected in normal processes [52].

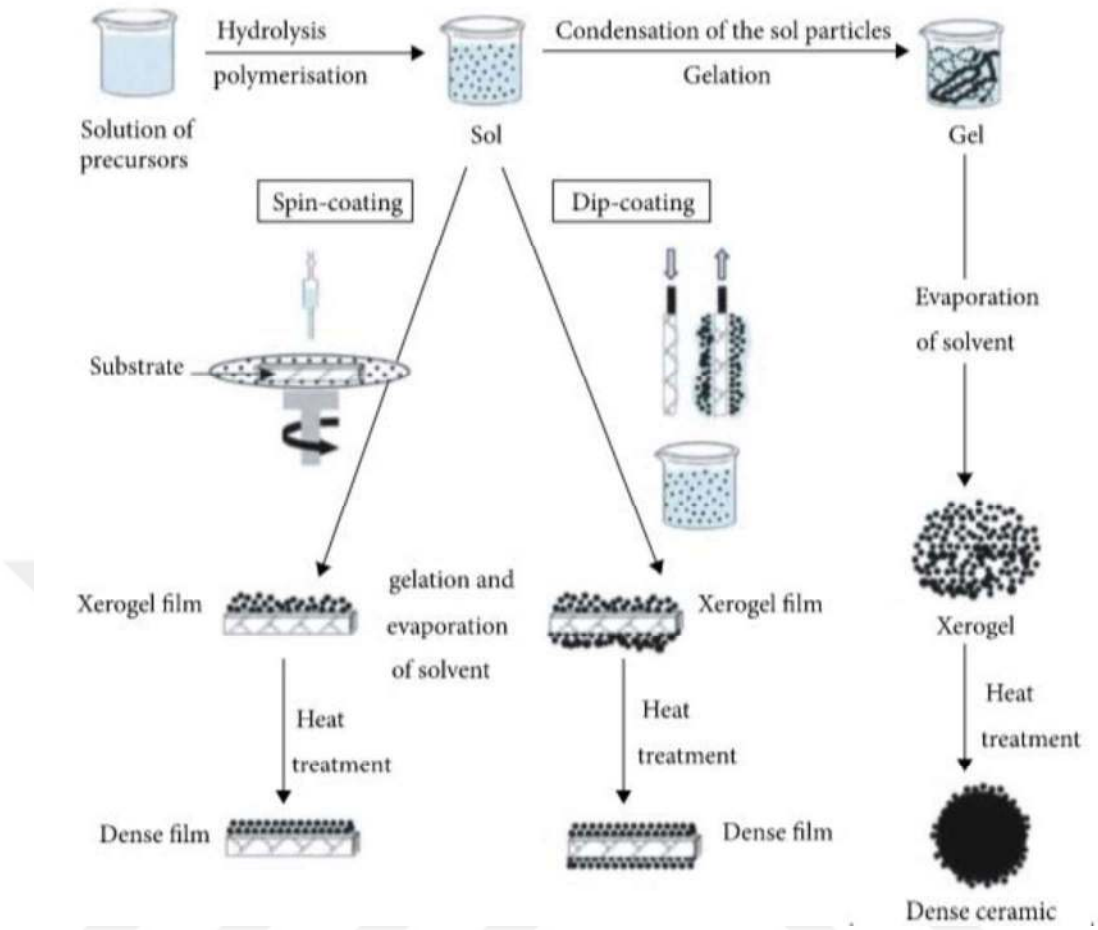

Figure 1.3 Overview of the sol-gel process [49].

The sol-gel method generally involves of the following basic steps:

- Hydrolysis of the precursors
- Condensation
- Gelation
- Aging
- Drying
- Annealing

1.3.2 Precursors of Sol-Gel Method

In the sol-gel method; solution is prepared using starting material, solvent, and catalysts.

1.3.2.1 Starting Material

Inorganic sols and gels are produced directly by synthesis from chemical reactants, usually dissolved in a liquid medium. The reactant containing a metal (M) cation in an inorganic sol or gel is called a chemical starting material. All soluble starting material are used in the sol-gel process. It can be defined as two main groups: metal salts and metal alkoxides.

- Metal salts → M_mX_n (X is an anionic group)
- Metal alkoxides → $M(OR)_x$ (R is an alkyl group)

Metal alkoxides actively participate in the reactions due to the highly electronegative OR group they contain. These compounds are highly reactive in the presence of moisture, heat or light [53,54].

1.3.2.2 Solvent

Due to the solution chemistry of metal salts and metal alkoxides is quite different, solvent choice should be made according to the type of starting material. The solvent can be water or inorganic solvent. Water for metal salts and alcohols for metal alkoxides are used as solvents. Alcohols such as CH_3OH (methanol), C_2H_5OH (ethanol), C_3H_3OH (propanol), C_4H_9OH (butanol) are used as precursors in the sol-gel method and react with metal oxides [54]. Some starting materials and solvents using in sol-gel process of TiO_2 is given in the Table 1.3.

Table 1.3 Starting materials and solvents using in sol-gel process of TiO_2.

Material	Chemical formula	Type	Solvent	Ref
Titanyl sulfate	$TiO(SO_4)$	Metal salt	Distilled Water	[55]
Titanium cloride	$TiCl_4$	Metal salt	Distilled Water	[56]
Titanium butoxide	$Ti(OC_4H_9)_4$	Metal alkoxide	Ethanol	[57]
Titanium isopropoxide	$Ti(OC_3H_7)_4$	Metal alkoxide	Ethanol	[58]

1.3.2.3 Catalyst

Catalysts used in the sol-gel method are divided into acid and base. Generally; acetic acid (CH_3COOH), nitric acid (HNO_3), hydrochloric acid (HCl), hydrofluoric acid (HF) and ammonium hydroxide (NH_4OH) are used as catalysts [59].

1.3.3 Reactions in The Sol-Gel Method

There are two main reactions in the preparation of the sol. These are hydrolysis and condensation reactions.

1.3.3.1 Hydrolysis reaction

The hydroxyl ion is bonded to the metal atom by the hydrolysis reaction.

$$M(OR)_4 + H_2O \rightarrow HO - M(OR)_3 + ROH \quad \textbf{(1.1)}$$

ROH is alcohol group compound. Depending on the amount of water and alcohol, hydrolysis reactions can continue until all OR groups are OH.

Hydrolysis reaction when there is enough alcohol and water;

$$M(OR)_4 + 4H_2O \rightarrow M(OH)_4 + 4ROH \quad \textbf{(1.2)}$$

1.3.3.2 Condensation reaction

The two materials undergoing hydrolysis are connected by an oxygen bridge.

$$(OR)_3M{-}OH + HO{-}M(OR)_3 \rightarrow (OR)_3{-}O{-}M(OR)_3 + H_2O \quad \textbf{(1.3)}$$

If one of the components is hydrolyzed, the reaction;

$$(OR)_3M{-}OR + HO{-}M(OR)_3 \rightarrow (OR)_3{-}O{-}M(OR)_3 + ROH \quad \textbf{(1.4)}$$

The products resulting from the reaction are hydrolyzed. These products recombine and a condensation reaction occurs [45,60].

1.3.4. Aging

The following stage after hydrolysis and condensation reactions is the aging stage. The waiting time for a wet gel to be stored for a long time and transformed into a stable structure with the reactions of the chemicals in it is called the aging process [61].

Aging is a step that also provides the formation of crystallization. In aging, the structure is reorganized as the structure decomposes and precipitation again. And products in crystal form are formed. As long as the gel is not aged, it remains in its amorphous form. As long as the gel is not aged, it remains in its amorphous form. Hydrothermal conditions are used to accelerate transformations in aging.

Aging not only provides crystallization, but also affects the drying phase of the sol-gel process. The capillary pressure that occurs during the drying phase is proportional to the interface area of the gel. If this interface area decreases with aging, the pressure that will occur during the drying phase decreases. Thus, stronger gel networks are formed and cracking that may occur during drying is prevented.

The aging time has significant effects on the phase crystallization, phase transformation, crystal size and thus on the surface area. Some substances that move away from the structure during aging also change the properties of the final product considerably. Oxygen vacancies were observed in the lattice due to desorption of hydroxyl ions after calcination in samples that were not sufficiently aged [54,62,63].

1.3.5 Drying

The drying process of a porous material can be divided into a few stages. Firstly; the body shrinks in an equal amount with the evaporated liquid volume, and the liquid-vapor interface remains on the outer surface of the body. When the body solidifies too much to shrink, the second stage begins and the liquid recedes inward by releasing the air-filled pores near the surface. A film of liquid help the external flow as air invades the pores, so evaporation continues to occur from the surface of the body. As a result, the liquid is isolated into the pockets and drying can only continue by diffusion of the outside vapor and evaporation of the liquid inside the body [54,64].

Drying the gel is one of the critical steps of the sol-gel. Drying is controlled by capillary pressure. During drying, shrinkage occurs in the gel due to capillary pressure, and the change in capillary pressure inside the pores can cause mechanical damage. Increased capillary pressure during drying can result in shrinkage and cracking [54].

In order to prevent these cracks, the stresses that will occur can be relieved by drying very slowly. In addition, many factors such as gelling, drying and heating rate, solids content of the sol, and composition geometry must be taken into account to prevent cracking [65].

1.4 Sol-Gel Film Coating Methods

Some application techniques used when coating thin films by Sol-gel method are listed below [66].

- Dip coating
- Spin coating
- Roller coating
- Slit coating
- Meniscus coating
- Doctor-Blade coating

Among these coating methods, dip and spin coating method are widely used for coating thin films.

1.4.1 Dip Coating Method

It is based on the principle of dipping the substrate in the prepared sol at a certain speed and with-drawal it at the same speed. The dip coating method can seperated into five stages. These five steps are shown in Figure 1.4. During the dipping stage, the substrate is submerged at a constant speed. It is kept in sol for a short time. Then the substrate is withdrawal with the dipping speed. In the deposition stage, parts of the substrate that is withdrew from the sol are covered with the sol. In the drainage stage, the sol which is coated on the substrate, is filtered drop by drop. During the evaporation stage; excess

sol that cannot be filtered from the substrate evaporates. Xerogel is obtained on the substrate. The xerogel formed on the substrate becomes a film after annealing.

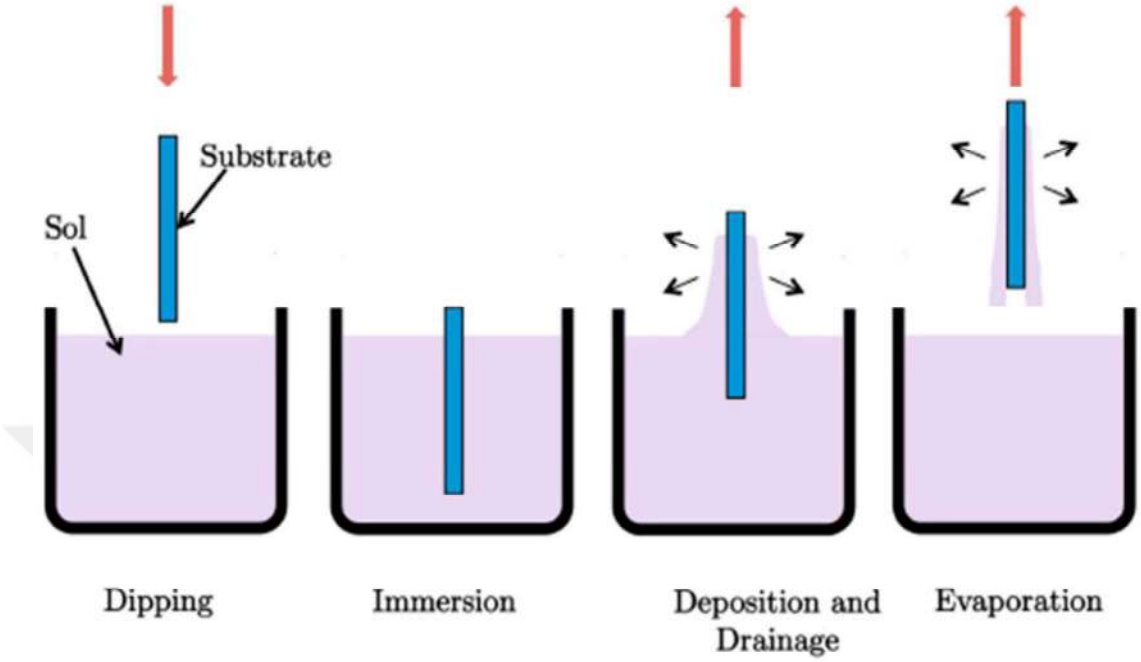

Figure 1.4 Stages of dip coating method [67].

The thickness of the coated film; It depends on the components of the solution, the dipping speed of the substrate and the viscosity. Some forces in the coating region control the film thickness. These forces are as follows [68]:

- Upward pulling force of the substrate due to viscosity
- Gravitational force
- Surface tension resultant force in the concave curve of the liquid
- The inertial force of the boundary layer of the liquid entering the coating zone.
- Surface tension gradient

The advantages of the Sol-Gel Dip Coating (SGDC) method can be summarized as follows [48]:

- Samples of all shapes and sizes can be coated

- Relatively inexpensive as the coating mechanism is simple
- Minimum pollution
- Possibility to work easily in a controlled atmosphere

The disadvantages of the sol-gel dipping method are as follows [48]:

- Too much solution needed to coating large substrates
- Necessity to coating both surfaces of the substrate

1.4.2 Spin Coating Method

This method is based on the principle of dripping sol onto the substrate while it is being rotated horizontally around an axis and spreading the sol onto the substrate surface with the effect of centrifugal force. Spin coating process can be broadly divided into 4 main steps sketched in Figure 1.5, which are deposition, spin up, spin off and evaporation.

During the deposition stage, sol is dropped on the substrate fixed to the rotating surface. The substrate that was initially mationless is rotated. The substrate should reach the desired rotational speed as soon as possible. Because the constant rotation speed will affect the uniformity of the film thickness. During spin up, sol dropped on the substrate spreads over the entire surface of the substrate by the effect of centrifugal force. During the spin-off stage, the excess sol flows to the environment. The film gradually becomes thinner and the removal of excess sol slows down. As the film thins, the resistance to flow increases and the concentration of non-volatile elements increases, increasing the viscosity. During the final stage, thinning occurs by evaporation. The advantage of the spin-coating method is that the sol wants to spread evenly on the substrate during the spin-off stage. This tendency increases due to the balance between the two main forces. These forces are centripetal force, which causes radially outward flow, and viscous force, which causes radially inward movement [69,70].

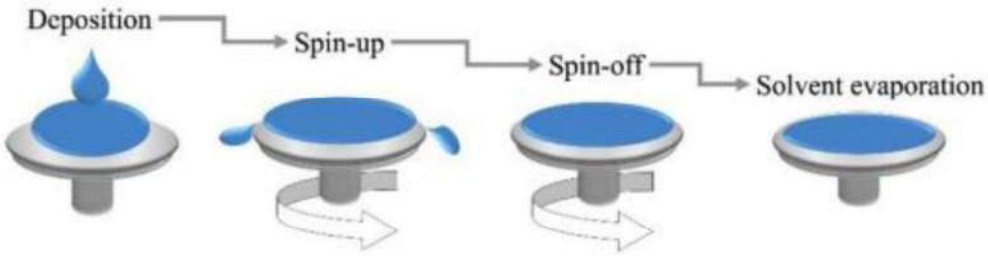

Figure 1.5 Stages of spin coating method [71].

The advantages of the sol-gel spin coating (SGSC) method can be summarized as follows [48]:

- Small amount of coating solution is used
- The process is very fast
- The process is suitable for multi-layer applications

The disadvantages of the sol-gel dipping method are as follows [48]:

- Suitable for round substrates
- It's hard to keep clean
- Homogeneous coating of large substrates is difficult
- In case of rapid evaporation of the solvent, homogeneous coatings cannot be obtained, and in the case of using solvents with high boiling points, it becomes difficult to obtain the desired film thickness.

1.5 Literature Review

Vorotilov et al. (1991) grew TiO_2 thin films on glass substrates by sol-gel spin coating method. They investigated the effect of solution content, gas moisture during deposition and heat treatment temperature on the film properties. X-ray diffraction spectra, optical and electrical properties quality were studied. In contrast to titanium ethoxide ($Ti(OC_2H_5)_4$) sols, titanium butoxide ($Ti(OC_4H_9)_4$) sols were found to be

more stable and could be prepared with a higher oxide content. They reported that gas moisture/hummudity during deposition had a negligible effect on film quality when the ratio of water content in sol was close to a certain maximum value (no precipitaion should appear). It has been observed that the films annealed at temperatures below 400°C are in amorphous structure and transform from amorphous structure to anatase structure at temperatures above this degree, and transformation from anatase phase to rutile phase begins between 600-800°C [72].

Wang et al. (2001) prepared nanosized TiO_2 by a aqueous sol-gel method using titanium butoxide was used as starting material of TiO_2. Using X-Ray diffractomery (XRD), Auger electron spectroscopy (AES) and X-Ray photoelectron spectroscopy (XPS), the thin films are characterized. As the films were annealed above 350 ^{0}C, its transformation from amorphous phase to anatase phase. The partially crystalline nature of the film resulted in high refractive indices: n=2.3 at 550 nm. The indirect and direct optical band-gaps of the anatase film was evaluated as 3.23 and 3.80 eV, respectively [73].

Naceur et al. (2012) grew TiO_2 thin films on silicon and quartz substrate by sol-gel spin coating method and investigated the effects of annealing on microstructural and optoelectronic properties. They annealed at different temperatures between 200 and 1000 ^{0}C. The microstructural and optical properties of the grown films were investigating using thermal gravimetric analyses (TGA), Raman spectroscopy, atomic force microscopy (AFM), XRD, UV-Vis and spectroscopic ellipsometry. XRD and Raman spectra showed that, starting from the annealing at 400 ^{0}C, the thin films crystallize in the anatase tetragonal phase and annealing at 1000 ^{0}C, the thin films changed into rutile structure. With increasing annealing temperature, the spherical shaped crystals became elongated and relatively flat. Optical band-gap values of thin films annealed between 200 ^{0}C and 1000 ^{0}C degrees decreased from 3.65 eV to 3.09 eV with increasing temperature. Annealing temperatures of thin films strongly affected the microstructural and optical properties [74].

Wong et al (2014) studied synthesis and characterization of TiO_2 thin films by sol-gel method in aqueous medium at room temperature. They investigated effect of aging time and starting material concentration of TiO_2 thin films. The solution were

synthesized using titanium (IV) isopropoxide hydrolysed in glacial acetic acid and deionized water and the solution was undergone aging for 1, 2, 3, 6 and 8 weeks. It was observed that the films coated un-aged were in amorphous structure, and after the aging process, the films crystallization into anatase phase. When aging time increased, anatase peaks became narrower and sharper. This showed that while crystallization occurred at RT, the longer the aging time, the better is the crystallinity [75].

Hwang et al (2012) investigated synthesis, characterization and photocatalytic properties of TiO_2 powders by using colloidal solution prepared from titanium isopropoxide as a starting material by sol-gel method. The effects of aging conditions such as aging time and temperature on the physical and chemical properties of TiO_2 were investigated. The average particle sizes of sols aged 0 h, 24 h, 72 h were calculated as 29 nm, 44 nm and 78 nm, respectively. This result clearly demonstrates that the aging time is important process in controlling the particle size. It was determined that the aging process affects the crystal size of TiO_2 powders. With increasing aging time, the surface area of the TiO_2 powder was increased in the range of 41 – 70 m^2/g [76].

Turabi (2019) grew TiO_2 thin films on glass substrate by sol-gel method. The solution was aged for 1, 7, 14, 21, 28, 35, 42 and 49 days and coated with different layers by spin coating method. The XRD peak intensity of the films obtained from the solutions aged up to 35 days increased and the FWHM value decreased. On the optical study, it was determined that solution aging causes a decrease in the band gap energy. It was determined that the FWHM value and band gap value of the films obtained after 35 days of solution aging increased. Additionaly, a decrease in the bandgap energy and crystallite sizes was reported with the increase of number of layers and annealing time. It was concluced that the crystallization of the film coated with the 35 days aged solution was better and increasing the number of layers and annealing time affected the XRD peak intensity, FWHM value, crystallite size and band gap energy. [77].

Miki et al., (2003) in their study; to obtain nanoporous films, TiO_2 solutions were prepared by hydrolysis of titanium (IV) isopropoxide and addition of trehalosedihydrate. The porous and thin TiO_2 films grew by heating up to 500 ^0C on the glass substrate by dip coating method. The maximum thickness of the film grew

by the dip coating method is 740 nm. The film consists of nano-sized particles (10-20 nm) and 7 nm pores. They determined that the specific surface area of the film was 163 m^2/g and porosity of the film was 65 % [78].

Malliga et al. (2014) investigated effect of film thickness on optical an structural properties of TiO_2 thin films on glass substrate from alkoxide solution by sol-gel spin coating method. The solution consist of titanium isopropoxide, acetic acid, ethanol. The characterization of the films grown as 4, 6, 8 and 10 layers was performed by XRD, UV-Visible spectroscopy, photoluminescence (PL) spectroscopy, field emission scanning electron microscope (FESEM) and energy dispersive X-ray spectroscopy (EDAX). It was determined thas as the number of layers increased, thecrystallite size increased from 6.3 nm to 35.5 nm and the peak intensities increased. As the film thickness increased, the transmittance decreased and there was a decrease in the band gap energy from 3.90 eV to 3.45 eV [79].

1.6 Objective

In this thesis TiO_2 thin films were coated on the glass substrates with different aging time, number of layers, dipping time and annealing temperature by sol-gel spin coating (SGSC) and sol-gel dip coating (SGDC) methods. The aim of the thesis is to investigate the effect of the sol-gel thin film growth parameters by characterizing structural (crystallite size, dislocation density, microstrain, avarage grain size, porosity), surface (homogenity and smoothness), and optical properties (energy bandgap, refractive index, dielectric constant and static dielectric constant) of the films.

CHAPTER 2

EXPERIMENTAL PROCEDURE

2.1 Substrate Selection and Preparation

According to the method we use, the film we will obtain must be homogeneous and smooth. Therefore, substrate selection becames important. The physical properties of the substrates on which the thin film will be formed are among the most effective factors for the quality of the thin film. Crystallization in the films formed depends on the crystal structure of the substrate and the propertions of the materials used. The glass was used as a substrate in our study. Glass is a very good substrate material that is abundantly found in nature. The glasses used in this thesis are hydrolic 3. class soda lime glass with high optical quality, colorless. It is produced by isolab by a fully automatic process to have a clean and dust-free surface. The standart thickness of the glasses is about 1 mm and the slide sizes are 26 mm x 78 mm.

Figure 2.1 The used ultrasonic bath

2.2 Substrate Cleaning

Crystallization depends on the cleanliness of the material used and the smoothness of the surface. Therefore, the glass substrate have been cleaned by ultrasonic cleaner (in Figure 2.1). The substrates was washed with detergent to purify of oil and dirt and clear rinsed. Then, substrates were kept in an ultrasonic bath for 5 minutes each in deionized water, methanol and again deionized water. The water remaining on the glass substrate was evaporated with the drying machine.

2.3 Solution Preparation

For growth of TiO_2, the solutions were prepared by using titanium tetraisopropoxide [$Ti\{OCH(CH_3)_2\}_4$] (Merck), ethanol [C_2H_5OH] (Sigma-Aldrich) and acetone [C_3H_6O] (Merck). TTIP (20 ml) was used as a starting material for TiO_2 solution. It was disolved by adding ethanol (30 ml) dropwise into TTIP when stirring on magnetic stirrer at 600 rpm (in figure 2.2) and stirred 10 minutes. Ethanol (15 ml) – acetone (7.5 ml) mixture was added dropwise into TiO_2 solution and stirred for 90 minutes. Then, the prepared solution was aged in a desiccator at room temperature for different lenghts of time (1, 7, 14, 21, 28, 56 days).

Figure 2.2 The used magnetic stirrer and spin coater

2.4 Preparation of TiO_2 Thin Films

2.4.1 Dip Coating

The cleaned glass substrates were dipped in the TiO_2 solution aged 1, 7, 14, 21, 28 and 56 days at a dipping speed of 5 mm/sec for 5, 10 and 20 seconds. After, the substrates were withdrew same speed and dried horizontally under ambient conditions followed by these was placed in an oven (in a Figure 2.3), kept at 100 ^{0}C for 30 minutes.

2.4.2 Spin Coating

The cleaned glass substrates were placed in a spin coater (in a Figure 2.2) and 5 drops of aged TiO_2 solution (1, 7, 14, 21, 28 and 56 days) were dropped onto the placed substrate surface. The spinning speed of the spin coater was adjust at 3000 rpm for 30 seconds. After the coated process, films were dried at 250 ^{0}C for 3 minutes in a drying oven followed by cooled to room temperature under ambient conditions. This process was repeated 3, 5 and 10 times for investigating the effect of the number of layers.

The solution was prepared again and subjected to aging for 28 days. The films were prepared with 3 layers (SGSC) and 10 seconds dipping time (SGDC). The prepared TiO_2 thin films were annealed at 300 ^{0}C, 400 ^{0}C, 500 ^{0}C, 600 ^{0}C and 700 ^{0}C for 1 hour in a tube furnace (in a Figure 2.3) for the researching effect of the annealing temperature.

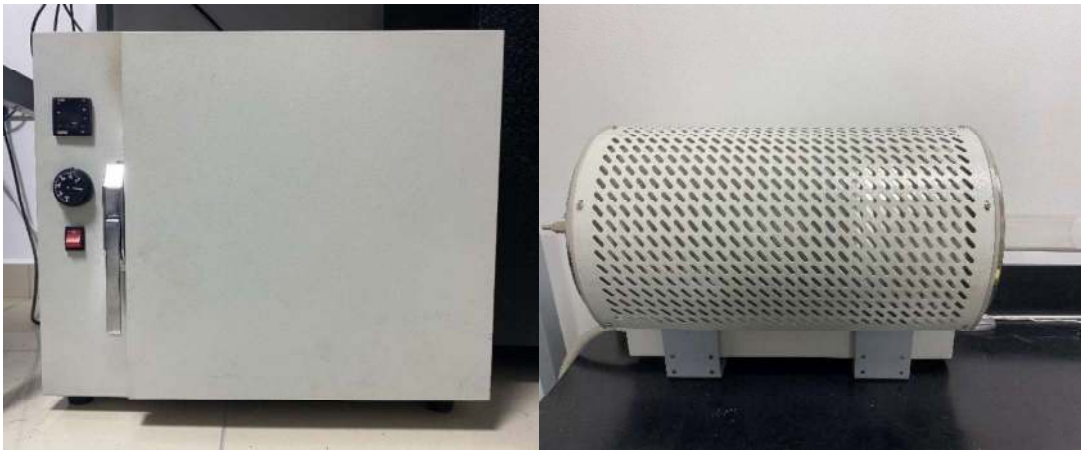

Figure 2.3 The used drying oven and tube furnace

2.5 Characterization

2.5.1 X-Ray Diffraction

XRD is a effective technique for determining the crystal structure of solid materials which are long-range order. However, it is find limited application for disordered and amorphous materials. The patterns obtained by XRD are a characteristic features of the material and a different diffraction pattern is obtained for each material. Based on the intensity of the peak in the patterns and the peak widhts, information about the crystallization level of the material can be obtained. Additionaly, the XRD analysis method offers the chance to get information about the material by providing some parameters, such as crystallite size, dislocation density and microstrain [80,81].

In this research, the structural properties of TiO_2 thin films produced by SGDC and SGSC methods was investigated by X-ray diffractometer (Miniflex 600, Rigaku) which shown in Figure 2.4. The XRD patterns were collected which uses a CuKα (λ=1.5405 Å) radiation source and 2θ range of 20 – 70 degrees with a step size of 0.02 by 2 min^{-1} steps operating at 40 kV accelerating voltage and 15 mA current. Crystal structure and structural properties of TiO_2 films were analyzed from some XRD patterns.

Figure 2.4 The used X-Ray Diffraction instrument

XRD works on the principle of Bragg's law. Bragg's Law equation is given as follow:

$$n \lambda = 2 d \sin \theta \quad \textbf{(2.1)}$$

Where, θ is the angle of incident of X-ray beams, d is the distance between atomic layers in a crystal, λ is the wavelenght of the incident X-rays beam and n is the diffraction order (usually n = 1). Hereby, [72]

$$d = \lambda / 2 \sin \theta \quad \textbf{(2.2)}$$

In current research work the (101) peak is used for anatase as given by the reference peaks. Scherrer equation was used to calculate the avarage crystallite size with peak broadening analysis.

$$D = k \lambda / \beta \cos (\theta) \quad \textbf{(2.3)}$$

Where, D is diameter of nanocrystals, k is a constant value (k=0.9), λ is the wavelenght of the used X-ray source (1.5405 Å), β is the full widht at half maximum lenght (FWHM), and θ is the anggle of diffraction [83,84].

The smallest repeating unit of the crystal lattice is the unit cell, the building block of a crystal. Defect prevent the unit cell to being arrenged in an order. The dislocation density, δ, were calculated by the following equation;

$$\delta = 1 / D^2 \quad \textbf{(2.4)}$$

Where, D is the avarage crystal size [85,86].

The microstrain (ε) was examined using the Stokes-Wilson equation [87]:

$$\varepsilon = \beta / 4 \tan (\theta) \quad \textbf{(2.5)}$$

2.5.2 Scanning Electron Microscope (SEM)

Micro and nanoscale structures of materials can be viewed by SEM. A topographic three-dimensional image is obtained with the SE (secondary electron) detector in the device. By the EDX (energy dispersive X-rays), the elemental content of the structures can be determined qualitatively and quantitatively.

Electron microscopy is based on the principle of reflection of electrons accelerated under high voltage by striking the material surface. By using these reflected electrons and accordingly X-rays, different analyzes are made and the topography of the surface is obtained. Field emission scanning electron microscope (FE-SEM) using for the analysis of the microstructural properties of the films was shown in Figure 2.5.

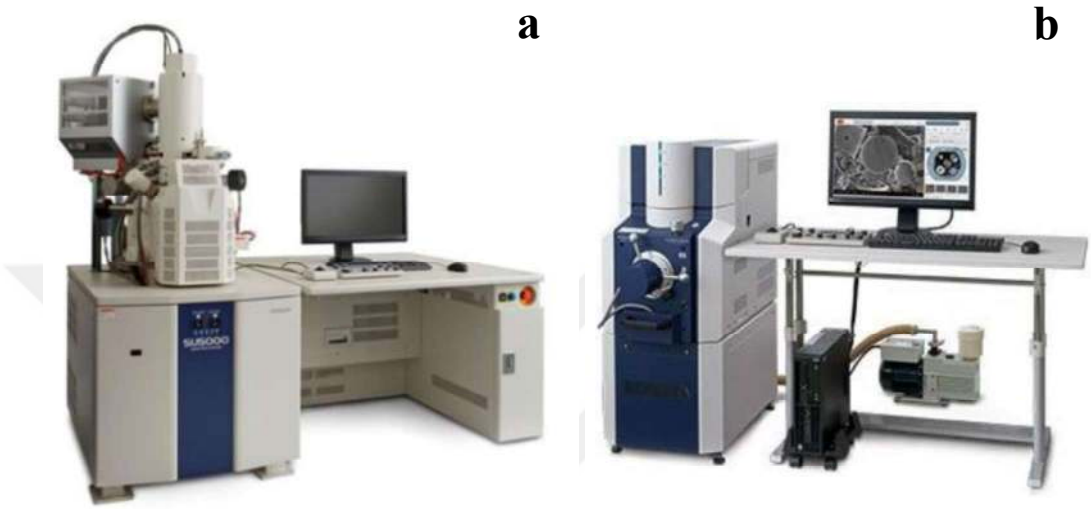

Figure 2.5 The used Scanning Electron Microscopes

The characterization of the surface morphologies of the grown films was examined with Hitachi SU 5000 FE-SEM (a) and FlexSEM 1000 II, HITACHI (b). The elemental content of the structures was determined with an X-MaxN 80 mm^2 EDS (energy dispersive) detector from Oxford Instruments with Hitachi SU 5000 FE-SEM. Average grain size was calculated using the ImageJ which is agraphic design program dedicated to analyzing images.

2.5.3 UltraViolet-Visible (UV-Vis) Spectroscopy

UV-Vis spectroscopy is an optical characterization technique used to measure the amount of light that is absorbed or transmitted by a sample at different wavelenghts of ultraviolet (200 - 400 nm), visible (400 – 800 nm) and near infrared (NIR) (800 – 2500 nm) light [88,89]. The optical absorbance of the thin films were measured in the wavelenght range of 200–1000 nm, at intervals of 10 nm, by using Shimadzu UV-VIS 2600 Spectrophotometer which shown in Figure 2.6.

Figure 2.6 The used UV-Visible Spectrometer

The ratio of the flux of incident electromagnetic energy to the distance unit in the direction of incident wave diffusion is known as the absorption coefficient. When the values of the absorption coefficient are high, ($\alpha > 10^4$) at high energies, it is clear that the absorption coefficient helps in determining the type of the electron transition since the incident photon's energy exceeds the forbidden energy gap. It is anticipated that direct electron transitions would occur, with electrons and photons retaining their energy and moment. However, it is anticipated that an indirect transition of the electron would occur when the values of the absorption coefficient are low ($\alpha > 10^4$) at low energies, and the electronic momentum is kept with the help of the phonon. The absorbance spectrum used to calculate the absorbance coefficient (α) by applied the following equation:

$$\alpha = (2.303 \times A) / t \quad \textbf{(2.6)}$$

where A is absorbance, t is the film thickness [90,91].

The thickness of the film was calculated using the gravimetric method,

$$t = (m_a - m_b) / (\rho S) \quad \textbf{(2.7)}$$

where m_a is mass of glass substrate after coating, m_b is mass of glass substrate before coating, ρ is the film density which is 4.23 g/cm^3 for the TiO_2 compound, S is the surface area.

The energy gap of films was determined using the Tauc's relation given as follow:

$$(\alpha\, hv) = A\,(hv - E_g)^n \qquad \textbf{(2.8)}$$

where, α is the absorption coefficient, hv is the incident photons' energy, A is a constant called the band tailing parameter, E_g is bandgap energy and ns is the power factors of transition mode, which is depending on the nature of material whether it is crystalline or amorphous [92].

In order to determine the bandgap energy of the films, the $(\alpha hv)^2$ vs hv graphs were drawn. The energy values of the point where the direction of the linear parts of these graphs intersects the hv axis at $(\alpha hv)^2 = 0$ were determined as the bandgap energy of the films.

Refractive index, n was calculated using three different models and these models have direct relation refractive index with the band-gap:

→ The Moss relation is given by [93],

$$Eg\, n^4 = k \qquad \textbf{(2.9)}$$

where Eg is a energy ban d-gap, k is a constant with a value of 108 eV.

→ Ravindra et al. relation is given by [94,95],

$$n = \alpha + ßEg \qquad \textbf{(2.10)}$$

with α = 4.084 and ß = (-0.62) eV^{-1}.

→ The Herve and Vandamme relation is given by [96,97],

$$n^2 = 1 + (A / (Eg + B))^2 \qquad \textbf{(2.11)}$$

where A value is 13.6 eV and B value is 3.4 eV.

The dielectric constant (ε_∞) was calculated by applied the following equation [98];

$$\varepsilon_\infty = n^2 \qquad \textbf{(2.12)}$$

where n is refractive index.

The static dielectric constant (ε_0) is related to the band-gap as shown the following equation [99];

$$\varepsilon_0 = 18.52 - 3.08\mathrm{Eg} \quad \textbf{(2.13)}$$

The porosity of thin films was calculated from the following relation in equation [100,101];

$$\text{Porosity (\%)} = (1 - (n^2-1) / (n_d^2-1)) \times 100 \quad \textbf{(2.14)}$$

where n_d is the refractive index of pore-free anatase (n_d = 2.52 [102]), and n is the refractive index of the porous thin films.

The optical conductivity (σ) of the film was calculated by applied the following equation [103];

$$\sigma = (\alpha\, n\, c) / (4\, \pi) \quad \textbf{(2.15)}$$

where α is the absorbance coefficient of the film, n is the refractive index and c is the speed of the light.

CHAPTER 3

RESULT AND DISCUSSION

3.1 XRD Spectrum Analysis

3.1.1 Aging Effect for SGSC TiO_2 thin Film

The XRD patterns for 1, 7, 14, 21, 28 and 56 days of SGSC TiO_2 thin films with 10 layers are given in Figure 3.1. According to the XRD data' the thin films reveals that there is no obviously diffraction peaks of the titanium dioxide but it only display a broadened peak in the range of Bragg's angles 2θ from 20º and 40º. It indicates an amorphous TiO_2 in presence, which is in accordance with the previously reported literature [104-106]. With increasing aging, no crystal formation were observed.

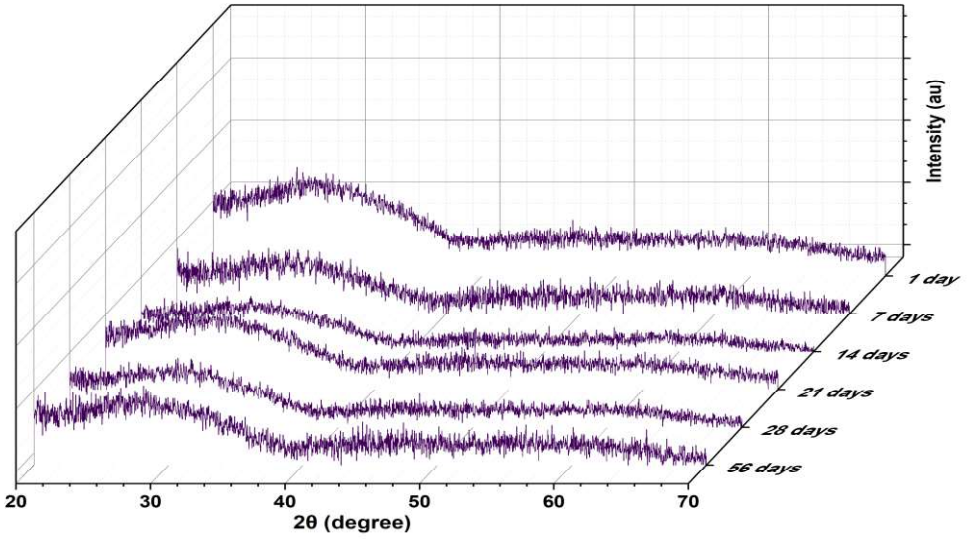

Figure 3.1 The XRD pattern of TiO_2 thin films for 1, 7, 14, 21, 28 and 56 days.

3.1.2 Annealing Temperature Effect for SGSC TiO_2 thin Film

XRD patterns of the SGSC TiO_2 thin films coated with the 28 days aged solution with 3 layers as a function of annealing temperature (as-grown, annealed at 300 ^{0}C, 400 ^{0}C, 500 ^{0}C and 600 ^{0}C) are given in Fig. 3.2. The as-grown and annealed at 300 ^{0}C films

exhibit amorphous behaviour. Films annealed at 400 °C began to crystallize in anatase form. The 2θ=24.61° peak value corresponding to the TiO_2 lattice plane (101). Previous work showed that thin films can be recrystallization from amorphous to anatase phase at between 300 ^{0}C and 400 ^{0}C [102,105]. Peaks at 37.53°, 47.77°, 53.59°, 54.74° and 62.49° matched with the lattice planes (004), (200), (105), (211) and (204), respectively were observed that begins to appear when increased annealing temperature from 400 ^{0}C to 600 ^{0}C. When the XRD peaks compared with values in the ICDD DB card number: 01-071-1168, all the peaks compromised with the tetragonal anatase TiO_2 structure [107-110] .

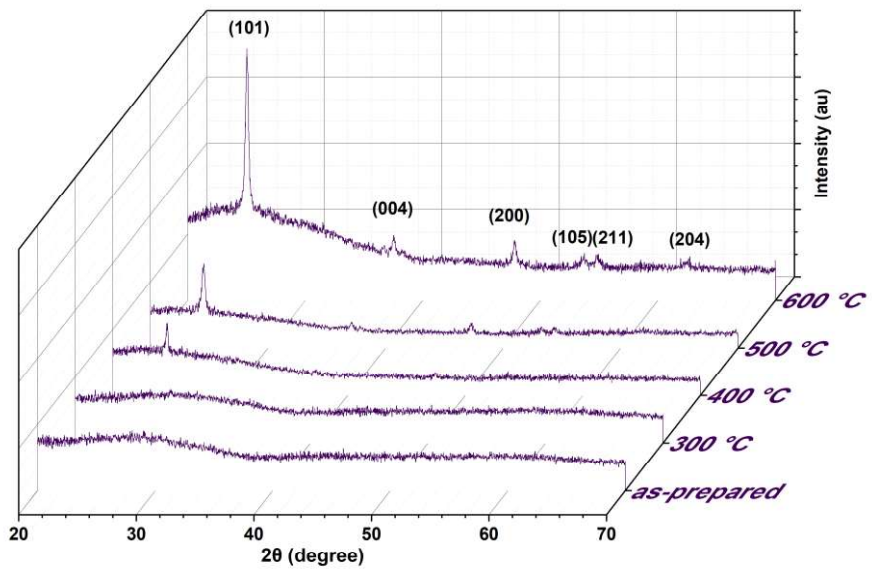

Figure 3.2 The XRD pattern of SGSC TiO_2 thin films by as-grown and annealed at 300 ^{0}C, 400 ^{0}C, 500 ^{0}C and 600 ^{0}C.

The lattice parameters; c/a ratio, volume, density, phase name, space group and number of titanium atoms per unit cell (Z) of SGSC TiO_2 thin films for annealed at 400 ^{0}C, 500 ^{0}C and 600 ^{0}C are given in Table 3.1. The thin films can be directly indexed to the tetragonal anatase structure (141:I41/amd). There are no other diffraction peaks detected, shows that the growth TiO_2 thin films have high purity. Lattice parameters are in the range of a = b = 3.771–3.833 Å, c = 9.373–9.578 Å and c/a is in the range of 2.446–2.523. When the annealing temperature increased from

400 ^{0}C to 600 ^{0}C, the lattice parameters and c/a ratio changed and these results are in agreement with previous works [111-113].

Table 3.1 Lattice information of SGSC TiO_2 thin films annealed at 400 ^{0}C, 500 ^{0}C and 600 ^{0}C.

Annealing Temp. ^{0}C	a (Å)	b (Å)	c (Å)	c/a	α=β=γ (^{0})	Volume (Å^3)	Calc. Density (g/cm^3)	Phase name	Space group	Z
400	3.771	3.771	9.514	2.523	90	135.30	3.892	TiO_2 Anatase	141: I41/amd	4
500	3.833	3.833	9.373	2.446	90	137.72	3.893			
600	3.809	3.809	9.578	2.514	90	138.99	3.842			

The other lattice parameters; 2θ degree, d-spacing, Full Width Half Maximum (FWHM), Crystallite size (D), Dislocation density (δ), Microstrain (ε) and peak intensity values are given in Table 3.2. The peak intensities increased for the (101) dominant peak from 208, 413 to 1541 for 400 ^{0}C, 500 ^{0}C and 600 ^{0}C annealing temperatures, respectively. These behaviour can be attribute to the increasing crystallization[114].

Table 3.2 Structural parameters of SGSC TiO_2 films annealed at 400 ^{0}C, 500 ^{0}C and 600 ^{0}C.

Annealing Temp. ^{0}C	hkl	2θ	d (Å)	FWHM (β)	D (nm)	δ (nm)$^{-2}$x10^3	ε x 10^3	Intensity
400	(101)	24.61	3.614	0.27	31.81	0.988	5.40	208
500	(101)	24.52	3.628	0.33	26.37	1.437	6.62	413
	(004)	37.09	2.422	0.22	39.54	0.639	2.86	45
	(200)	47.26	1.922	0.34	358.9	7.76 x10^{-3}	3.39	63
600	(101)	25.02	3.556	0.33	25.18	1.437	6.49	1541
	(004)	37.53	2.395	0.27	30.84	1.051	3.47	157
	(200)	47.77	1.903	0.23	113.6	77.4 x10^{-3}	2.27	205
	(105)	53.59	1.699	0.33	103.5	94.2 x10^{-3}	2.85	69
	(211)	54.74	1.677	0.34	40.51	0.609	2.87	87
	(204)	62.49	1.485	0.40	21.05	2.256	2.88	53

The FWHM and crystallite size of anatase was calculated from the diffraction peaks with using Eq. 2.3. The crystallite size for (101) plane of SGSC films are calculated as 31.81 nm, 26.37 nm and 25.18 nm for 400 ^{0}C, 500 ^{0}C and 600 ^{0}C annealing temperature respectively. It is seen that the crystallite size decreased with increasing annealing temperature [115]. The lower FWHM and higher crystal size atributed to the higher crystallization. According to XRD results, it can be said that SGSC films annealed at 400 ^{0}C have better crystallization.

3.1.3 Annealing Temperature Effect for SGDC TiO_2 thin Film

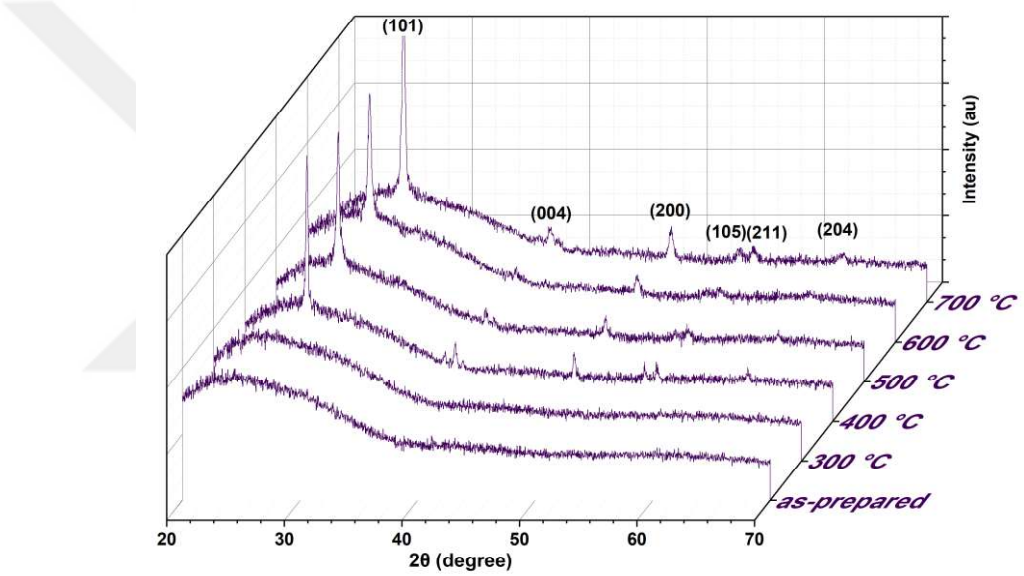

Figure 3.3 The XRD pattern of SGDC TiO_2 thin films by as-grown and annealed at 300 ^{0}C, 400 ^{0}C, 500 ^{0}C, 600 ^{0}C and 700 ^{0}C.

XRD patterns of the SGDC TiO_2 thin films coated with the 28 days aged solution with 10 seconds dipping time are given Figure 3.3 as a function of annealing temperature (as-grown, annealed at 300 ^{0}C, 400 ^{0}C, 500 ^{0}C, 600 ^{0}C and 700 ^{0}C). The SGDC TiO_2 films as-grown and annealed at 300 ^{0}C exhibit amorphous behaviour. The presence of peaks in the XRD pattern for 400 ^{0}C, 500 ^{0}C, 600 ^{0}C and 700 ^{0}C annealing temperature represent the formation of nanocrystalline TiO_2 films. This results are in agreement with the previous research [116].

Table 3.3 Lattice information of SGDC TiO2 thin films annealed at 400 0C, 500 0C, 600 0C and 700 ^{0}C.

Annealing Temp. ^{0}C	a (Å)	b (Å)	c (Å)	c/a	α=β=γ (^{0})	Volume (Å^3)	Calc. Density (g/cm^3)	Phase name	Space group	Z
400	3.790	3.790	9.488	2.504	90	136.28	3.249			
500	3.791	3.791	9.504	2.507	90	136.55	3.249	TiO_2	141:	4
600	3.793	3.793	9.446	2.491	90	135.89	3.905	Anatase	I41/amd	
700	3.767	3.767	9.481	2.517	90	134.53	3.249			

Lattice parameters; c/a ratio, volume, density, phase name, space group and number of titanium atoms per unit cell (Z) of SGDC TiO_2 thin films for annealed at between 400 ^{0}C and 700 ^{0}C are given in Table 3.3. When the X-ray diffraction peaks compared with values in the ICDD DB card number: 01-086-1157, all the peaks compromised with the anatase TiO_2 structure. Lattice parameters of SGDC films annealed at between 400 ^{0}C – 700 ^{0}C are changed in the range of a = b = 3.767 Å - 3.793 Å, c = 9.446 Å – 9.504 Å and c/a ratio = 2.491 – 2.517.

The other parameters; 2θ degree, d-spacing, FWHM, Crystallite size (D), Dislocation density (δ), Microstrain (ε) and peak intensity of SGDC TiO_2 thin films annealed at 400 ^{0}C, 500 ^{0}C, 600 ^{0}C and 700 ^{0}C values are given in Table 3.4. All films have close 2θ=25.25º, 37.90º, 47.97º, 53.99º, 54.97º and 62.79º corresponding to the TiO_2 lattice planes (101), (004), (200), (105), (211) and (204), respectively. The (105) and (204) lattice planes are not observed in annealed at 600 ^{0}C films. The peak intensities for (101) plane in all films are increased from 1455, 1241, 1175 to 1776 with increasing annealing temperature. In contrast to the SGSC TiO_2 thin films, the peak intensities of the (101) planes for SGDC TiO_2 thin films decreased with increasing annealing temperature up to 600 ^{0}C. And a dramatically increasing was observed at SGDC film annealed at 700 ^{0}C.

Table 3.4 Structural parameters of SGDC TiO_2 films annealed at 400 ^{0}C, 500 ^{0}C, 600 ^{0}C and 700 ^{0}C.

Annealing Temp. ^{0}C	hkl	2θ	d (ang.)	FWHM (β)	D (nm)	δ $(nm)^{-2}x10^3$	ε x 10^3	Intensity
400	(101)	25.25	3.524	0.17	50.07	0.393	3.31	1455
	(004)	37.90	2.37	0.15	55.59	0.324	1.91	233
	(200)	47.97	1.895	0.15	134.7	$55.1x10^{-3}$	1.47	220
	(105)	53.99	1.697	0.10	288.7	$11.9x10^{-3}$	0.86	151
	(211)	54.97	1.668	0.10	117.8	$72.1x10^{-3}$	0.74	165
	(204)	62.79	1.479	0.11	75.44	0.175	0.79	116
500	(101)	24.24	3.525	0.21	38.83	0.663	4.27	1241
	(004)	37.80	2.422	0.22	37.76	0.701	2.8	145
	(200)	48.00	1.922	0.34	57.53	0.302	3.33	177
	(105)	53.93	1.698	0.29	110.7	$81.6x10^{-3}$	2.49	74
	(211)	54.95	1.669	0.32	37.19	0.723	2.69	134
	(204)	62.74	1.479	0.20	41.53	0.579	1.43	88
600	(101)	25.26	3.523	0.31	27.17	1.354	6.04	1175
	(004)	37.75	2.381	0.21	39.52	0.640	2.68	95
	(200)	48.4	1.903	0.25	55.72	0.322	2.43	151
	(105)	-	-	-	-	-	-	-
	(211)	55.02	1.677	0.34	33.81	0.875	2.85	79
	(204)	-	-	-	-	-	-	-
700	(101)	25.48	3.493	0.32	26.33	1.443	6.18	1776
	(004)	37.89	2.372	0.46	18.12	3.045	5.85	173
	(200)	48.18	1.887	0.40	41.17	0.589	3.9	291
	(105)	54.14	1.693	0.42	55.14	0.328	3.59	118
	(211)	55.29	1.660	0.32	32.07	0.972	2.67	133
	(204)	62.96	1.475	0.38	21.88	2.088	2.71	97

The crystal size for (101) plane for SGDC TiO_2 thin films annealed at 400 ^{0}C, 500 ^{0}C, 600 ^{0}C and 700 ^{0}C are calculated as 50.07 nm, 38.83 nm, 27.17 nm and 26.33 nm, respectively. With increasing annealing temperature from 400 ^{0}C to 700 ^{0}C, the crystallite size are decreased for SGDC films. Also, FWHM, dislocation density and microstrain values are increased with increasing annealing temperature.

3.2 SEM Analysis

3.2.1 Aging Effect on SGSC TiO_2 Thin Films

SEM images at 1000x and 10000x magnification of the as-grown SGSC TiO_2 thin films grown on the glass substrate at different aging days with 3 layers are given Figure 3.4 and Figure 3.5, respectively.

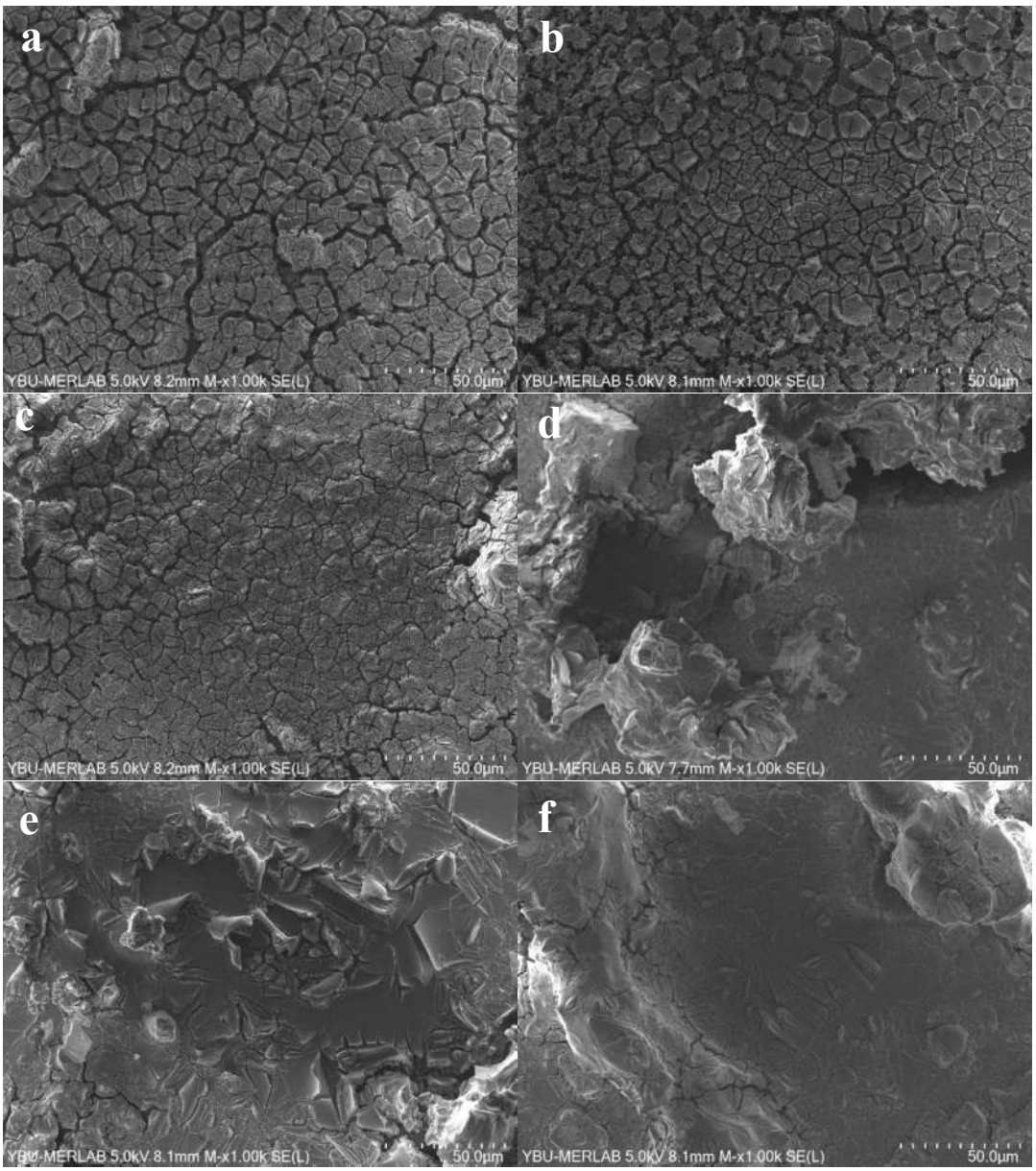

Figure 3.4 The SEM images (1kx) of SGSC TiO_2 films for aged 1 (a), 7 (b), 14 (c), 21 (d), 28 (e) and 56 (f) days.

It can be seen from Figure 3.4 (a) that the coating surface is non-homogeneous and severe cracking. The formation of cracks has been explained by a number of mechanism, including capillary force, which develops during the rapid evaporation of solvent from the coating surface during drying stage, a decrease in the bond strength between TiO_2 nanoparticles as the film is thick, and a significant mismatch between the thermal expansion coefficients of the glass substrate and TiO_2 nanoparticles [117,118].

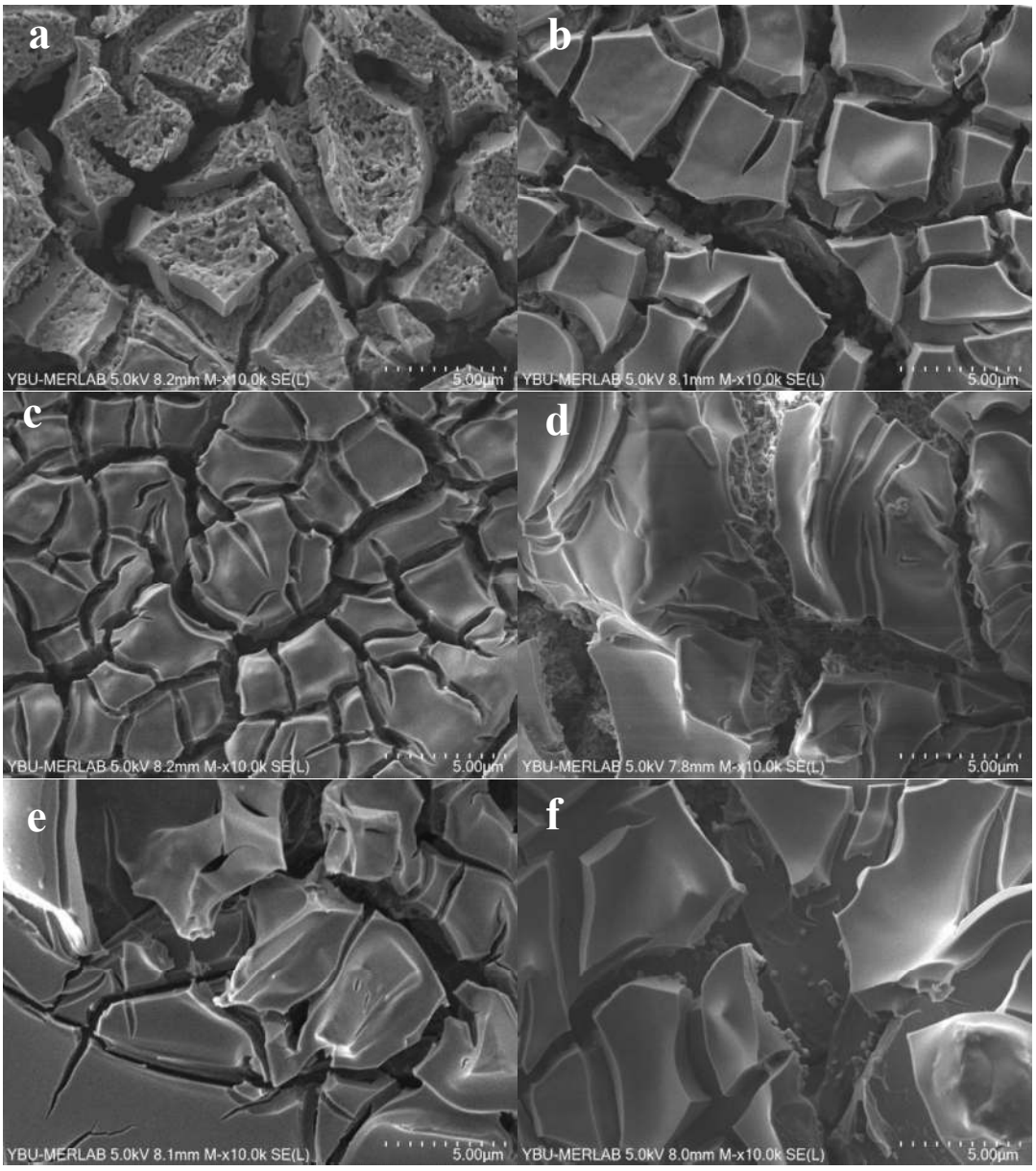

Figure 3.5 The SEM images (10kx) of SGSC TiO_2 films for aged 1 (a), 7 (b), 14 (c), 21 (d), 28 (e) and 56 (f) days.

With higher magnification, the morphologies of coating surface became clear and shown sponge like structure of TiO_2 nanostructures (Figure 3.5). This structre is formed by single nanosized TiO_2 particles bound together, resulting in an arrangement randomly of holes and cavities. Similar structures have been seen in previous works [119]. From 1 day to 14 days smaller cracks and grains size decreasing and interparticle space observed. As can be seen that (Fig. 3.4(d)) the large agglomeration occured on the coating surface of aged 21 days. For 56 days, the coating surface of the SGSC films shows that more uniform and smooth surface, less and small cracks.

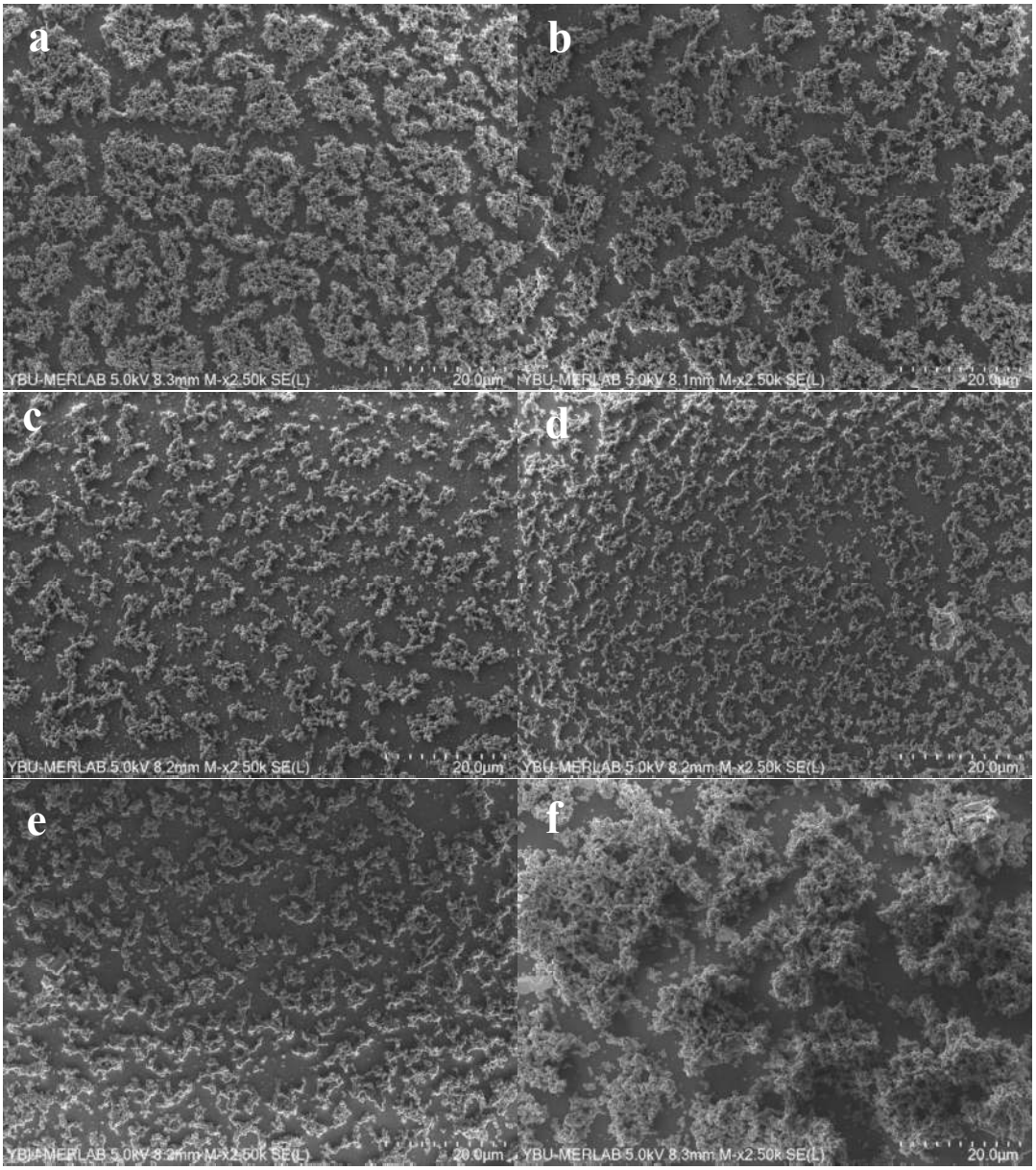

Figure 3.6 The SEM images (2.5kx) of SGDC TiO_2 films for aged 1 (a), 7 (b), 14 (c), 21 (d), 28 (e) and 56 (f) days.

3.2.2 Aging Effect on SGDC TiO_2 Thin Films

SEM images at 2500x and 20000x magnification of the as-grown SGDC TiO2 thin films grown on the glass substrate at different aging days with 10 seconds dipping time are given in Figure 3.6 and Figure 3.7, respectively.

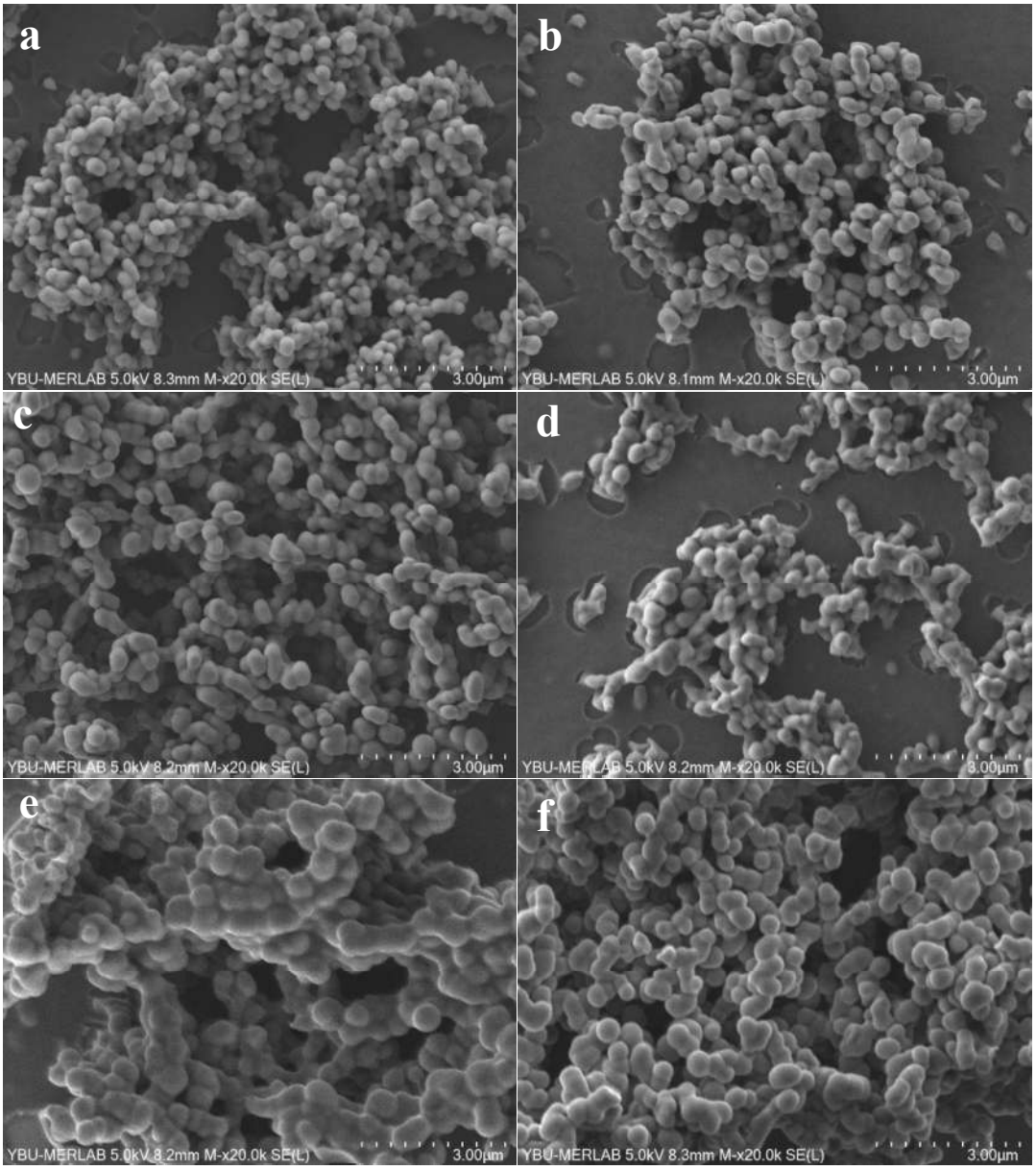

Figure 3.7 The SEM images (20kx) of SGDC TiO_2 films for aged 1 (a), 7 (b), 14 (c), 21 (d), 28 (e) and 56 (f) days.

It can be seen from figure 3.6 that the coating surface morphologies shows good uniformity, smooth, homogeneity with cracks and holes. All films shows island-like

structures of TiO_2 nanoparticles. When the aging day increased from 1 day to 28 days, larger island-like structures decreased and holes became larger. Also, exhibited a more homogeneous distribution. At film aged 56 days, the larger and non-uniform structure with larger holes seen. The particles of SGDC films are about in spherical form, in aggrement with previous work [103,120-123]. The Figure 3.8 shows the avarage grain size of the TiO_2 nanoparticles for differend aged days. The avarage grain sizes values were calculated 292 nm, 346 nm, 376 nm, 340 nm, 481 nm and 476 nm for 1, 7, 14, 21, 28 and 56 aging day, respectively.

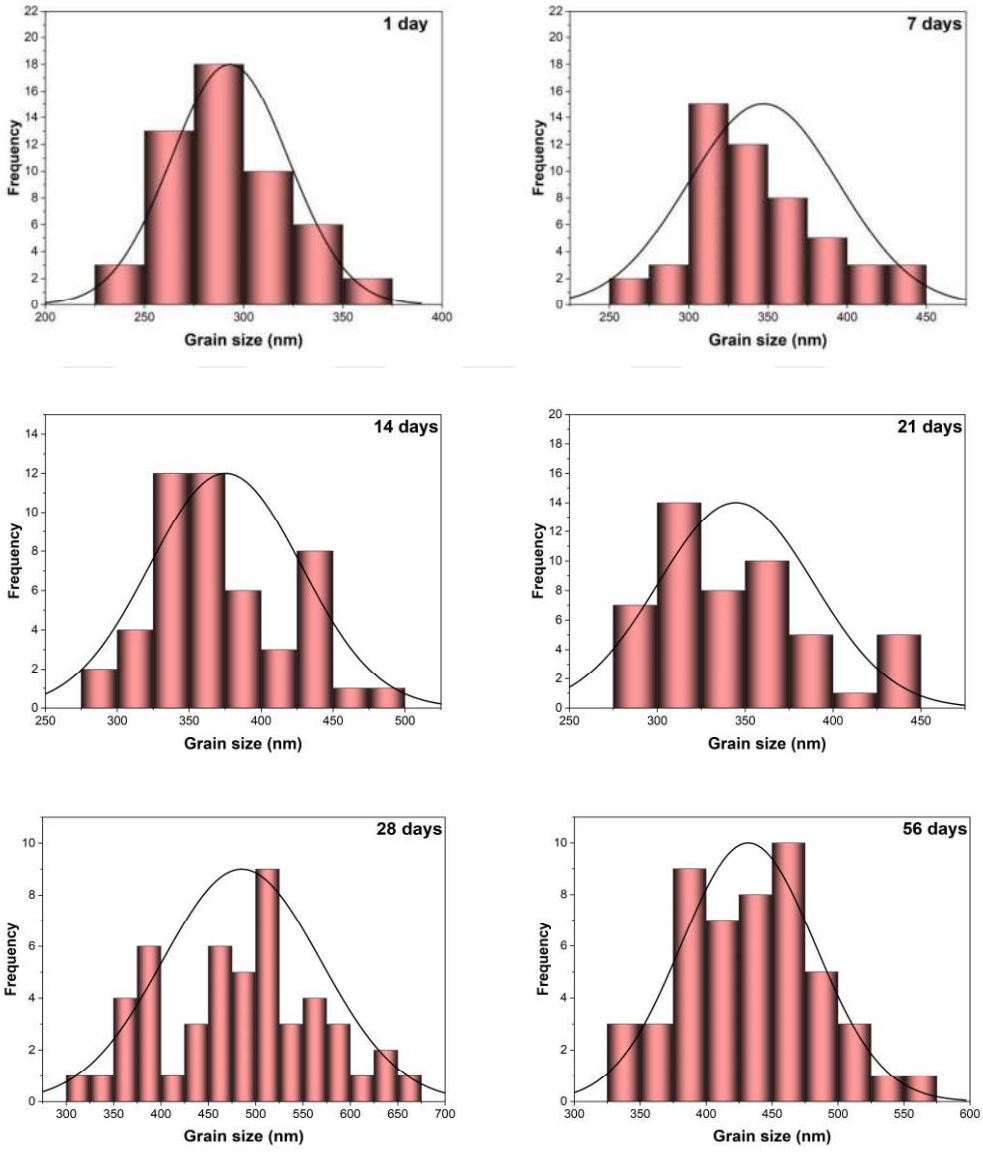

Figure 3.8 Histogram showing the particle size distribution pattern for the corresponding SEM images of SGDC TiO_2 thin films for different aged days.

3.2.3 Number of Layers Effect on SGDC TiO_2 Thin Films

The SEM images at 1000x and 5000x magnification for SGSC TiO_2 thin films for different number of layers for 56 days aged with 3 layers are given Figure 3.9

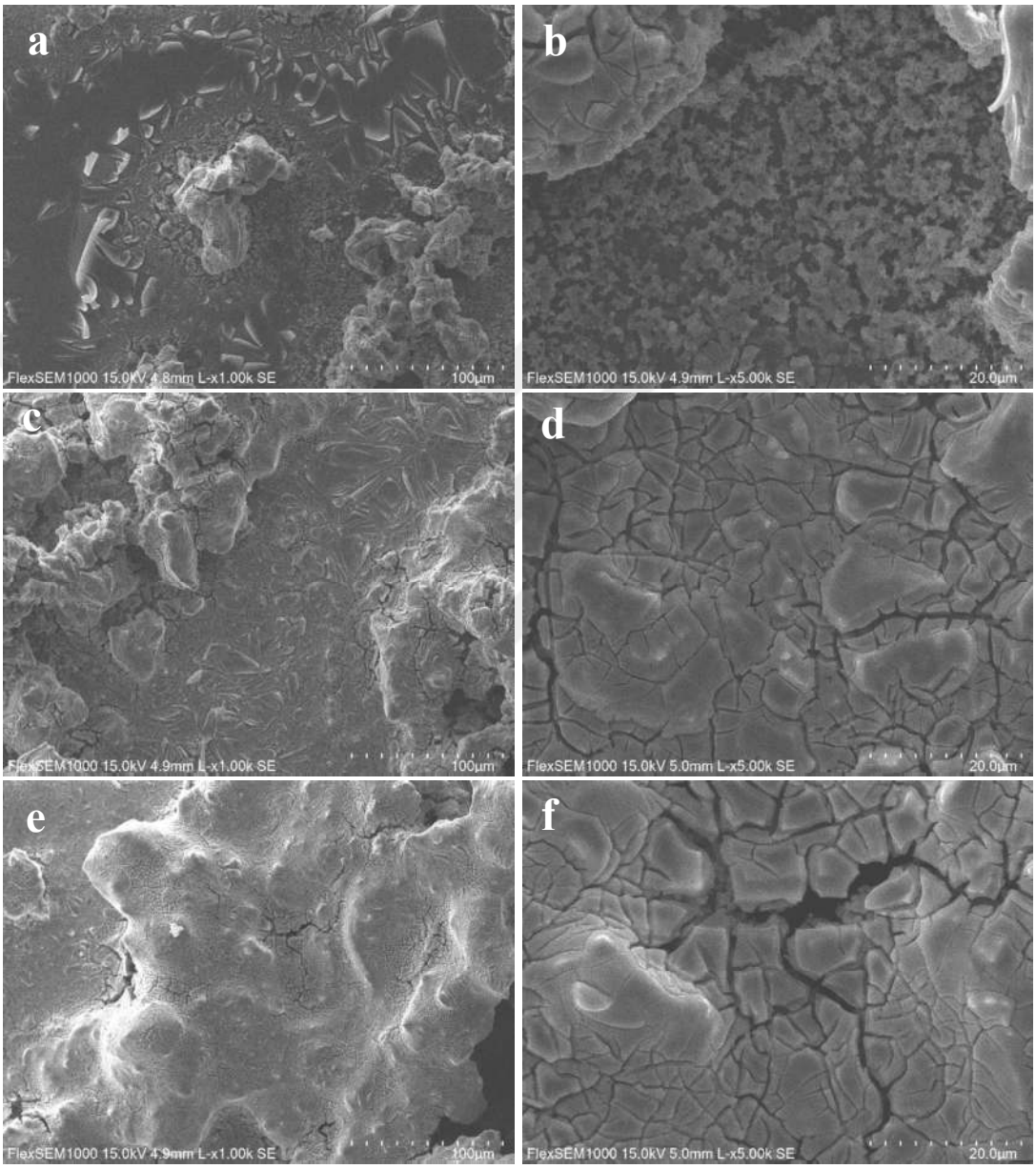

Figure 3.9 The SEM images (1kx and 5kx) of SGSC TiO_2 thin films for 3 (a, b), 5 (c, d) and 10 (e, f) layers for aged 56 days.

The cracks and holes observed. It was observed that with the increase of the number of layers, the cracks increase due to the drying process [124]. It can be seen that an obvious agglomeration phenomena exist. Various factors such as capillary absorption,

solid bridge, Van der Waals and hydrogen bonding can cause agglomeration formation [125].

3.2.4 Dipping Time Effect on SGDC TiO_2 Thin Films

The SEM images at 1000x and 5000x magnification for SGDC TiO_2 thin films for different dipping time for 56 days aged are given Figure 3.10.

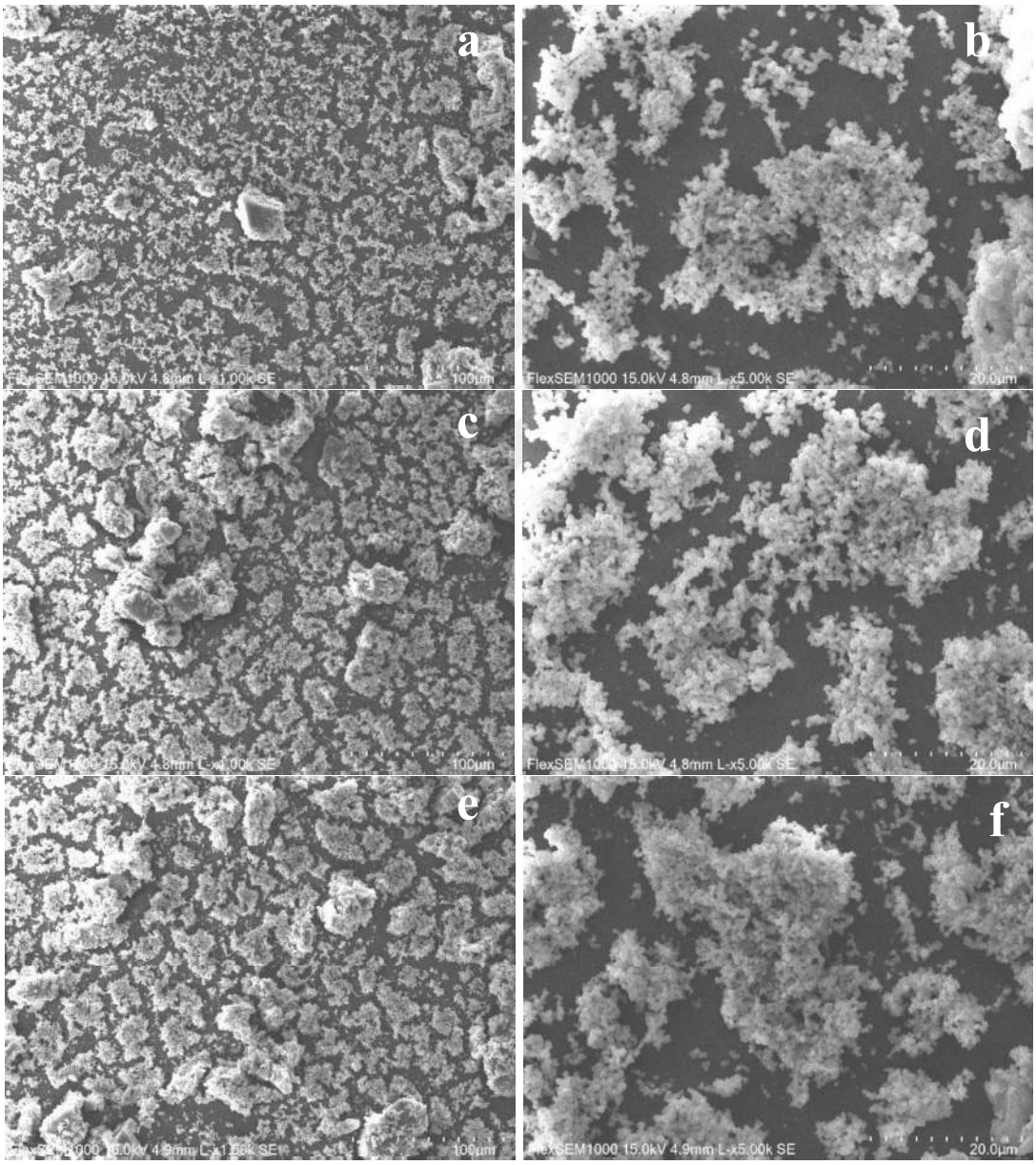

Figure 3.10 The SEM images (1kx and 5kx) of SGDC TiO2 thin films for 5 (a, b), 10 (c, d) and 20 (e, f) seconds dipping time for aged 56 days.

With the increasing dipping time, island-like structres were increased. And agglomeration increasing observed. Brinker and Scherer reported that the small particles inclined to agglomerate due to the high surface energy [45].

3.2.5 Annealing Effect on SGSC TiO_2 Thin Films

SEM images at 1000x and 10000x magnification of the SGSC TiO_2 thin films grown on the glass substrate for as-grown, and annealed at 300 ^{0}C, 400 ^{0}C, 500 ^{0}C, 600 ^{0}C and 700 ^{0}C with 3 layers are given in Figure 3.11 and Figure 3.12 respectively.

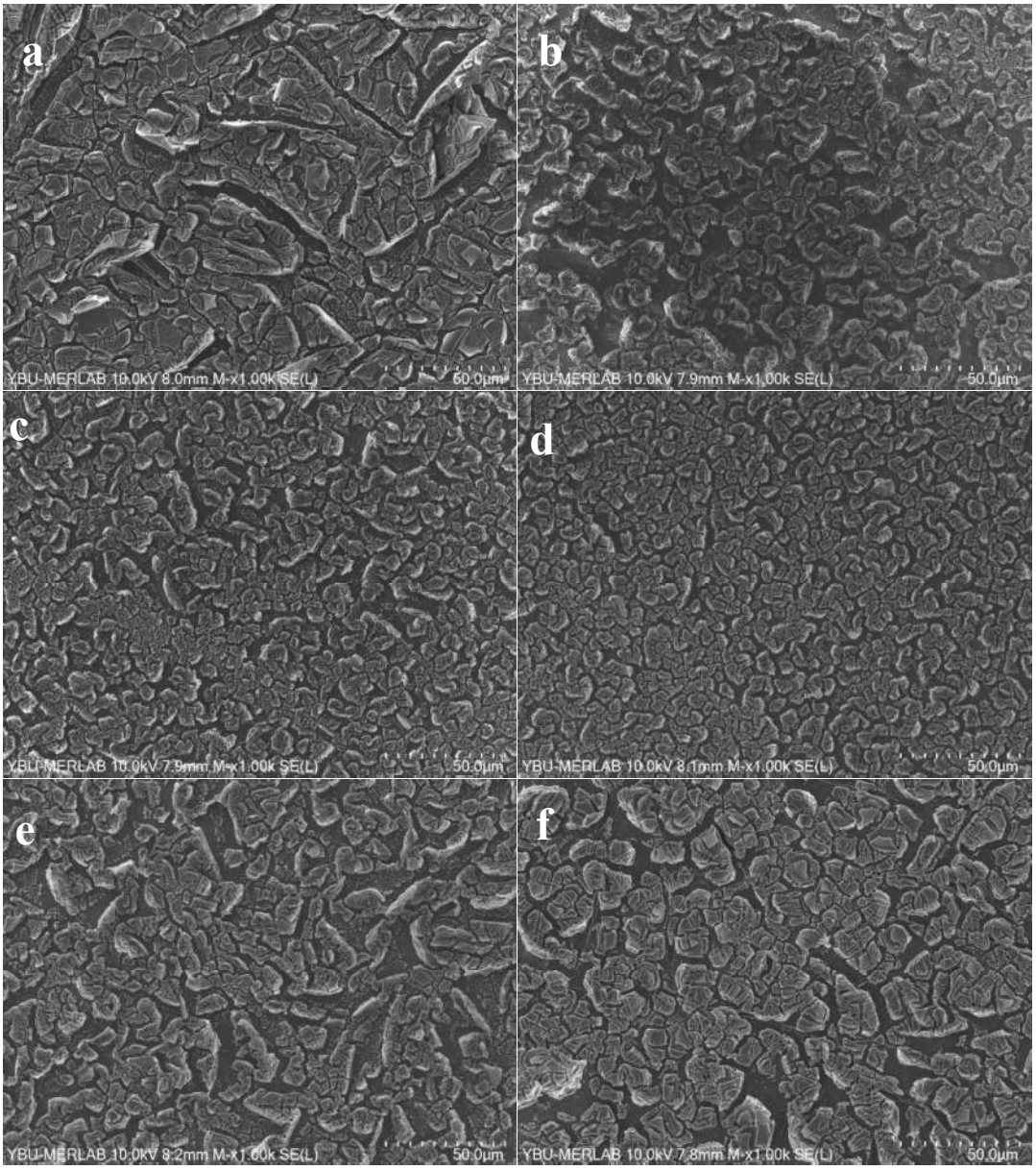

Figure 3.11 The SEM images (1kx) of SGSC TiO_2 films for as-grown (a), annealed at 300 ^{0}C (b), 400 ^{0}C (c), 500 ^{0}C (d), 600 ^{0}C (e) and 700 ^{0}C (f).

When annealing temperature increasing up to 500 ^{0}C, the uniformity, particle distribution and smoothess were increased but above 500 ^{0}C dramatically decreased. According to the SEM images, it can be said that the TiO_2 particles more homogeneously covered at 500 ^{0}C annealing temperature.

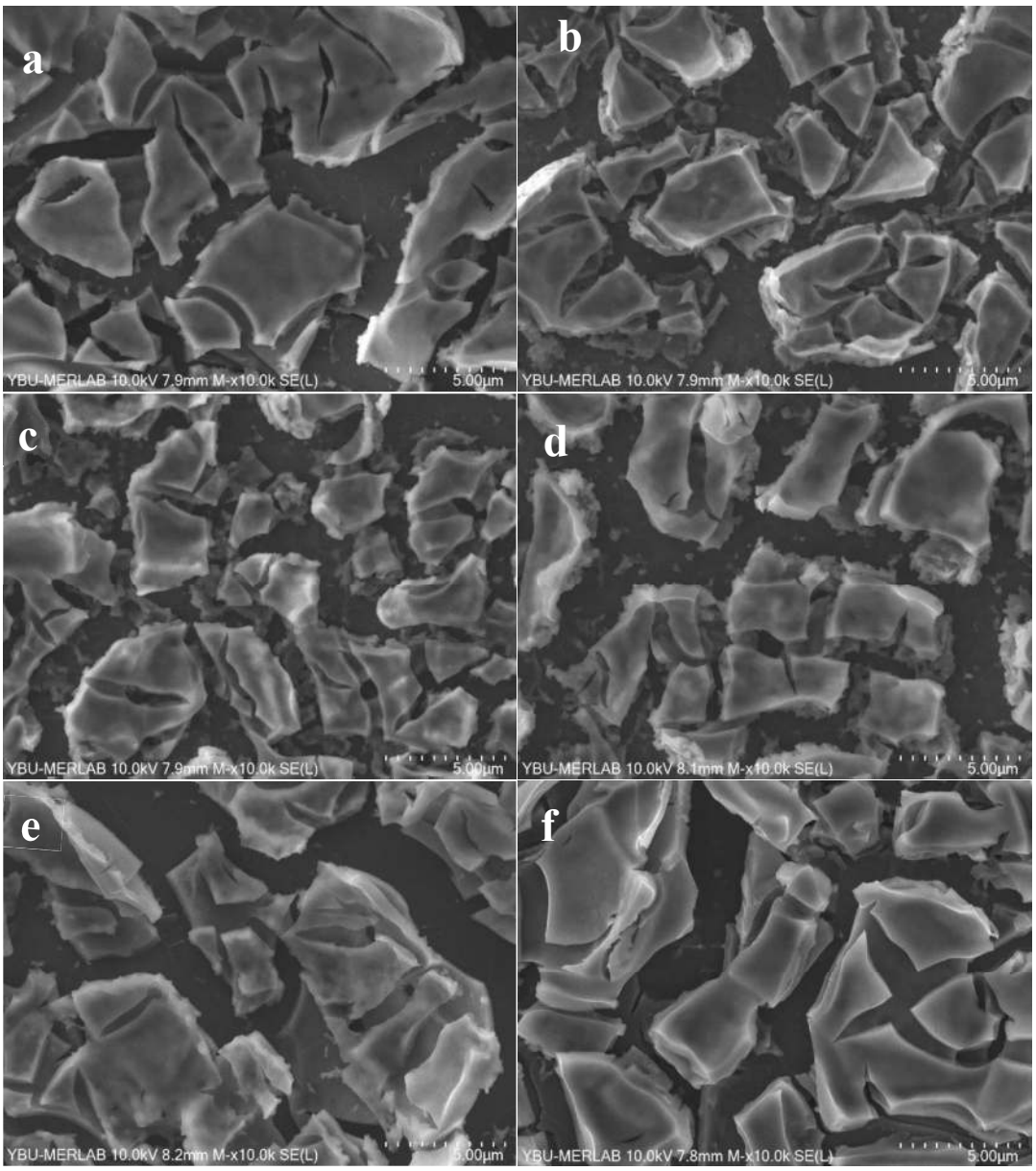

Figure 3.12 The SEM images (10kx) of SGSC TiO_2 films for as-grown (a), annealed at 300 ^{0}C (b), 400 ^{0}C (c), 500 ^{0}C (d), 600 ^{0}C (e) and 700 ^{0}C (f).

3.2.6 Annealing Effect on SGDC TiO_2 Thin Films

Figure 3.13 and Figure 3.14 shows the SEM images at magnification 2500x and 20000x magnification of SGDC TiO_2 thin films for different annealing temperature with 10 seconds dipping time. The as-grown films shows island-like structure. When the SGDC films annealed at from 300 ^{0}C to 700 ^{0}C, island-like structres grew by merging and holes on the surface increased. All the SGDC films were composed of spherical particles.

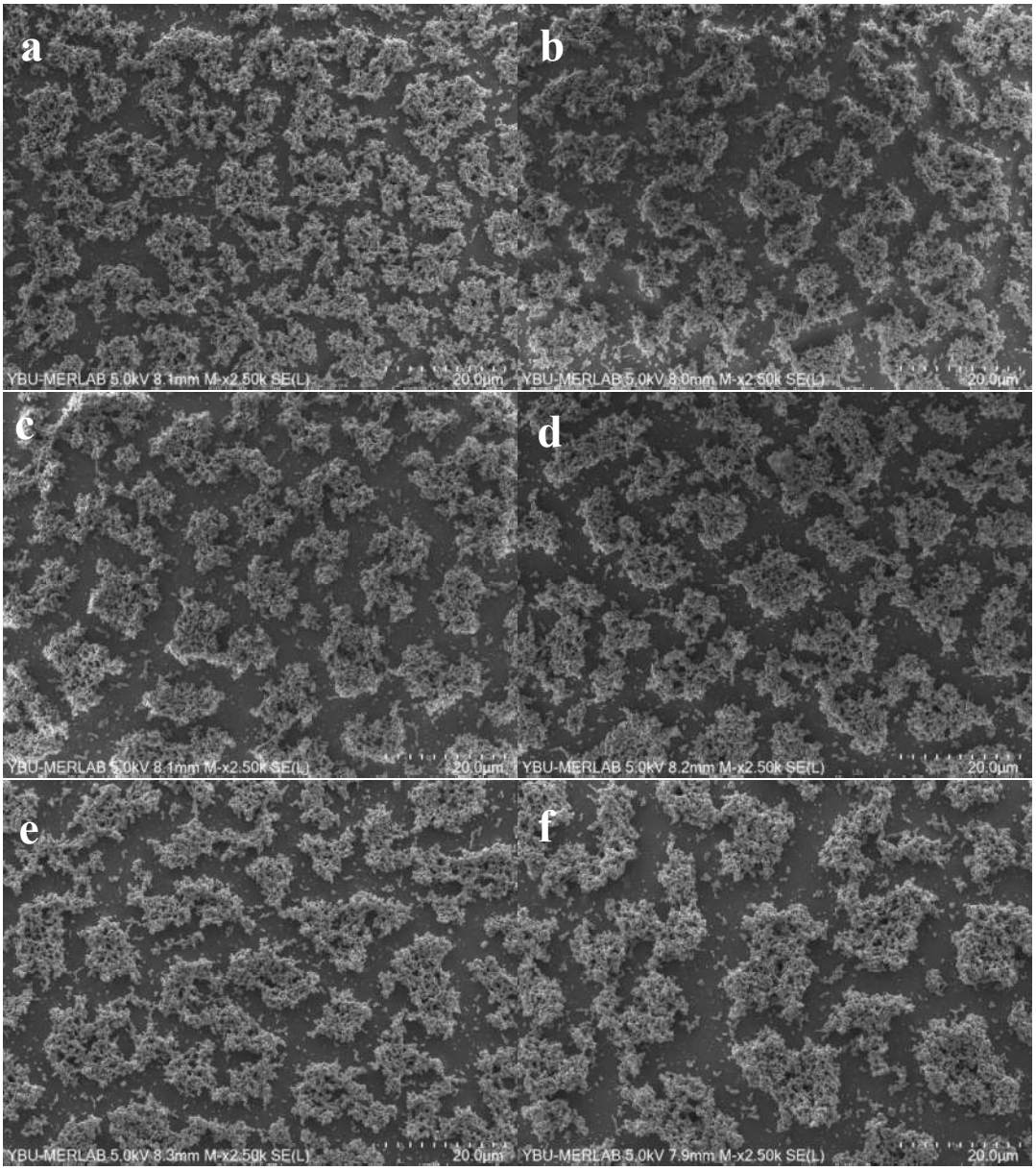

Figure 3.13 The SEM images (2.5kx) of SGDC TiO_2 thin films for as-grown (a), annealed at 300 ^{0}C (b), 400 ^{0}C (c), 500 ^{0}C (d), 600 ^{0}C (e) and 700 ^{0}C (f).

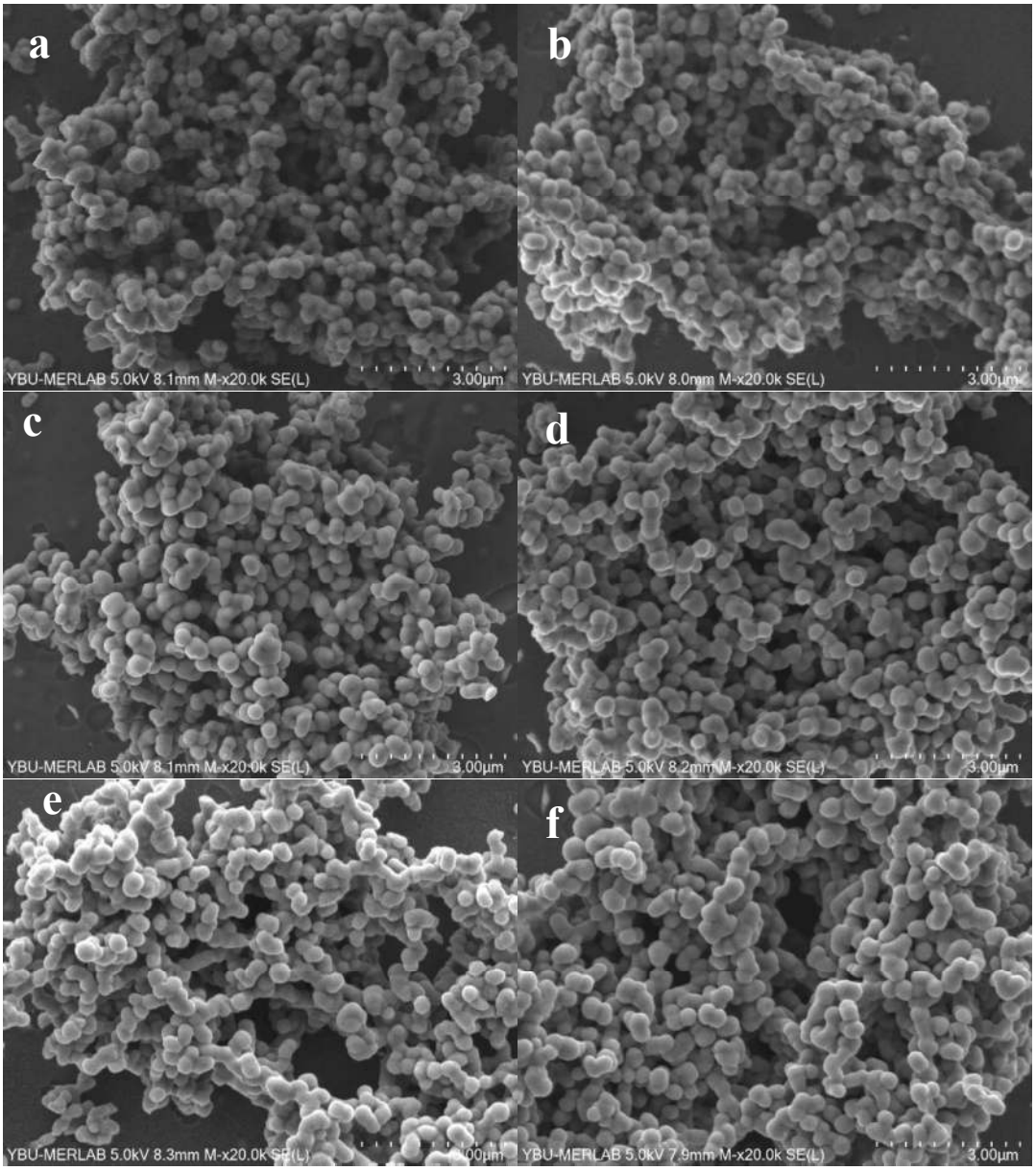

Figure 3.14 The SEM images (20kx) of SGDC TiO_2 thin films for as-grown (a), annealed at 300 ^{0}C (b), 400 ^{0}C (c), 500 ^{0}C (d), 600 ^{0}C (e) and 700 ^{0}C (f).

In Figure 3.15, structures of spherical particles of SGDC TiO_2 thin films annealed at 700 ^{0}C with 10 seconds dipping time are clearly seen at larger magnification (100kx). Similar structures have been seen in previous works [126]. When the interlocking spherical structres are analyzed, it is seen that they are formed by the merging of smaller particles.

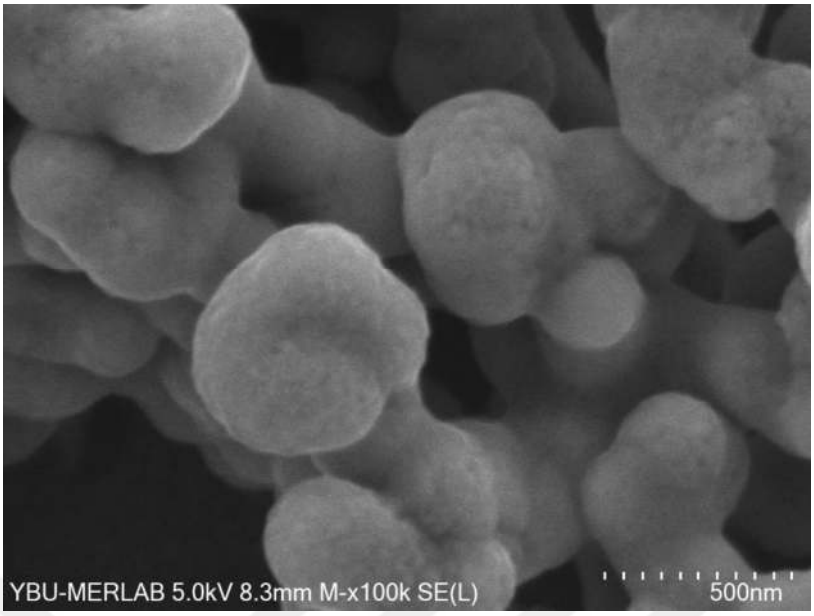

Figure 3.15 The SEM images (100kx) of SGDC TiO_2 thin films annealed at 700 ^{0}C.

Histogram showing the particle size distribution pattern for the corresponding SEM images of SGDC TiO_2 thin films as-grown and annealed at 300 ^{0}C, 400 ^{0}C, 500 ^{0}C, 600 ^{0}C and 700 ^{0}C are given in Figure 3.16. The average grain sizes were calculated as 337 nm, 328 nm, 325 nm, 336 nm, 350 nm and 371 nm, respectively. With increasing annealing temperature, the sturucture transfomed from the amourphous to anantase and the avarage grain size increased.

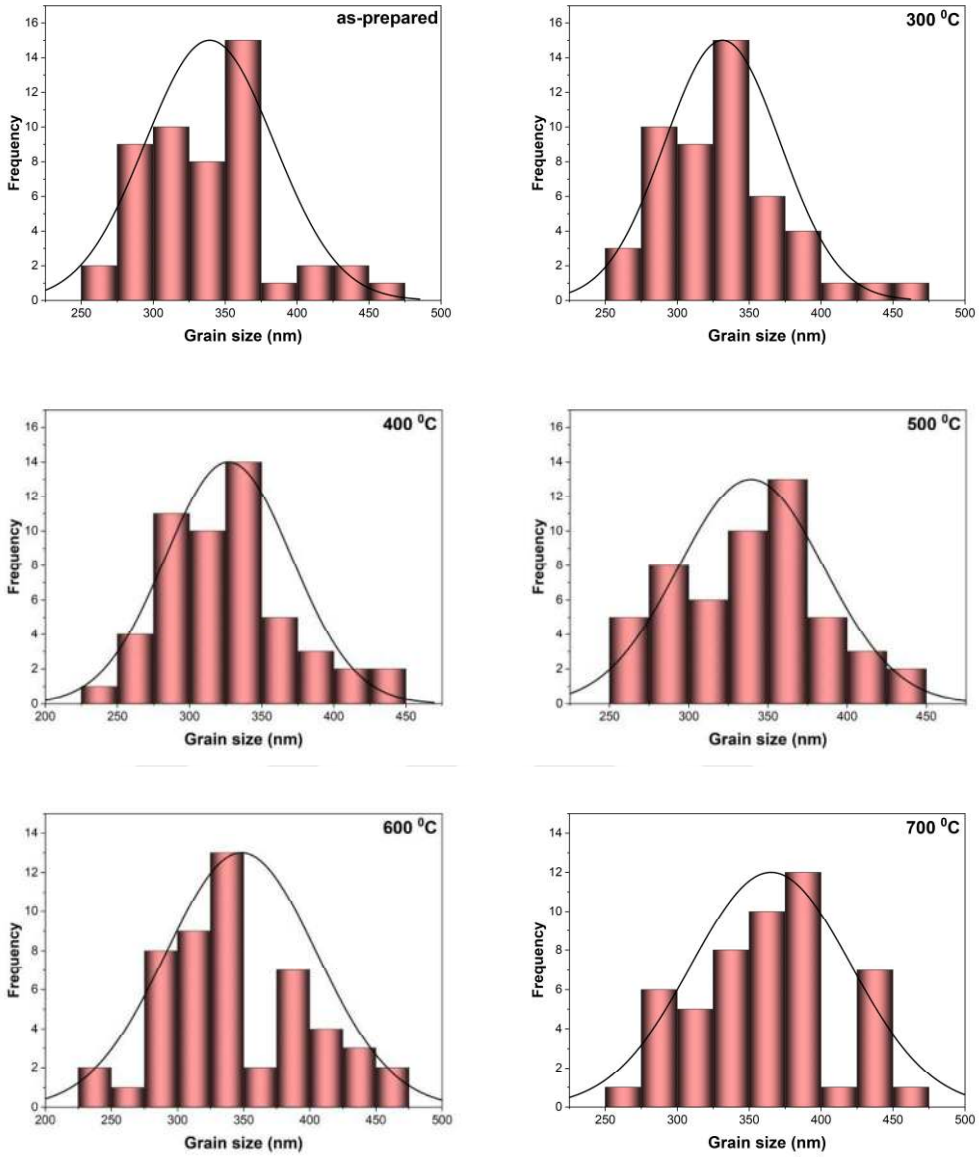

Figure 3.16 Histogram showing the particle size distribution pattern for the corresponding SEM images of SGDC TiO_2 thin films at different annealing temperature.

3.3 EDX Analysis

3.3.1 Annealing Effect on SGSC TiO_2 Thin Films

The Energy-Dispersive X-Ray spectra of SGSC TiO_2 thin films for as-grown and annealed at 300 ^{0}C, 400 ^{0}C, 500 ^{0}C, 600 ^{0}C and 700 ^{0}C are given in the Fig.3.17. EDX spectra of all thin films have mainly exposed the presence of titanium and oxygen atoms and as a result materialization of SGSC TiO_2 films was confirmed [127-129].

The peak at Lα=0.4522 keV, where the electron from M orbital filled in the hole left by the kicked out electron in L orbital and Kα=4.508 keV, where the electron from L orbital filled in the hole in K orbital provided evidence that the Ti elements were present. The peak at Kα=0.5249 keV, where the electron from L orbital filled in the hole in K orbital are provided evidence that the O elements were present. The peaks associated with silicon were due to the glass substrate. Thermal exposure often activates the diffusion of Si from the thin film on glass substrate [130-132].

With the increasing annealing temperature, molecular weight percentage of Ti element was gradually increased from 17.0 % to 41.0 % and molecular weight percentage of O element was gradually decreased from 64.9 % to 42.2 %, in agreement with previous studies [133]. The EDX analysis of thin film annealed at 700 ^{0}C which is highest Ti content are revealed a molecular weight percentage of 41 % for Ti and 42.2 % for O.

3.3.2 Annealing Effect on SGDC TiO_2 Thin Films

The EDX spectra of SGDC TiO_2 thin films glass substrate for as-grown and annealed at 300 ^{0}C, 400 ^{0}C, 500 ^{0}C, 600 ^{0}C and 700 ^{0}C are given in the Fig.3.18. The EDX result showed that the TiO_2 films was primarily composed of titanium and oxygen elements which is proper with the stoichiometric of TiO_2.

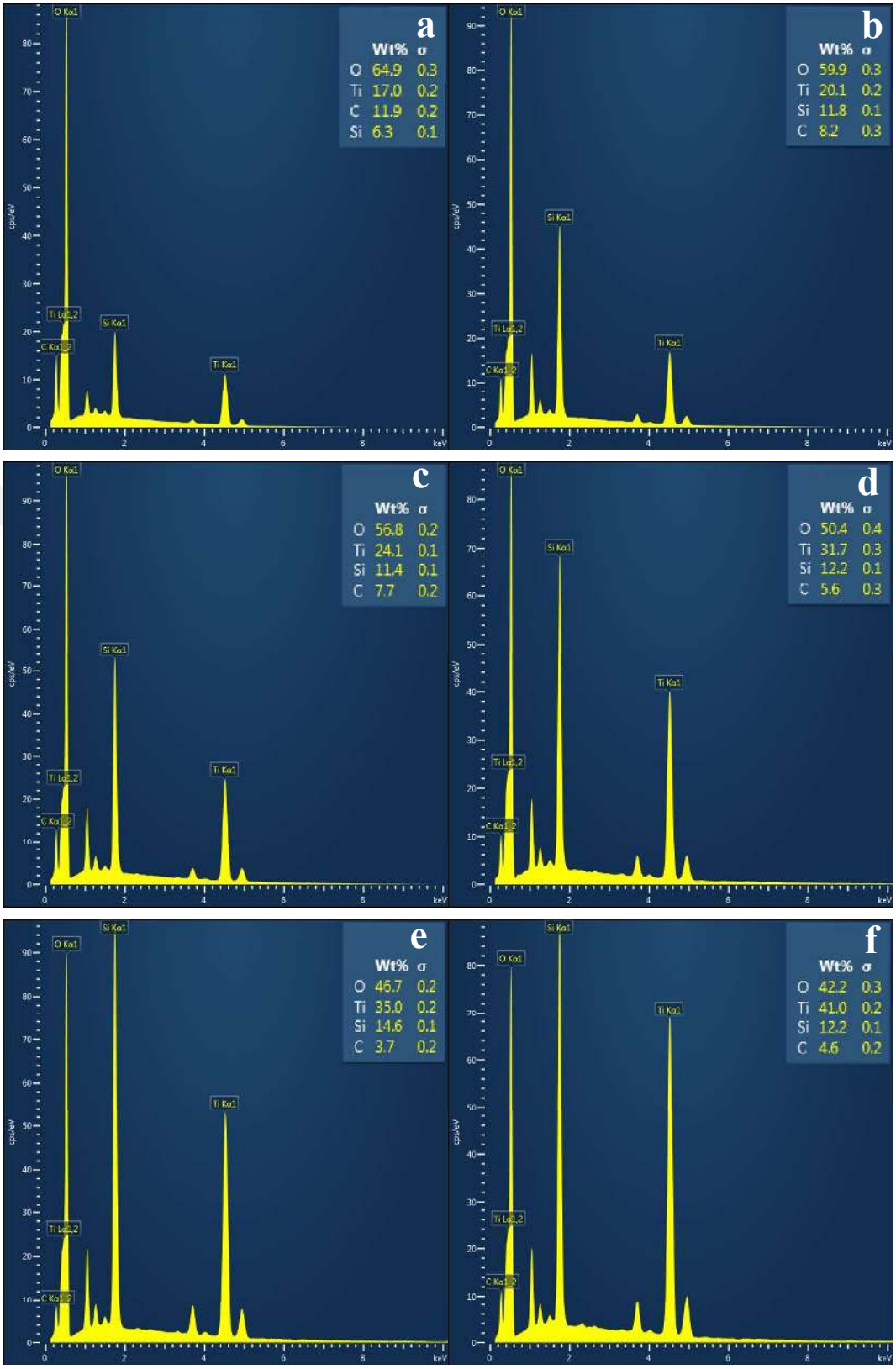

Figure 3.17 The EDX analysis of SGSC TiO_2 thin films for as-grown (a), annealed at 300 ^{0}C (b), 400 ^{0}C (c), 500 ^{0}C (d), 600 ^{0}C (e) and 700 ^{0}C (f).

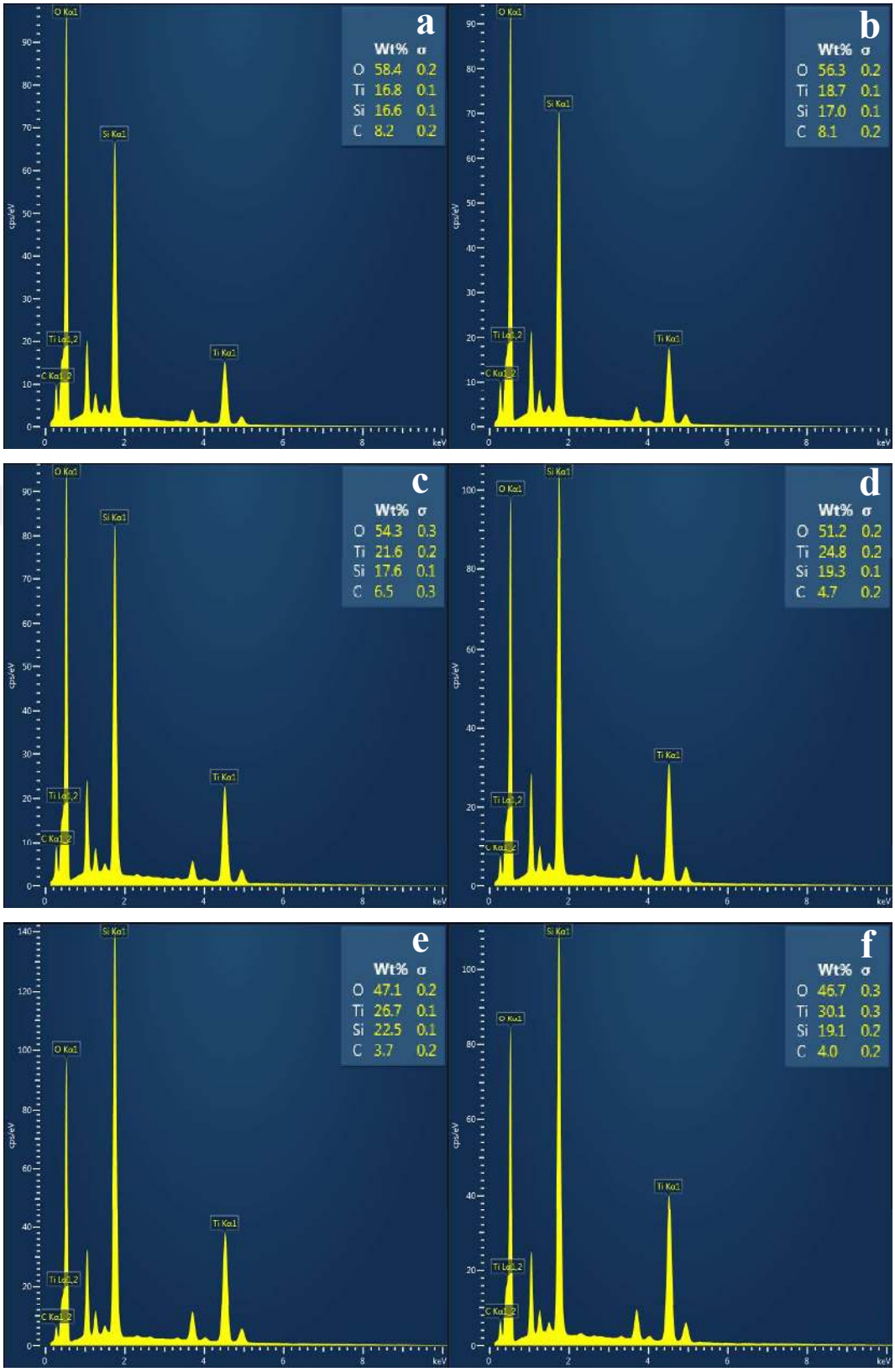

Figure 3.18 The EDX analysis of SGDC TiO_2 thin films for as-grown (a), 300 ^{0}C (b), 400 ^{0}C (c), 500 ^{0}C (d), 600 ^{0}C (e) and 700 ^{0}C (f).

With increasing annealing temperature, molecular weight percentage of Ti element was gradually increased from 16.8 % to 30.1 % and molecular weight percentage of O element was gradually decreased from 58.4 % to 46.7 %. The variation of molecular weight percentage of Ti element for SGSC and SGDC thin films according to the annealing temperature is shown in the Fig.3.19. When the SGSC and SGDC films compared, its observed that SGSC showed a higher increase in the percentage of Ti than SGDC films with increasing annealing temperature.

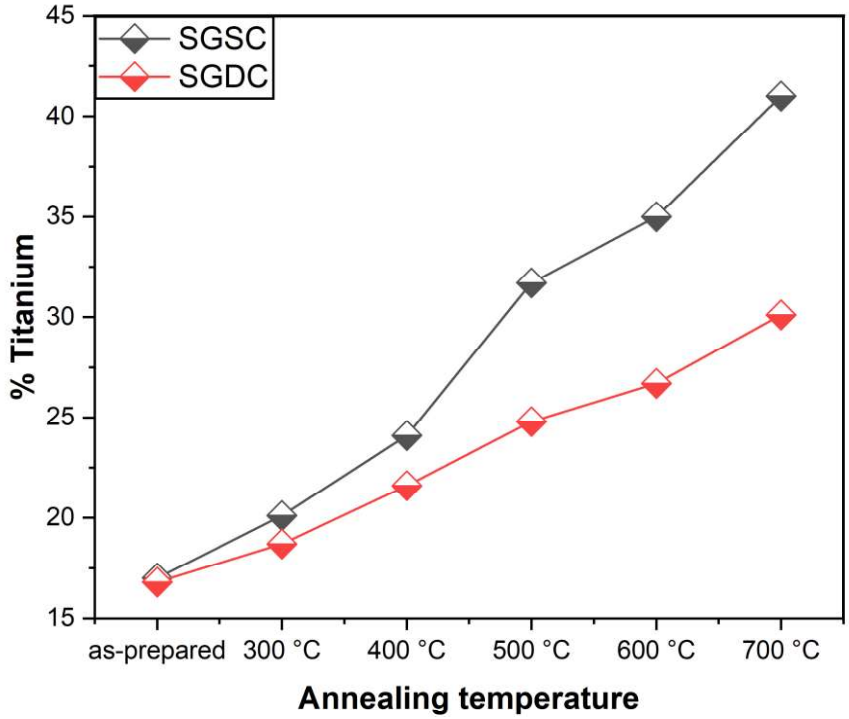

Figure 3.19 Titanium content changing with the annealing temperature.

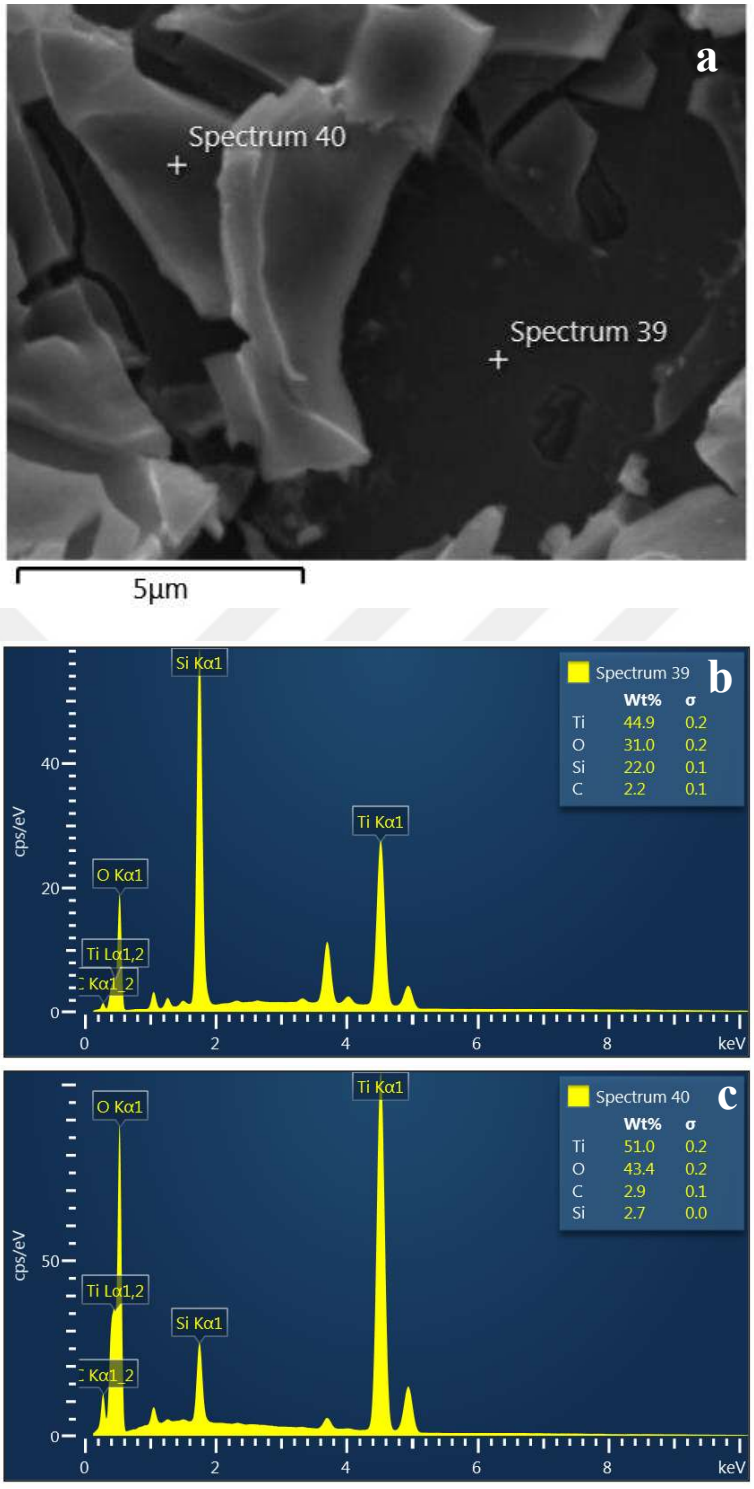

Figure 3.20 (a) SEM images of SGSC TiO_2 thin film annealed at 700 ^{0}C, (b) EDX analysis of spectrum 39 and (c) spectrum 40.

The Fig.3.20 (a) show EDX analysis of the SGSC TiO_2 thin films annealed at 700 ^{0}C. 2 points were marked on the base and on the surface which is spectrum 39 and 40,

respectively. The EDX analysis of these point are given in Fig.3.20 (b) and (c). It can be seen that molecular weight percentage for point at the base (spectrum 39) are 44.9 % for Ti, 31.0 % for O and 22.0 % for Si. Whereas, molecular weight percentage for point at the surface (spectrum 40) are 51.0 % for Ti, 43.4 % for O and 2.7 % for Si. When the point at the base and surface compared, it was observed that increase in Ti and O content and a dramatically decrease in the Si content due to the distance from the glass substrate.

3.4 Absorbance and Band-Gap Analysis

3.4.1 Aging Effect on SGSC TiO_2 Thin Films

The optical absorption spectra of the SGSC TiO_2 thin films for 1, 7, 14, 21, 28 and 56 days aged with 3 layers are given in the Fig.3.21.

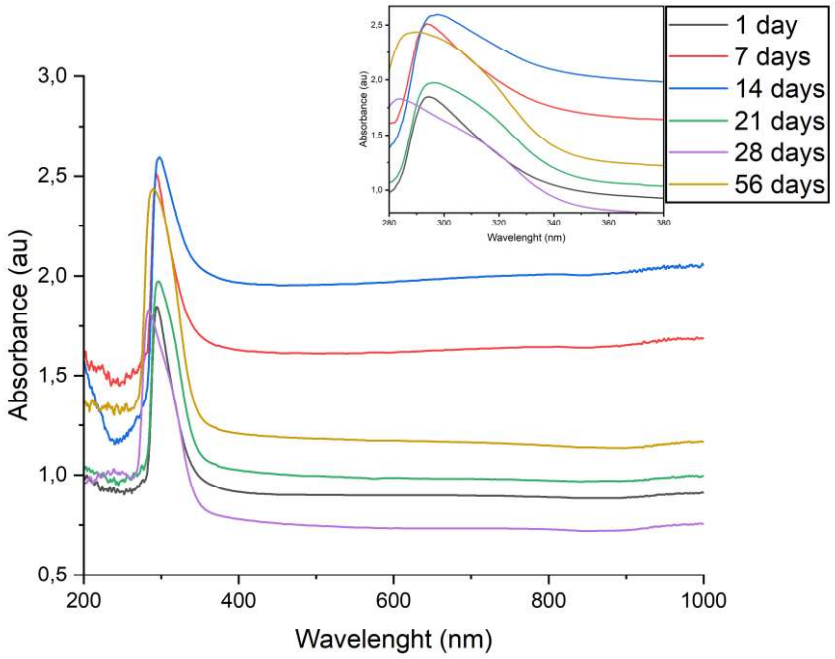

Figure 3.21 The optical absorption spectra of the SGSC TiO_2 films for different aging day with 3 layers.

The absorption peaks for different aging days was exhibited strong absorption below 400 nm. Also, it was observed that the absorption spectra for aged 7 and 14 days have higher visible light absorption capacity. Maximum absorption is observed at around

290 nm. The spectra of all thin films consist of a sharp absorption threshold around 410 nm. Similar result was indicated in the other studies [134-136]. Which is attributed to the electron transition O2p → Ti3d from the valance band (VB) to the conduction band (CB) [137]. It was observed that absorption treshold of SGSC TiO_2 thin films are shifted toward different wavelenght with increasing aging days, in agreement with previous work [138].

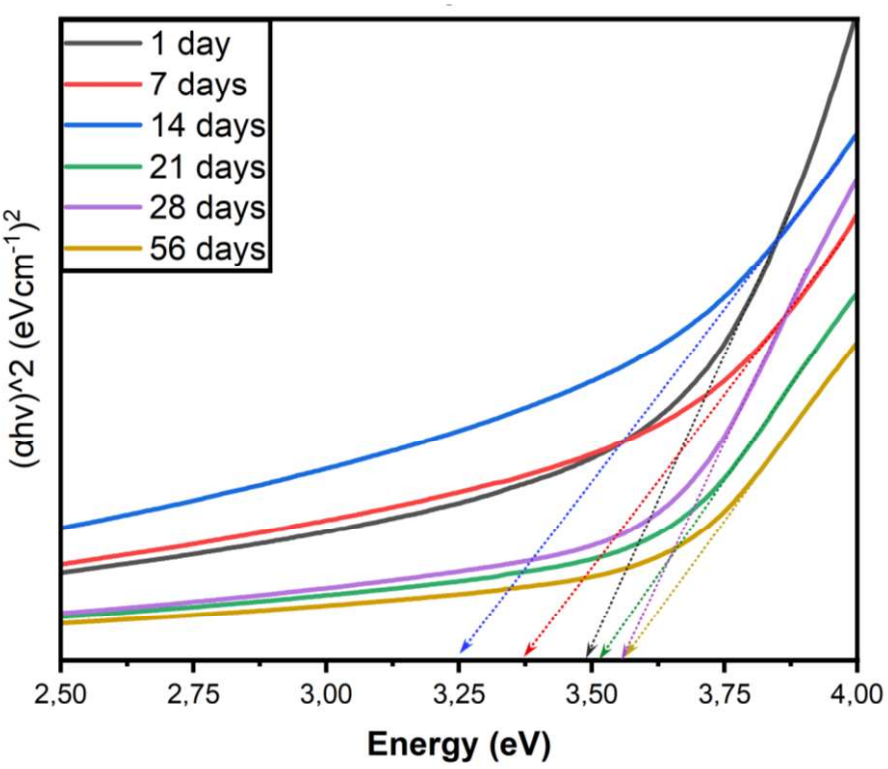

Figure 3.22 Plot of (αhv)^2 versus energy for SGSC TiO_2 thin films for different aging time for 3 layers.

It was reported by the authors of [139] that the direct transition was more fovurable in anatase TiO_2 nanoparticles. The plot of $(\alpha hv)^2$ versus energy (hv) are given in Figure 3.22, to determine the bandgap values of SGSC TiO_2 thin films for different aging time (1, 7, 14, 21, 28 and 56 days) with 3 layers. The obtained bandgap value are given Table 3.5. The bandgap values are varied between 3.22 eV and 3.56 eV [140-142]. It can be seen that when the aging day increased from 1 day to 14 days, bandgap value significantly decreased, corresponding to absorption treshold shifted towards higher

wavelenghts. After that increased with increasing aging day. It is seen in the previous studies that the bandgap value changes with the effect of aging time [143].

3.4.2 Aging Effect on SGDC TiO_2 Thin Films

The optical absorption spectra of the SGDC TiO_2 thin films for 1, 7, 14, 21, 28 and 56 days aged with 10 seconds dipping time are given in the Fig. 3.23.

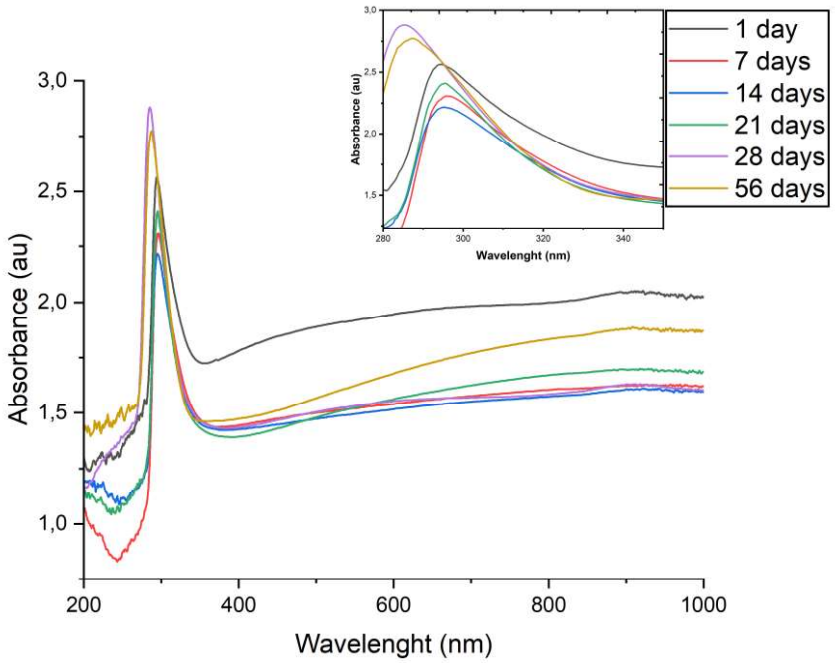

Figure 3.23 The optical absorption spectra of SGDC TiO_2 thin films for different aging day with 10 second dipping time.

When the aging day increased from 1 day to 56 days, absorption treshold shifted towards the shorter wavelenghts. Maximum absorption are seen for aged between 1 and 21 days are at around 295 nm. After that for aged 28 and 56 days decreased at around 285 nm. Similar results at same aging day was also reached at SGSC TiO_2 thin films. The bandgap values of the SGDC TiO_2 thin films for aged 1, 7, 14, 21, 28 and 56 days were calculated by Tauc's relation $(\alpha hv)^2$ - hv graph are shown in Fig. 3.24. The obtained bandgap values are given in Table 3.5. It can be seen that with increasing aging day from 1 day to 56 days, the bandgap values gradually increased from 3.32 eV to 3.57 eV (seen in Figure 3.25).

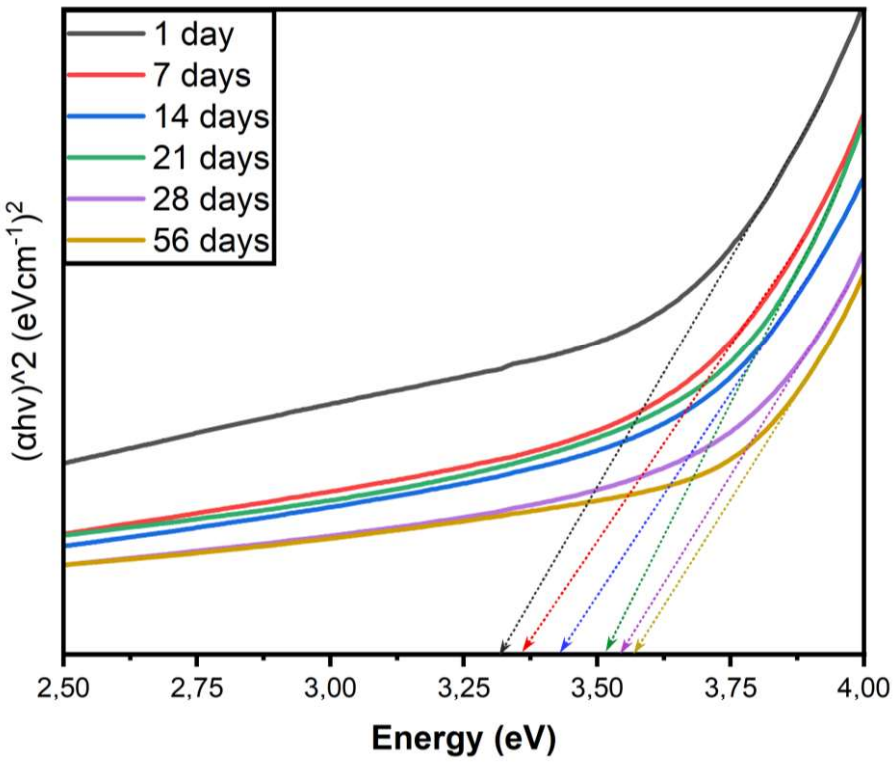

Figure 3.24 Plot of (αhv)^2 versus energy for SGDC TiO_2 thin films for different aging time for 10 seconds dipping time.

Table 3.5 Band-gap value of SGSC and SGDC TiO_2 thin films for different aging time for 3 layers and 10 second dipping time.

Band-gap	**1 day**	**7 days**	**14 days**	**21 days**	**28 days**	**56 days**
SGSC	3.48 eV	3.36 eV	3.22 eV	3.51 eV	3.55 eV	3.56 eV
SGDC	3.32 eV	3.36 eV	3.43 eV	3.52 eV	3.55 eV	3.57 eV

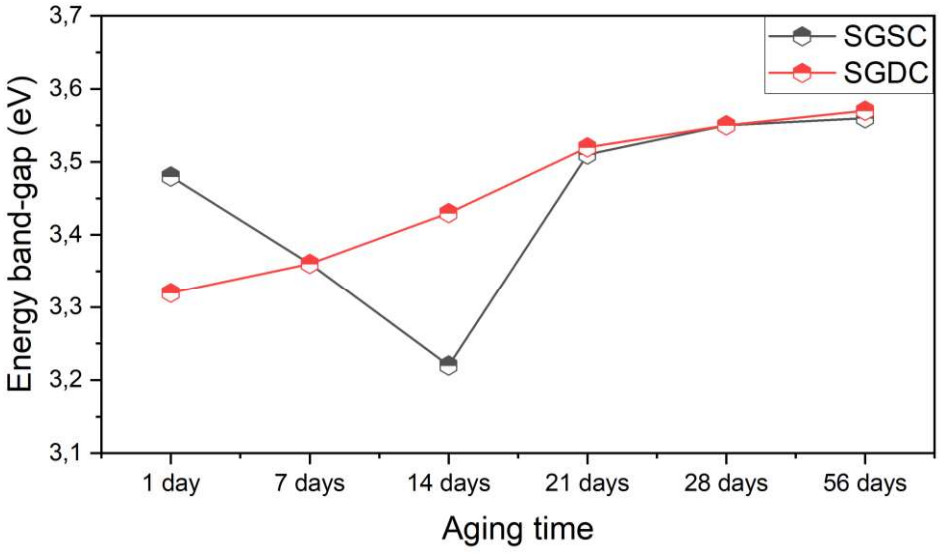

Figure 3.25 Band-gap changing with the aging time for SGSC and SGDC TiO_2 thin films.

The fact that the films are nanocrystalline nature may explain why we observed a higher bandgap value in this work [144]. It can said that this phenomenon is explained by variations in phase transformation and film composition [145]. The expansion of the bandgap can be explained by well known Burstein-Moss (BM) effect [146]. Transitions can only at higher energy levels in the CB because of the lowest states in the CB are blocked. This phenomenon frequently seen in degenerated semiconductor. Therefore, it is interpreted that blue shift in the energy bandgap shows a carrier density increased [147].

3.4.3 Number of Layers Effect on SGSC TiO_2 Thin Films

The absorption spectra of the SGSC TiO_2 thin films for 3, 5 and 10 layers with different aging days is given in Fig. 3.26.

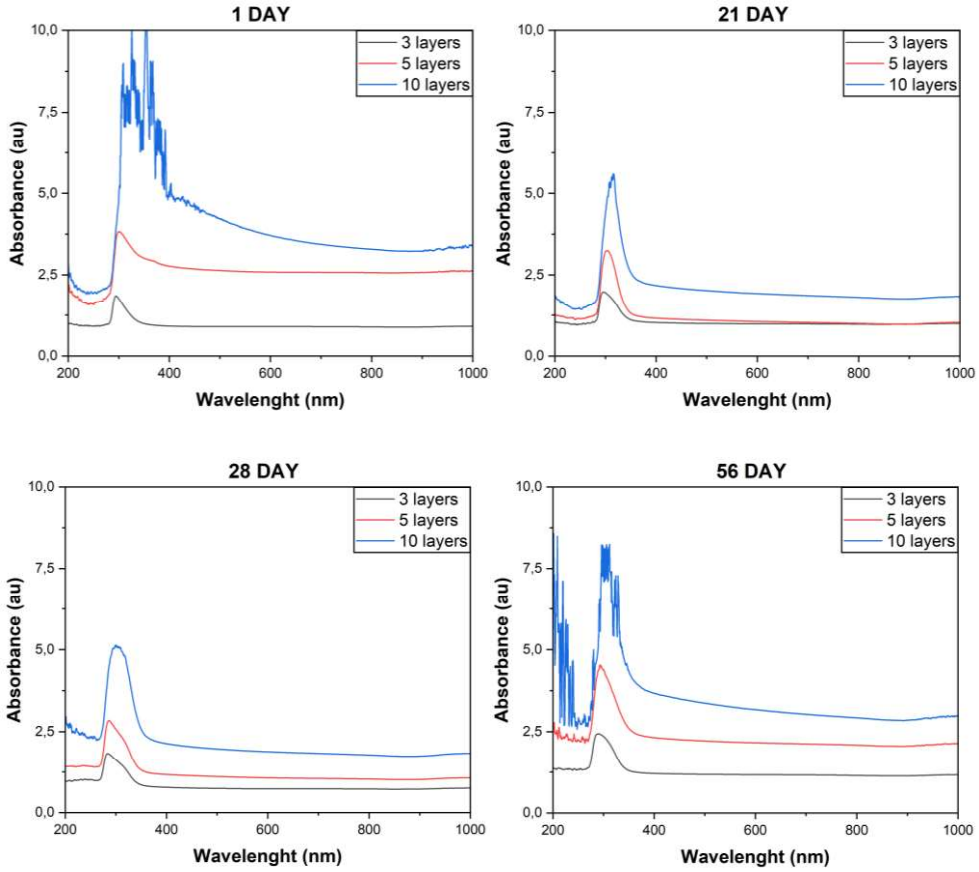

Figure 3.26 The optical absorption spectra of the SGSC TiO_2 thin films for aged 1, 21,28 and 56 days for 3, 5 and 10 layers.

The noise seen in films for 10 layers was not observed for aged 21 and 28 days thin films. The absorption peaks shifted towards higher wavelenght with increasing number of layer. According to reports, large agglomeration of TiO_2 particles scatter less light than evenly dispersed particles, and TiO_2's light scattering performance is strongly dependent on particle size [148]. With increasing number of layer, larger agglomeration are seen in the SEM images, in agreement with these results. The plot of $(\alpha hv)^2$ versus energy of SGSC TiO_2 thin films for 3, 5 and 10 layers for different aging day are shown in the Fig. 3.27. The obtained bandgap values are given in the Table 3.6. With increasing number of layer, the bandgap value decreased. Similar results have been observed in previous studies [21,149].

The increase in grain size of TiO_2 layers cause a decreasing in the bandgap. Additionally, defect levels in the TiO_2 forbidden band were caused the formation of several subbands. So, the bandgap energy value is decreased [21,150-152].

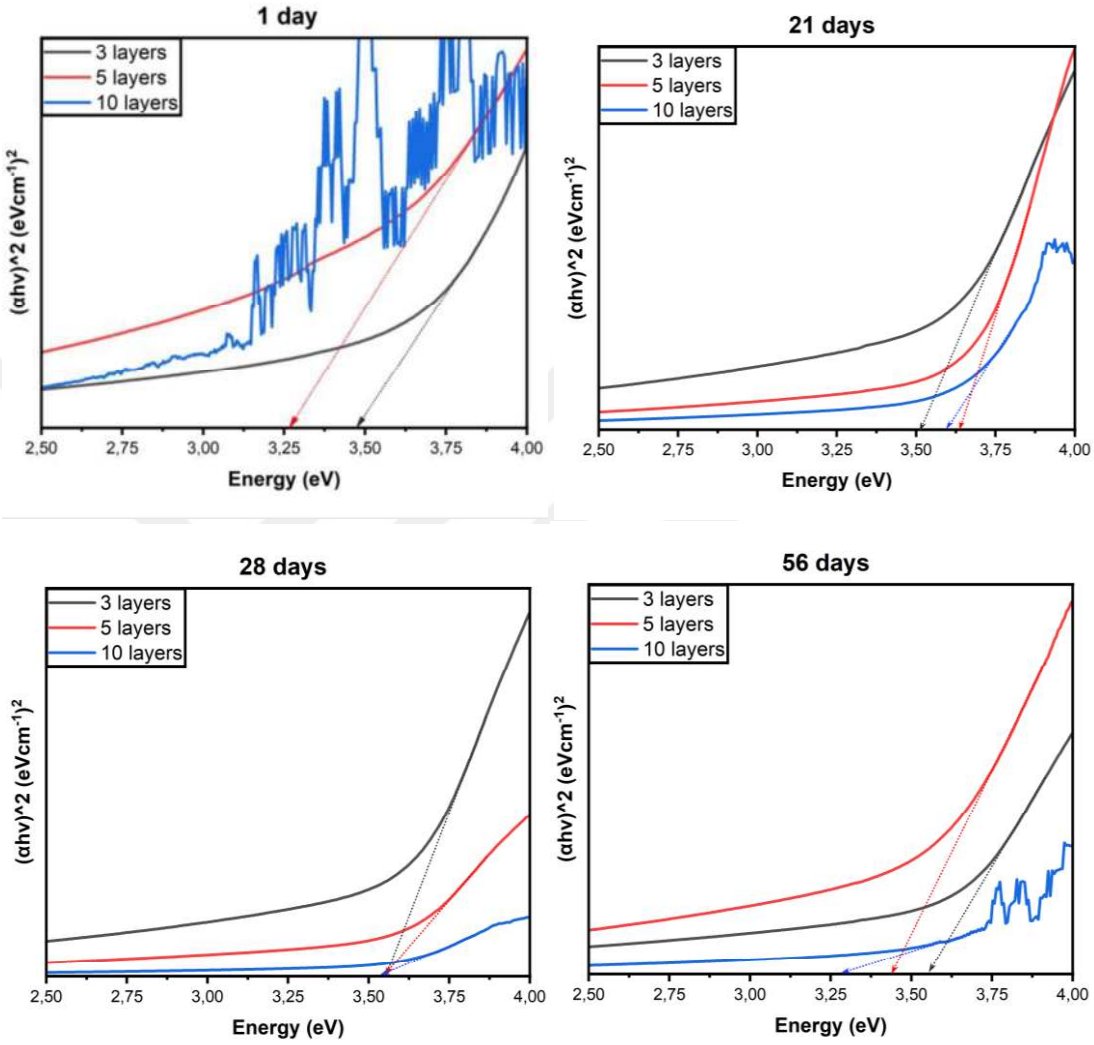

Figure 3.27 Plot of (αhv)^2 versus energy for SGSC TiO_2 thin films for different aging time for 3, 5 and 10 layers.

3.4.4 Dipping Time Effect on SGDC TiO_2 Thin Films

The Figure 3.28 show the absorption spectra of the SGDC TiO_2 thin films for 5, 10 and 20 seconds dipping time with different aging days. It was not observed significant change with increasing dipping time. The plot of $(\alpha hv)^2$ versus energy are shown in the Figure 3.29. The determined bandgap values are given in the Table 3.6.

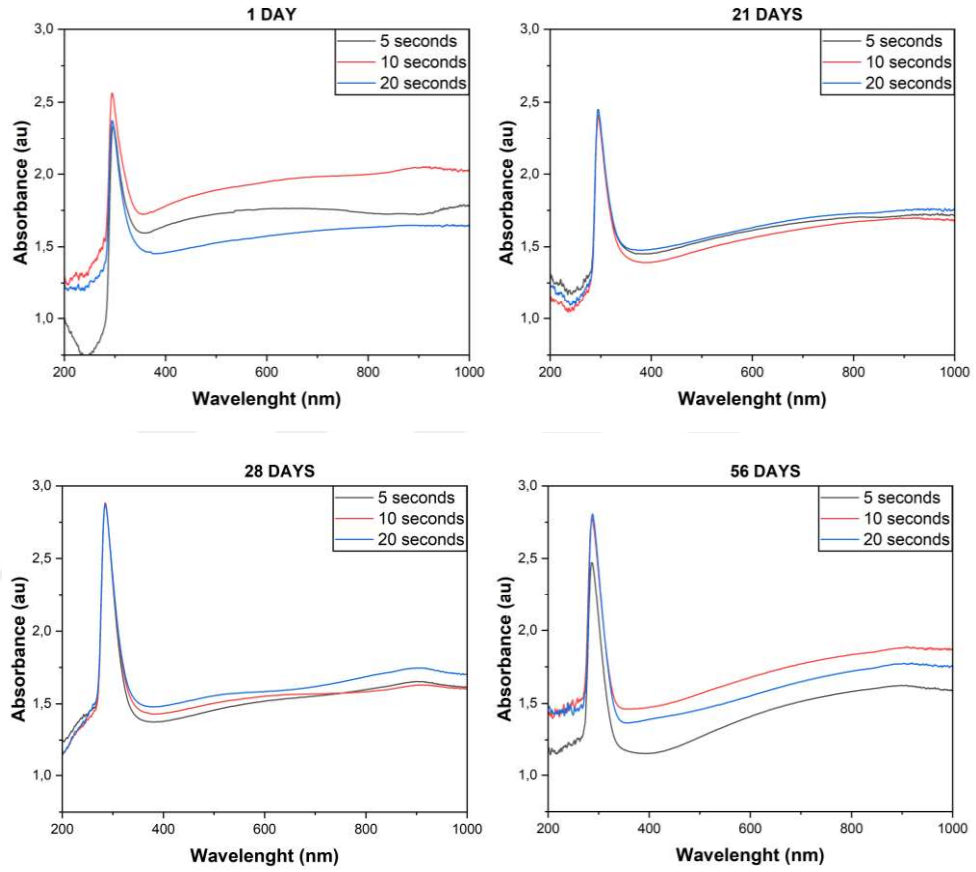

Figure 3.28 The optical absorption spectra of SGDC TiO_2 thin films for aged 1, 21, 28 and 56 days for 5, 10 and 20 seconds dipping time.

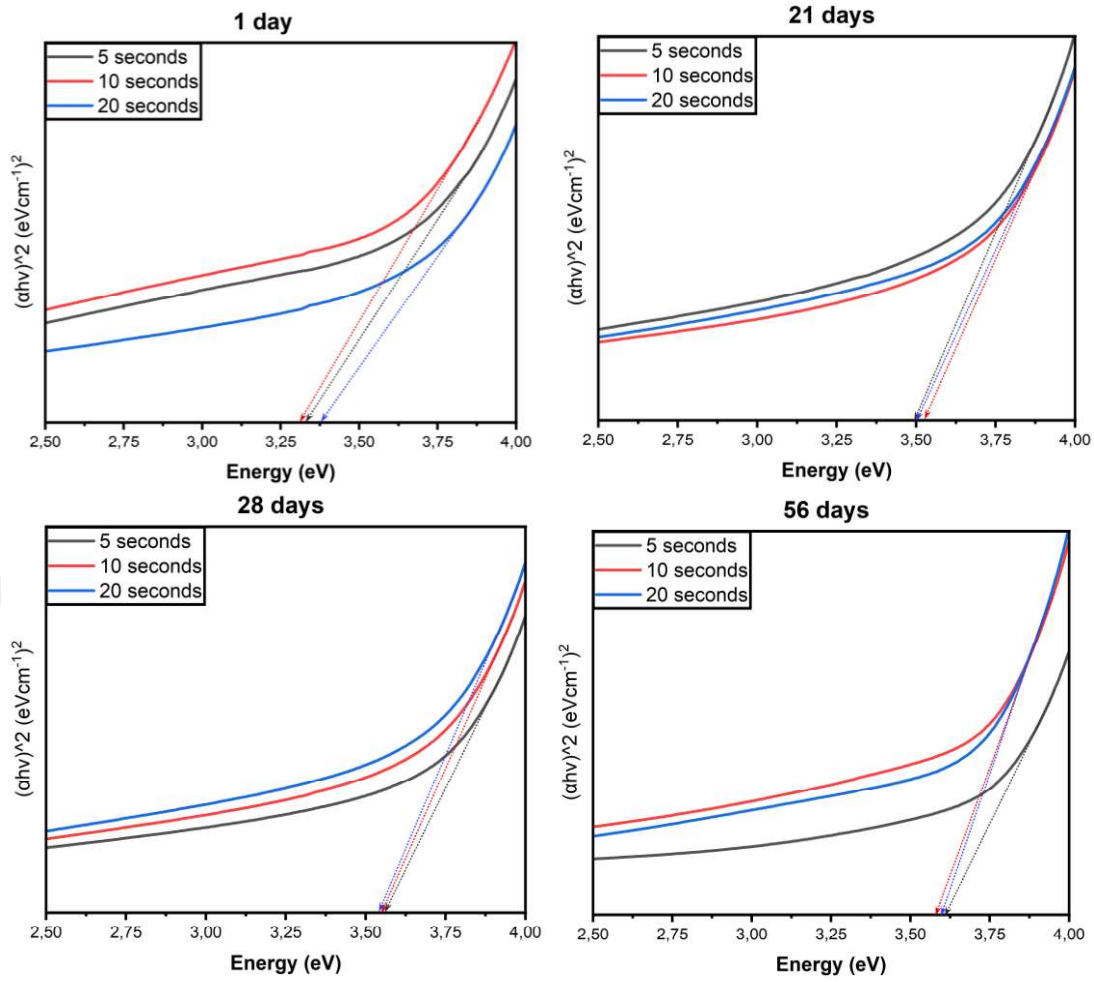

Figure 3.29 Plot of (αhv)^2 versus energy for SGDC TiO_2 thin films for different aging time for 5, 10 and 20 seconds dipping time.

Table 3.6 Band-gap value of SGSC and SGDC TiO_2 thin films for 1, 14, 21 and 28 days aging time for different layers number and dipping time.

SGSC Band-gap	**3 layers**	**5 layers**	**10 layers**	**SGDC Band-gap**	**5 seconds**	**10 seconds**	**20 seconds**
1 day	3.48 eV	3.27 eV	-	**1 day**	3.33 eV	3.32 eV	3.37 eV
21 days	3.51 eV	3.63 eV	3.59 eV	**21 days**	3.49 eV	3.52 eV	3.50 eV
28 days	3.55 eV	3.54 eV	3.53 eV	**28 days**	3.56 eV	3.55 eV	3.54 eV
56 days	3.56 eV	3.44 eV	3.29 eV	**56 days**	3.61 eV	3.57 eV	3.59 eV

3.4.5 Annealing Effect on SGSC TiO_2 Thin Films

The Figure 3.30 are shown the optical absorption spectra of SGSC TiO_2 thin films as-grown, annealed at 300 ^{0}C, 400 ^{0}C, 500 ^{0}C and 600 ^{0}C for aged 28 days for 3 layers. The absorption spectra of films annealed at 700 ^{0}C could not be obtained.

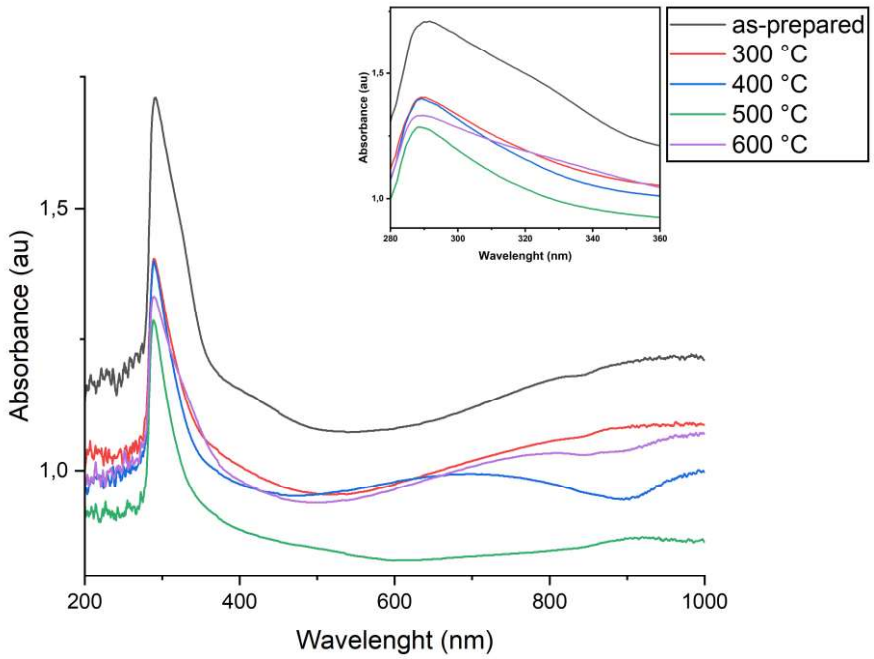

Figure 3.30 The optical absorption spectra of SGSC TiO_2 thin films annealed at different temperatures.

It is seen that annealing affect led to a decreasing in the ultraviolet and visible light absorption capacity of the growth films, these results in agreement with previous studies [153]. The bandgap values of the SGSC TiO_2 thin films was determined by Tauc's relation by using $(\alpha h\nu)^2$ vs energy graph (Fig. 3.31). With increasing annealing temperature, bandgap values decreased from 3.16 eV to 2.97 eV up to 600 ^{0}C. Similar changing indicated in the previous works [154-158]. As a result of the annealing process, small grains become larger grains due to reasons such as breaking the unwanted bonds and reorgaizing the atoms, and reducing the defects therefore the packing density increased. Consequently, the bandgap value are decreased [77,116].

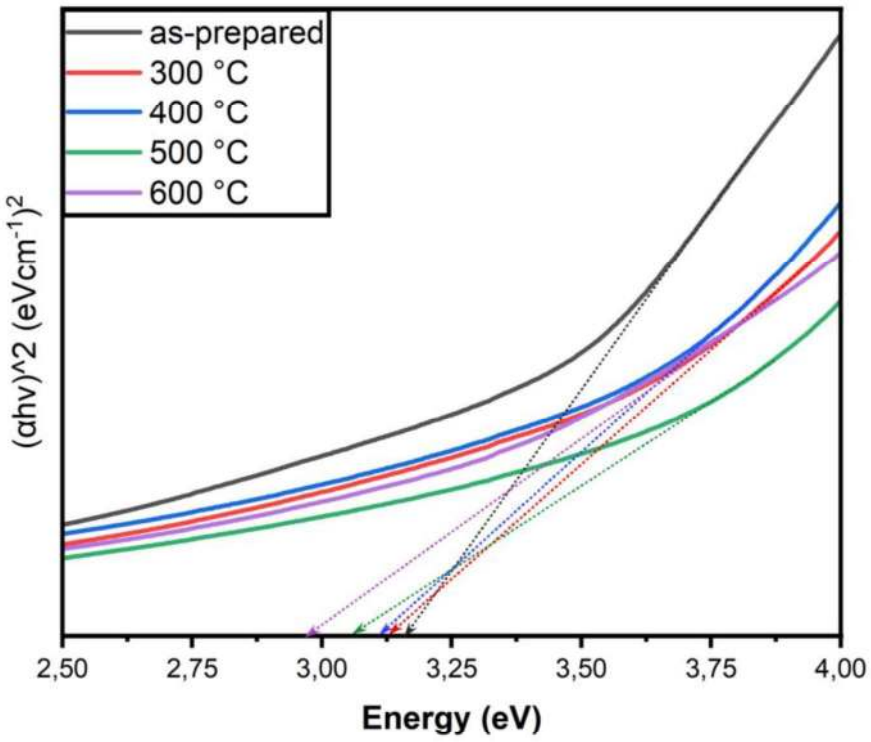

Figure 3.31 Plot of (αhv)^2 versus energy for SGSC TiO_2 thin films annealed at different temperature.

3.4.6 Annealing Effect on SGDC TiO_2 Thin Films

Figure 3.32 show the optical absorption spectra of SGDC TiO_2 thin films as-grown and annealed at 300 ^{0}C, 400 ^{0}C, 500 ^{0}C, 600 ^{0}C and 700 ^{0}C for 28 days aged with 10 seconds dipping time.

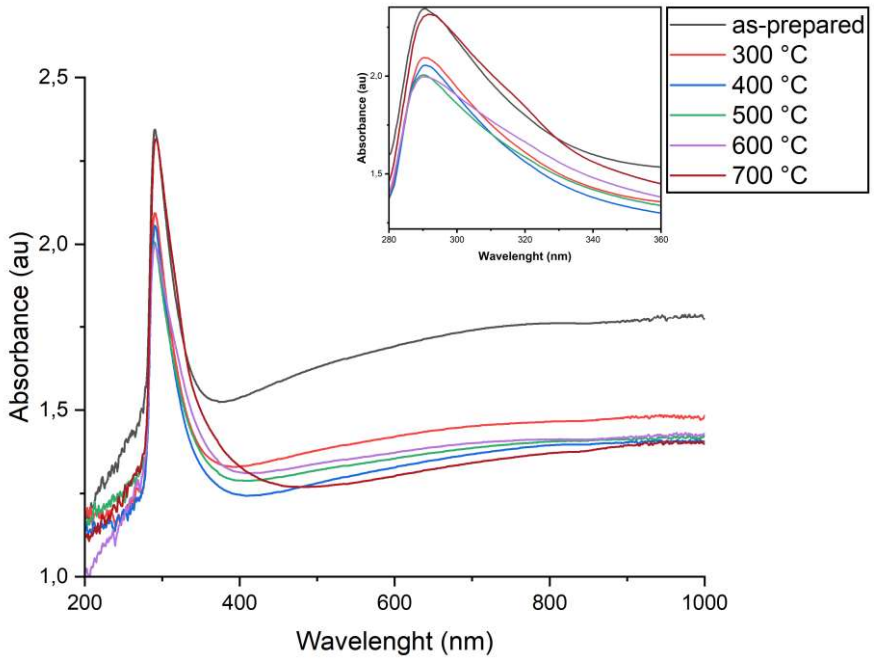

Figure 3.32 The absorption spectra of SGDC TiO_2 thin films annealed at different temperatures.

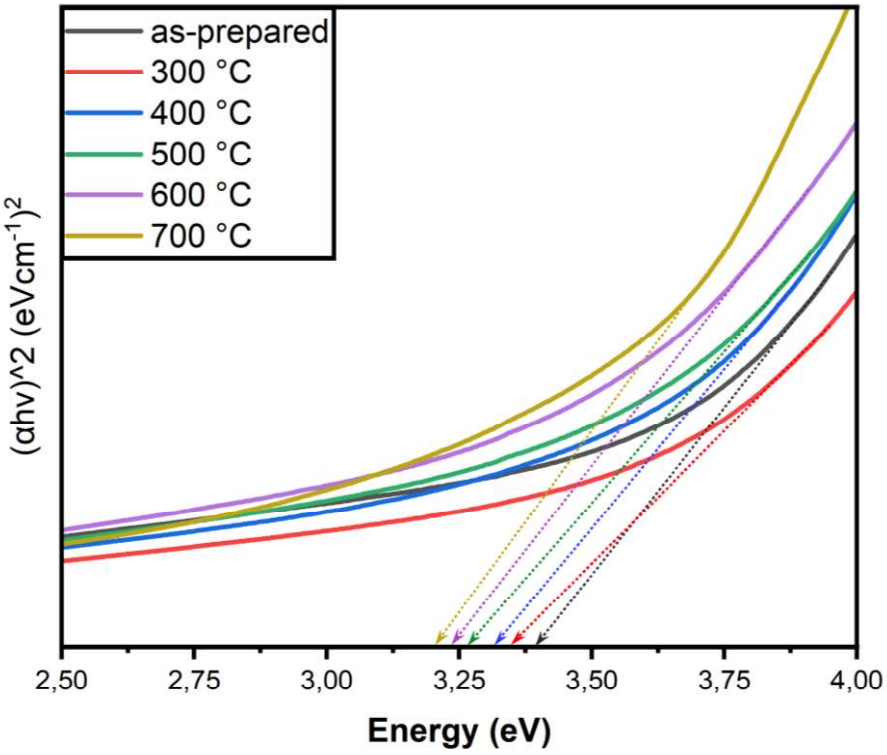

Figure 3.33 Plot of (αhv)^2 versus energy for SGDC TiO_2 thin films annealed at different temperature.

Table 3.7 Band-gap value of SGSC and SGDC TiO_2 thin films annealed at different temperatures.

	As-grown	**300 ^{0}C**	**400 ^{0}C**	**500 ^{0}C**	**600 ^{0}C**	**700 ^{0}C**
SGSC	3.16 eV	3.13 eV	3.11 eV	3.06 eV	2.97 eV	-
SGDC	3.39 eV	3.35 eV	3.32 eV	3.26 eV	3.23 eV	3.20 eV

It was seen that the visible light absorption capacity of the films decreased with the annealing process. The linearity of the Tauc plot of $(\alpha hv)^2$ vs hv for the SGDC TiO_2 thin films for as-grown and annealed at 300 ^{0}C, 400 ^{0}C, 500 ^{0}C, 600 ^{0}C and 700 ^{0}C are shown in the Fig. 3.33. The determined bandgap values are given in the Table 3.7. The bandgap values of the thin films decreased from 3.39 eV to 3.20 eV with increasing annealing temperature. Similar results for SGDC TiO_2 films have been observed in previous studies [159].

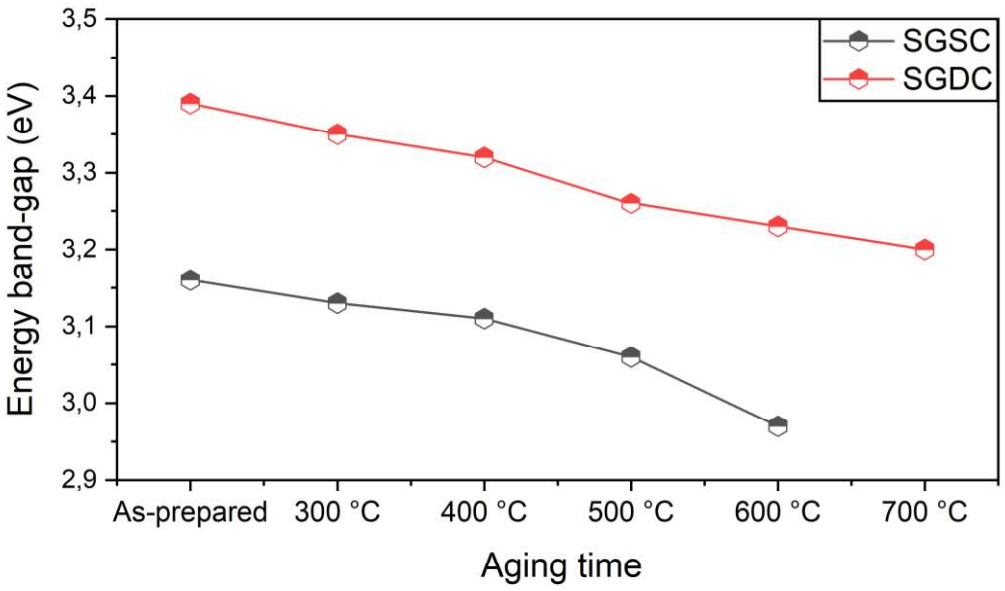

Figure 3.34 Bandgap changing with the annealing temperature for SGSC and SGDC TiO_2 thin films.

Figure 3.34 show a comparision the bandgap changing with the annealing effect for SGSC and SGDC thin films. The difference between in the bandgap values of both coating methods are nearly 0.20 eV. When the compared SGSC and SGDC TiO_2 thin films, with the increasing of annealing temperature, the same changing behaviour is

seen in two growth thecniques and with increasing annealing temperature the bangap values are decereased.

3.5 Refractive Index, Porosity, Dielectric Constant and Optical Conductivity

3.5.1 Aging Effect on SGSC and SGDC TiO_2 Thin Films

Table 3.8 Refractive index (n), porosity (P), dielectric constant (ε_∞) and static dielectric constant (ε_o) values of SGSC and SGDC TiO_2 thin films as a function of aging day.

Aging (day)	Bandgap (eV)	ε_o	Moss rel.			Ravindra et al. rel.			Herve-Vandamme rel.		
			n	P (%)	ε_∞	n	P (%)	ε_∞	n	P (%)	ε_∞
SGSC - 1	3.48	7.80	2.36	14.6	5.57	1.93	49.3	3.71	2.22	27.0	4.91
7	3.36	8.17	2.38	12.7	5.67	2.01	43.9	4.01	2.25	24.4	5.05
14	3.22	8.60	2.41	10.4	5.79	2.09	37.2	4.36	2.29	21.1	5.22
21	3.51	7.71	2.36	15.0	5.55	1.91	50.1	3.64	2.21	27.6	4.87
28	3.55	7.59	2.35	15.6	5.52	1.88	52.4	3.55	2.20	28.4	4.83
56	3.56	7.56	2.35	15.7	5.51	1.87	52.9	3.52	2.20	28.6	4.82
SGDC - 1	3.32	8.29	2.39	12.1	5.70	2.03	42.0	4.10	2.26	23.5	5.10
7	3.36	8.17	2.38	12.7	5.67	2.01	43.9	4.00	2.25	24.4	5.05
14	3.43	7.96	2.37	13.8	5.61	1.96	47.1	3.83	2.23	25.9	4.97
21	3.52	7.68	2.35	15.1	5.54	1.90	51.1	3.62	2.21	27.8	4.86
28	3.55	7.59	2.35	15.6	5.51	1.88	52.4	3.55	2.20	28.4	4.83
56	3.57	7.52	2.35	15.9	5.50	1.87	53.3	3.50	2.19	28.8	4.81

The refractive index of the films was determined by using Moss (equation 2.9), Ravindra (equation 2.10) and Herve-Vandamme relations (equation 2.11). The dielectric constant and porosity values were calculated by using 2.12 and 2.14 equations. The calculated refractive index, porosity, dielectric constant and static dielectric constant values for SGSC (3 layers) and SGDC (10 seconds dipping time) TiO_2 thin films for 1, 7, 14, 21, 28 and 56 days aged are given in the Table 3.8.

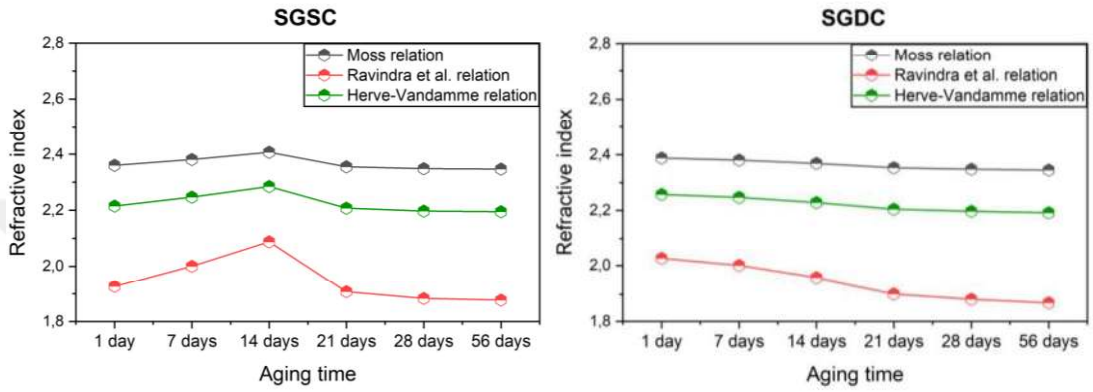

Figure 3.35 Refractive index of SGSC and SGDC TiO_2 thin films versus aging time, calculated using Moss relation, Ravindra et al. relation and Herve-Vandamme relation.

The calculated refractive index by Moss relation are between 2.35–2.41 for SGSC and 2.35–2.39 for SGDC films. According to Ravindra et al. relation, the refractive index of SGSC and SGDC films were defined as in the range of 1.87-2.09 and 1.87-2.03, respectively. On the other hand, the refractive index of SGSC and SGDC were calculated by Herve-Vandamme relation as between 2.20–2.29 and 2.26-2.19, respectively for different aging day. The Figure 3.35 show the refractive index vs aging time values using the Moss, Ravindra and Herve-Vandamme relations. The variation in refractive index can be attributed to optical absorption and variety of impurities and defects in the thin films [160]. These refractive index values are in agreement with the previous studies [161,162].

The static dielectric constant of SGSC and SGDC thin films were calculated as in the range of 7.52 – 8.60. The porosity values were calculated using refractive index are in the range of 10.4 % - 15.9 %, 37.2 % - 53.3% and 21.1 % - 28.8 %, for Moss, Ravindra and Herve-Vandamme relations respectively. With decreasing porosity, density of

TiO_2 thin films increased. Lower porosity values were observed for SGSC thin films aged 14 days and SGDC thin films aged 1 day. The dielectric constant changing with increasing aging day were calculated between 5.50 – 5.79, 3.50 – 4.36 and 4.81 – 5.22, for Moss, Ravindra and Herve-Vandamme relation respectively.

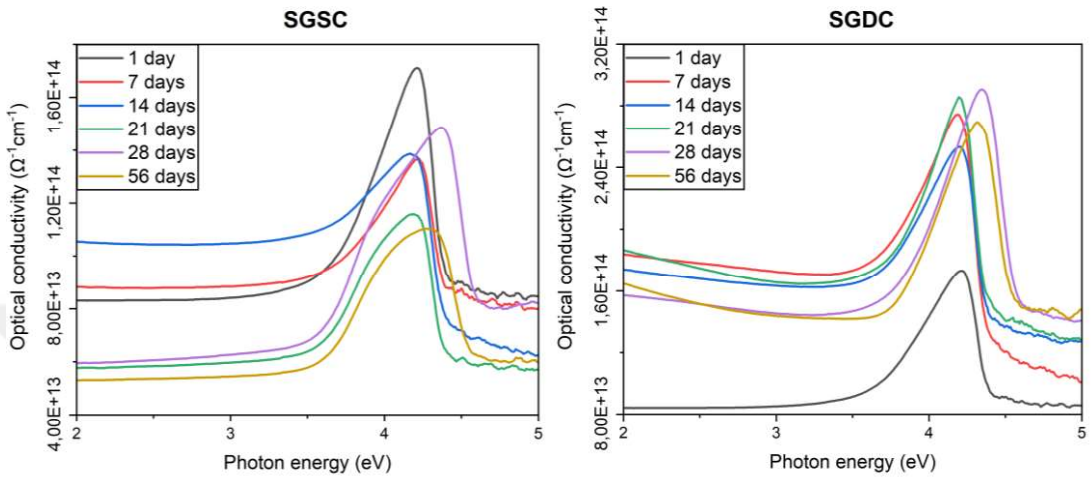

Figure 3.36 Optical conductivy-photon energy plot for SGSC and SGDC TiO_2 thin films for different aging day.

The Figure 3.36 show the optical conductivity versus photon energy plot for SGSC and SGDC TiO_2 thin films with different aging time. Increasing aging days caused a change in the optical conductivity.

3.5.2 Layer and Dipping Time Effect on SGSC and SGDC TiO_2 Thin Films

The calculated refractive index, porosity, dielectric constant and static dielectric constant value of the SGSC for 3, 5 and 10 layers and SGDC for 5, 10 and 20 seconds dipping time with aged 56 days are given in the Table 3.9. The static dielectric constant was calculated in the range of 7.40 – 8.39. According to the Moss relation, the refractive index values were determined in the range of 2.34 – 2.39 for the different number of layers and dipping time. On the other hand, the calculated refractive index values by Ravindra relation were changed between 1.85 – 2.04. With using Herve-Vandamme relation, the lowest refractive index values were calculated between 2.18 - 2.27.

Table 3.9 Refractive index (n), porosity (P), dielectric constant (ε_∞) and static dielectric constant (ε_o) values of SGSC and SGDC TiO_2 thin films for aged 56 days as a function of number of layer and dipping time.

Layer-Dipping time	Ban dgap (eV)	ε_o	Moss rel.			Ravindra et al. rel.			Herve-Vandamme rel.		
			n	P (%)	ε_∞	n	P (%)	ε_∞	n	P (%)	ε_∞
SGSC - 3	3.56	7.56	2.35	15.8	5.51	1.88	52.6	3.52	2.20	28.6	4.82
5	3.44	7.93	2.37	14.0	5.60	1.95	47.5	3.81	2.23	26.1	4.95
10	3.29	8.39	2.39	11.6	5.73	2.04	40.6	4.18	2.27	22.8	5.13
SGDC-5	3.61	7.40	2.34	16.5	5.47	1.85	55.0	3.41	2.18	29.7	4.76
10	3.57	7.52	2.35	15.9	5.50	1.87	53.3	3.50	2.19	28.8	4.81
20	3.59	7.46	2.34	16.2	5.49	1.86	54.2	3.45	2.19	29.3	4.79

It was observed that with the increasing number of layers, the refractive index, dielectric constant and static dielectric constant increased and porosity decreased. Similar results with increasing number of layers was achieved in previous studies [163]. Lower porosity and higher refractive index were observed at SGSC films for 10 layers. These decrease in the porosiy is due to film densification and filling of pores with increasing number of layers [164].

3.5.3 Annealing Temperature Effect on SGSC and SGDC TiO_2 Thin Films

The determined refractive index, porosity, dielectric constant and static dielectric constant value for SGSC (3 layers) and SGDC (10 seconds dipping time) with as-grown and annealed at 300 ^{0}C, 400 ^{0}C, 500 ^{0}C, 600 ^{0}C and 700 ^{0}C are given in the Table 3.10. The calculated static dielectric constant are changed between 8.08 – 9.37. According to Moss relation, the refractive index was determined in the range of 2.38 – 2.46 for different anneling temperature. The refractive index values calculated by using Ravindra relation are changed between 1.98 – 2.24. According to Herve-Vandamme relation, the lowest refractive index values were calculated between 2.24

- 2.36. The refractive index changing as a function of annealing temperature for each relation is given in the Figure 3.37.

Table 3.10 Refractive index (n), porosity (P), dielectric constant (ε_∞) and static dielectric constant (ε_o) values of SGSC and SGDC TiO_2 thin films as a funciton of annealing temperature.

Annealing Temp.	Bandgap (eV)	ε_o	Moss rel.			Ravindra et al. rel.			Herve-Vandamme rel.		
			n	P (%)	ε_∞	n	P (%)	ε_∞	n	P (%)	ε_∞
SGSC as- grown	3.16	8.79	2.42	9.43	5.85	2.13	34.3	4.52	2.30	19.7	5.30
300 ^{0}C	3.13	8.88	2.42	8.90	5.87	2.14	32.8	4.59	2.31	18.9	5.34
400 ^{0}C	3.11	8.94	2.43	8.55	5.89	2.16	31.8	4.65	2.32	18.4	5.36
500 ^{0}C	3.06	9.10	2.44	7.65	5.94	2.19	29.3	4.78	2.33	17.2	5.43
600 ^{0}C	2.97	9.37	2.46	5.98	6.03	2.24	24.7	5.03	2.36	14.8	5.56
SGDC as- grown	3.39	8.08	2.38	13.2	5.64	1.98	45.3	3.93	2.24	25.0	5.01
300 ^{0}C	3.35	8.20	2.38	12.6	5.68	2.01	43.4	4.03	2.25	24.1	5.06
400 ^{0}C	3.32	8.29	2.39	12.1	5.70	2.03	42.0	4.10	2.26	23.5	5.10
500 ^{0}C	3.26	8.48	2.40	11.1	5.76	2.06	39.2	4.26	2.27	22.1	5.17
600 ^{0}C	3.23	8.57	2.41	10.6	5.78	2.08	37.7	4.33	2.28	21.4	5.21
700 ^{0}C	3.20	8.66	2.41	10.1	5.81	2.10	36.3	4.41	2.29	20.6	5.25

It can be seen that with increasing annealing temperature, refractive index, dielectric constant and static dielectric constant values increased for SGSC and SGDC TiO_2 thin films and porosity decreased. Similar result was achieved in previous studies [165].

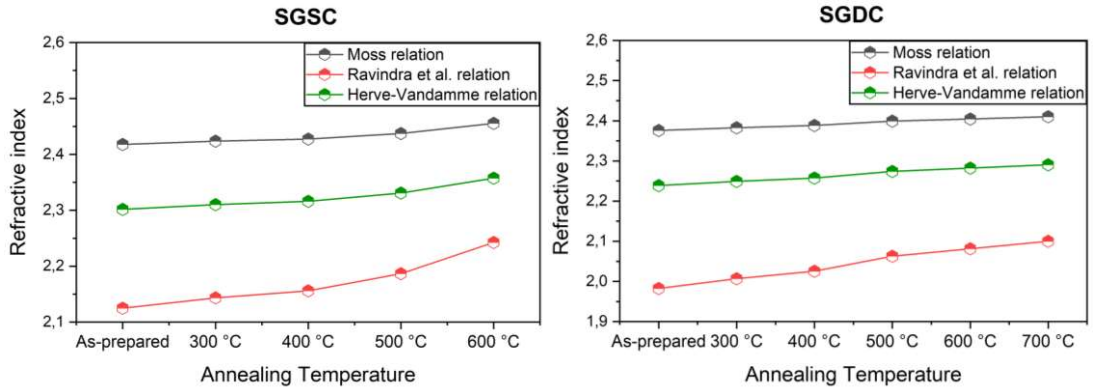

Figure 3.37 Refractive index of SGSC and SGDC TiO_2 thin films versus annealing temperature, calculated using Moss relation, Ravindra et al. relation and Herve-Vandamme relation.

The optical conductivity versus incident photon energy plot of SGSC and SGDC TiO_2 thin films for as-grown and annealed at 300 ^{0}C, 400 ^{0}C, 500 ^{0}C, 600 ^{0}C and 700 ^{0}C are given in the Figure 3.38. It was seen that with the increasing annealing temperature, optical conductiviy decreased for each coating methods.

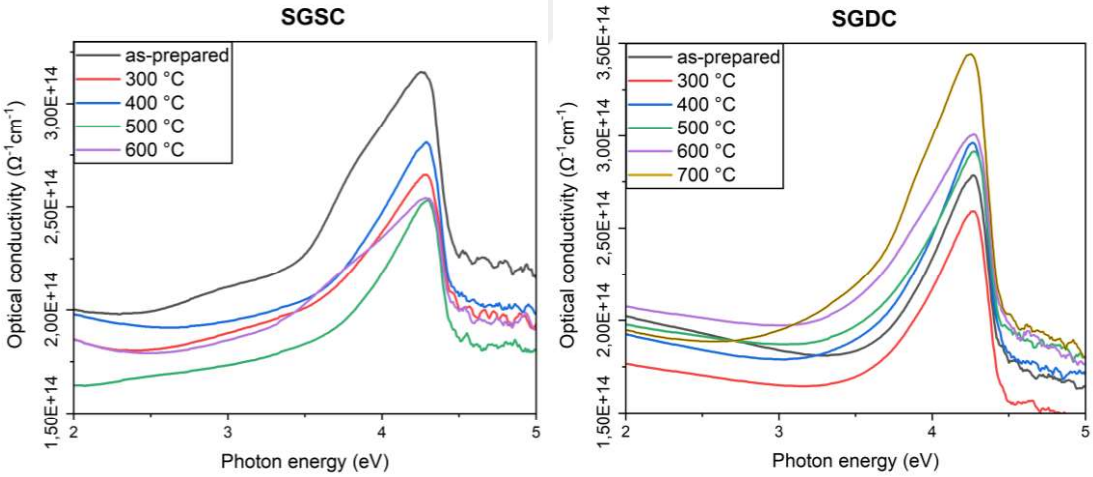

Figure 3.38 Optical conductivy-photon energy plot for SGSC and SGDC TiO_2 thin films for different annealing temperature.

CHAPTER 4

CONCLUSION

In this thesis, the structural and optical properties of TiO_2 thin films grown on glass substrate by sol-gel spin coating and sol-gel dip coating methods were investigated. XRD, SEM and UV-Vis spectroscopy measurements are used for characterization. For these aim some growth parameter have been considred; aging day of the solution, number of layer, dipping time and annealing temperature.

With using the structural analysing results, the crystallite size, dislocation density, microstrain, avarage grain size values, and with using the optical results energy bandgap, refractive index, porosity, dielectric constant and static dielectric constant values were calculated for each growth process.

In the first part of the study, the prepared solution was aged 1, 7, 14, 21, 28 and 56 days. Thin films were grown on glass substrate by using SGSC and SGDC methods. Using the aged solutions, Number of layers and dipping time effect on the thin film were investigated. For these aim, 3, 5 and 10 layers and 5, 10 and 20 seconds dipping time considered, the Thin films were dried at 250 ^{0}C for 3 minutes for SGSC growth and 100 ^{0}C for 30 minutes for SGDC growth . To investiagte the annealing effect on the for all these growth parameters, TiO_2 thin films were annealed at 300 ^{0}C, 400 ^{0}C, 500 ^{0}C, 600 ^{0}C and 700 ^{0}C for 1 hour.

The XRD results of SGSC aged TiO_2 thin films showed amorphous phase. With the annealing of the films, recrystallization from amorphous to anatase structure was occured at above 400 ^{0}C. The dominant (101) peak is nearly at 24.61^o corresponding to the lattice plane was observed in all crystal structure. The other lattice plane (004), (200), (105), (211) and (204) appeared with annealing. The crystallite size for (101) planes in all SGSC and SGDC films was calculated as 31.81, 26.37, 25.18 nm and 50.07, 38.83, 27.17, 26.33 nm, with increasing annealing temperature. It was observed that, the crystallite size decreased and FWHM, dislocation density and microstrain increased with increasing annealing temperature. According to XRD results, the better

crystallization was observed at 400 ^{0}C for each coating methods. The interplanar spacing, FWHM, dislocation density and microstrain were calculated as 3.614 Å, 0.27º, 0.000988 nm^{-2} and 5.40x10^{-3} for SGSC TiO_2 thin films annealed at 400 ^{0}C and 3.524 Å, 0.17º, 0.000393 nm^{-2} and 3.31x10^3 for SGDC films at 400 ^{0}C.

From the SEM imaging, it was observed that surface of the SGSC films are non-homogeneous and severe cracking. The increasing aging time was caused a change of the agglomeration size, homogenity, cracks and smoothness of the coating surface. From the SEM images of the SGDC thin film, all films was showed island-like structure. With the increasing aging time, these structure size decreased and holes increased. The particles of island-like structures are about in spherical form. The average grain size of SGDC thin film for 1, 7, 14, 21, 28 and 56 days aged was determined as 292, 346, 376, 340, 481 and 476 nm, respectively. With the increasing number of layers, it was observed that, larger agglomeration formed, homogenity and particle distribution improved and the holes decreased. From the SEM imaging of 5, 10 and 20 seconds dipping time, size of island-like structure increased and larger agglomeration shown. When we look at the annealing effect results, it was observed that, the increasing annealing temperature caused a morphological changing on the coating surface. The average grain size of SGSC films annealed at 700 ^{0}C was calculated as 47 nm. With the increasing annealing temperature from room temperature to 700 ^{0}C, the average grain size of SGDC films was determined as 337, 328, 325, 336, 350 and 371.

From the EDX analysis, content of the titanium element in the SGSC films was gradually increased from 17.0 % to 41.0 % with increasing annealing temperature. The molecular weight percentage of titanium elements at 700 ^{0}C was observed as 41 % for Ti, 42.2 % for O and 12.2 % for Si element. The Si elements was due to the glass substrate. The content of the Ti element in the SGDC was gradually increased from 16.8 % to 30.1 % with increasing annealing temperature. The higher content of the Ti was observed as 41.0 % at 700 ^{0}C for SGSC thin film.

From the UV-Visible spectroscopy measurements, the absorption threshold was observed at around 410 nm for all grown TiO_2 films. The bandgap values of the SGSC films were calculated as 3.48, 3.36, 3.22, 3.51, 3.55 and 3.56 eV with increasing aging

time from 1, 7, 14, 21, 28 to 56 days, respectively. The lowest energy bandgap value was observed for 14 days aged thin film. The bandgap values for SGDC films were determined as 3.32, 3.36, 3.43, 3.52, 3.55 and 3.56 eV for aged 1, 7, 14, 21, 28 and 56 days, respectively. It was observed that, with the increasing aging day, the bandgap values gradually increased. The number of layers and dipping time was caused a changing in the band structure. The bandgap values of films as-grown and annealed at 300 ^{0}C, 400 ^{0}C, 500 ^{0}C, 600 ^{0}C and 700 ^{0}C was calculated as 3.16, 3.13, 3.11, 3.06 and 2.97 eV for SGSC films and 3.39, 3.35, 3.32, 3.26, 3.23 and 3.20 eV for SGDC films, respectively. As can be seen that the bandgap values for each using coating methods gradually decreased with increasing annealing temperature.

The refractive index by using Moss relation was calculated as 2.36, 2.38, 2.41, 2.36, 2.35 and 2.35 for SGSC and 2.39, 2.38, 2.37, 2.35, 2.35 and 2.35 for SGDC for aged 1, 7, 14, 21,28 and 56 days, respectively. The lowest refractive index value was observed at SGDC for 56 aged thin film and the highest value was observed at SGSC for 14 days aged thin film. The porosity, dielectric constant and static dielectric constant values of the SGSC thin film for 14 days aged and SGDC for 56 days aged were calculated as 10.4 %, 5.79, 8.60 and 15.9 %, 5.50, 7.52, respectively. The rafractive index for as-grown and annealed at 300 ^{0}C, 400 ^{0}C, 500 ^{0}C, 600 ^{0}C and 700 ^{0}C were calculated as 2.42, 2.42, 2.43, 2.44 and 2.46 for SGSC TiO_2 thin films and 2.38, 2.38, 2.39, 2.40, 2.41 and 2.41 for SGDC thin films, respectively. The lowest refractive index value was seen at SGDC as-grown and highest value was seen at SGSC annealed at 600 ^{0}C. The porosity, dielectric constant and static dielectric constant value was determined as 13.2 %, 5.64 and 8.08 for SGDC as-grown thin film and 5.98 %, 6.03 and 9.37 for SGSC thin film annealed at 600 ^{0}C. It was observed that optical conductivity changed with the annealing temperature.

As a result we can summarize and say that the growt thecnique and the growt paramaters of the different growth thecniques effect the structural, optical and the other properties of the thin film. So according to the our aim, we can choose and we can optimize the growth parameters. In this thesis, it has been tried to do this and to optimize the growth parameters for two different growth methods and to draw a road map for those who will work on this subject from now on.

FUTURE STUDIES;

1. Investigating the effects of the other sol-gel parameters
    - Different Precursors effect (TTIP, TiBu, $TiCl_4$)
    - Differnetn Solvent effect (Ethanol, Methanol, Propanol)
    - Different Catalyst effect (Hydrocloric acid, Nitric acid, Acetic acid)
    - pH effect
    - ZnO+TiO_2 (layer by layer)
    - Doping effect
2. Compared the Hydrothermal and Sol-Gel methods
    - Hydrothermal growth on films coated by sol-gel

REFERENCES

[1] Durmaz, D., Sol-jel döndürmeli kaplama tekniği ile TiO2 filmlerinin üretimi ve karakterizasyonu (Master's thesis, ESOGÜ, Fen Bilimleri Enstitüsü),(2019).

[2] Chen, X., & Mao, S. S., Titanium dioxide nanomaterials: synthesis, properties, modifications, and applications. *Chemical reviews*, *107*(7), 2891-2959, (2007).

[3] Matthews, R. W., Photooxidation of organic impurities in water using thin films of titanium dioxide. Journal of Physical Chemistry, 91(12), 3328-3333, (1987).

[4] RINO, J.P., STUDART, N., Structural correlations in titanium dioxide. Physical Review 1999; 59(2):6643

[5] Akrami, S., Watanabe, M., Ling, T. H., Ishihara, T., Arita, M., Fuji, M., & Edalati, K., High-pressure TiO2-II polymorph as an active photocatalyst for CO2 to CO conversion. *Applied Catalysis B: Environmental*, *298*, 120566 (2021).

[6] Fahmi, A., Minot, C., Silvi, B., & Causa, M., Theoretical analysis of the structures of titanium dioxide crystals. Physical Review B, 47(18), 11717, (1993).

[7] Bazu, T., Sol-Gel Yöntemi ile Kaplanarak Kendini Temizleyen Yüzeylerin Elde Edilmesi ve Karakterizasyonu (Doctoral dissertation, Yüksek Lisans Tezi, Gazi Üniversitesi Fen Bilimleri Enstitüsü, Ankara, Türkiye), (2013).

[8] Mo, S. D., & Ching, W. Y., Electronic and optical properties of three phases of titanium dioxide: Rutile, anatase, and brookite. Physical review B, 51(19), 13023, (1995).

[9] Chang, Y., Supported TiO2 photocatalyst synthesis and some applications to water purification. University of Calgary, (2004).

[10] Elbushra, H., Ahmed, M., Wardi, H., & Eassa, N., Synthesis and characterization of TiO2 using sol-gel method at different annealing temperatures. MRS Advances, 3(42-43), 2527-2535, (2018).

[11] Wu, S., Luo, X., Long, Y., & Xu, B., Exploring the phase transformation mechanism of titanium dioxide by high temperature in situ method. In IOP Conference Series: Materials Science and Engineering (Vol. 493, No. 1, p. 012010). IOP Publishing, (2019, March).

[12] Ranade, M. R., Navrotsky, A., Zhang, H. Z., Banfield, J. F., Elder, S. H., Zaban, A., ... & Whitfield, H. J., Energetics of nanocrystalline TiO2. Proceedings of the National Academy of Sciences, 99(suppl_2), 6476-6481, (2002).

[13] Taç, B., Gümüş ile katkılanmış tio2 ince filmlerin üretimi ve karakterizasyonu (Doctoral dissertation, Süleyman Demirel Üniversitesi Fen Bilimleri Enstitüsü), (2014).

[14] Shon, H., Phuntsho, S., Okour, Y., Cho, D. L., Kim, K. S., Li, H. J., ... & Kim, J. H., Visible light responsive titanium dioxide (TiO 2). Applied Chemistry for Engineering, 19(1), 1-16, (2008).

[15] Brock, T., Groteklaes, M., & Mischke, P., European coatings handbook. Vincentz Network GmbH & Co KG, (2000).

[16] Hanaor, D. A., & Sorrell, C. C., Review of the anatase to rutile phase transformation. Journal of Materials science, 46, 855-874, (2011).

[17] Kılıçoğlu, B. Didem. "Nanoboyutlu TiO2 esaslı antibakteriyel kaplama." Thesis (PhD), Yıldız Teknik Üniversitesi Fen Bilimleri Enstitüsü, (2009).

[18] Fujishima, A., Photosensitized electrolytic oxidation on semiconducting n-type TiO_2 electrode. Kogyo Kagaku Zasshi, 72, 108-113, (1969).

[19] Frank, S. N., & Bard, A. J., Heterogeneous photocatalytic oxidation of cyanide ion in aqueous solutions at titanium dioxide powder. Journal of the American Chemical Society, 99(1), 303-304, (1977).

[20] Aytekin, B., Yanma yöntemiyle TiO2 sentezi, karakterizasyonu ve adsorpsiyon özellikleri, (2015).

[21] Khan, M. I., Bhatti, K. A., Qindeel, R., Althobaiti, H. S., & Alonizan, N., Structural, electrical and optical properties of multilayer TiO2 thin films deposited by sol–gel spin coating. Results in physics, 7, 1437-1439, (2017).

[22] Vydianathan, K., Nuesca, G., Peterson, G., Eisenbraun, E. T., Kaloyeros, A. E., Sullivan, J. J., & Han, B., Metalorganic chemical vapor deposition of titanium oxide for microelectronics applications. Journal of Materials Research, 16(6), 1838-1849, (2001).

[23] Huusko, J., Lantto, V., & Torvela, H., TiO2 thick-film gas sensors and their suitability for NOx monitoring. Sensors and Actuators B: Chemical, 16(1-3), 245-248, (1993).

[24] Hara, K., Sayama, K., Ohga, Y., Shinpo, A., Suga, S., & Arakawa, H., A coumarin-derivative dye sensitized nanocrystalline TiO2 solar cell having a high solar-energy conversion efficiency up to 5.6%. Chemical Communications, (6), 569-570, (2001).

[25] Banerjee, S., Dionysiou, D. D., & Pillai, S. C., Self-cleaning applications of TiO2 by photo-induced hydrophilicity and photocatalysis. Applied Catalysis B: Environmental, 176, 396-428, (2015).

[26] Çeşmeli, S., & Biray Avci, C., Application of titanium dioxide (TiO2) nanoparticles in cancer therapies. Journal of drug targeting, 27(7), 762-766, (2019).

[27] Xie, J., & Hung, Y. C., UV-A activated TiO2 embedded biodegradable polymer film for antimicrobial food packaging application. Lwt, 96, 307-314, (2018).

[28] Weir, A., Westerhoff, P., Fabricius, L., Hristovski, K., & Von Goetz, N., Titanium dioxide nanoparticles in food and personal care products. Environmental science & technology, 46(4), 2242-2250, (2012).

[29] Hsu, C. L., & Sheu, D. C., Disinfection ability of TiO2-containing coating (Doctoral dissertation, Thesis for Master of Science Department of Bioengineering, Tatung University, Taipei, Taiwan), (2004).

[30] Biçer, E. D., Sol–Jel yöntemi ile hazırlanan TiO2–SiO2 nanokompozit ince filmlerin fiziksel ve mekanik özelliklerinin incelenmesi (Doctoral dissertation, Fen Bilimleri Enstitüsü), (2015).

[31] Nix, W. D., Mechanical properties of thin films. Metallurgical transactions A, 20, 2217-2245, (1989).

[32] Suthar, D., Chuhadiya, S., Sharma, R., & Dhaka, M. S., An overview on the role of ZnTe as an efficient interface in CdTe thin film solar cells: a review. Materials Advances, (2022).

[33] Liu, G., Processing of CdS/CdTe solar cell and the growth model of CdTe thin film, (2016).

[34] Hasan, M. M., Haseeb, A. S. M. A., Saidur, R., Masjuki, H. H., & Hamdi, M., Influence of substrate and annealing temperatures on optical properties of RF-sputtered TiO2 thin films. Optical Materials, 32(6), 690-695, (2010).

[35] Blešić, M. D., Šaponjić, Z. V., Nedeljković, J. M., & Uskoković, D. P., TiO2 films prepared by ultrasonic spray pyrolysis of nanosize precursor. Materials letters, 54(4), 298-302, (2002).

[36] Byrappa, K., Lokanatha Rai, K. M., & Yoshimura, M., Hydrothermal preparation of TiO2 and photocatalytic degradation of hexachlorocyclohexane and dichlorodiphenyltrichloromethane. Environmental technology, 21(10), 1085-1090, (2000).

[37] Wang, C., Deng, Z. X., & Li, Y., The synthesis of nanocrystalline anatase and rutile titania in mixed organic media. Inorganic Chemistry, 40(20), 5210-5214, (2001).

[38] Jung, S. C., Kim, B. H., Kim, S. J., Imaishi, N., & Cho, Y. I., Characterization of a TiO2 photocatalyst film deposited by CVD and its photocatalytic activity. Chemical Vapor Deposition, 11(3), 137-141, (2005).

[39] Shimizu, Y., Kuwano, N., Hyodo, T., & Egashira, M., High H2 sensing performance of anodically oxidized TiO2 film contacted with Pd. Sensors and Actuators B: Chemical, 83(1-3), 195-201, (2002).

[40] Lv, P., Fu, W., Mu, Y., Sun, H., Su, S., Chen, Y., ... & Yang, H., Photoelectrochemical property of CdS and PbS cosensitized on the TiO2 array by novel successive ionic layer adsorption and reaction method. Journal of Alloys and Compounds, 621, 30-34, (2015).

[41] SORAR, İ., & SARIGÜL, H., Sol-jel yöntemiyle hazırlanan tio2 filmlerin optik ve elektrokromik özellikleri. Marmara Fen Bilimleri Dergisi, 28(2), 81-88, (2008).

[42] Li, W., Fries, D. P., & Malik, A., Sol–gel stationary phases for capillary electrochromatography. Journal of Chromatography A, 1044(1-2), 23-52, (2004).

[43] Ebelmen, J. J., Recherches sur les combinaisons des acides borique et silicique avec les ethers, (1846).

[44] Uhlmann, D. R., Zelinski, B. J. J., Wnek, G. E., Brinker, C. J., Clark, D. E., & Ulrich, D. R., Better ceramics through chemistry. In Mat. Res. Soc. Symp. Proc. (Vol. 32, pp. 59-70), (1984).

[45] Brinker, C. J., & Scherer, G. W., Sol-gel science: the physics and chemistry of sol-gel processing. Academic press, (2013).

[46] Znaidi, L., Sol–gel-deposited ZnO thin films: A review. Materials Science and Engineering: B, 174(1-3), 18-30, (2010).

[47] Bardakçı, S., Sol-Jel yöntemi ile Hazırlanan Tio 2 Ince Filmlerin Optik Özelliklerinin Belirlenmesi (Doctoral dissertation, Sakarya Universitesi (Turkey)), (2007).

[48] Şam, E. D., Saf ve katkılı TiO2 filmlerin optik, yapısal ve fotoaktivite özellikleri, (2007).

[49] Bokov, D., Turki Jalil, A., Chupradit, S., Suksatan, W., Javed Ansari, M., Shewael, I. H., ... & Kianfar, E., Nanomaterial by sol-gel method: synthesis and application. Advances in Materials Science and Engineering, 2021, 1-21, (2021).

[50] Özler, F. B., Titanyum ve alaşımlarının sol-jel daldırma yöntemiyle yüzey modifikasyonu (Doctoral dissertation, Fen Bilimleri Enstitüsü), (2007).

[51] Türhan, İ., TiO2 ve katkılı TiO2 ince filmlerinin hazırlanması ve karakterizasyonu, (2000).

[52] Jones, R. W., Fundamental Principles of Sol--Gel Technology. The Institute of Metals, 1990,, 12, (2000).

[53] Kloskowski, A., Pilarczyk, M., Chrzanowski, W., & Namieśnik, J., Sol-gel technique—a versatile tool for adsorbent preparation. Critical Reviews in Analytical Chemistry, 40(3), 172-186, (2010).

[54] TOYGUN, Ş., KÖNEÇOĞLU, G., & KALPAKLI, Y., General principles of sol-gel. Sigma Journal of Engineering and Natural Sciences, 31(4), 456-476, (2013).

[55] Periyat, P., Baiju, K. V., Mukundan, P., Pillai, P. K., & Warrier, K. G. K., Aqueous colloidal sol–gel route to synthesize nanosized ceria-doped titania having high surface area and increased anatase phase stability. Journal of sol-gel science and technology, 43, 299-304, (2007).

[56] Baiju, K. V., Periyat, P., Wunderlich, W., Krishna Pillai, P., Mukundan, P., & Warrier, K. G. K., Enhanced photoactivity of neodymium doped mesoporous

titania synthesized through aqueous sol–gel method. Journal of sol-gel science and technology, 43, 283-290, (2007).

[57] Senain, I., Nayan, N., & Saim, H., Structural and electrical properties of TiO2 thin film derived from sol-gel method using titanium (IV) butoxide. International Journal of Integrated Engineering, 2(3), (2010).

[58] Verma, A., Basu, A., Bakhshi, A. K., & Agnihotry, S. A., Structural, optical and electrochemical properties of sol–gel derived TiO2 films: Annealing effects. Solid State Ionics, 176(29-30), 2285-2295, (2005).

[59] Pope, E. J. A., & Mackenzie, J. D., Sol-gel processing of silica: II. The role of the catalyst. Journal of non-crystalline solids, 87(1-2), 185-198, (1986).

[60] Livage, J., & Sanchez, C., Sol-gel chemistry. Journal of Non-Crystalline Solids, 145, 11-19, (1992).

[61] Pierre, A. C., Introduction to sol-gel processing. (2nd ed.), Springer Nature, (2020).

[62] Hsiang, H. I., & Lin, S. C., Effects of aging on the phase transformation and sintering properties of TiO2 gels. Materials Science and Engineering: A, 380(1-2), 67-72, (2004).

[63] Clapsaddle, B. J., Sprehn, D. W., Gash, A. E., Satcher Jr, J. H., & Simpson, R. L., A versatile sol–gel synthesis route to metal–silicon mixed oxide nanocomposites that contain metal oxides as the major phase. Journal of non-crystalline solids, 350, 173-181, (2004).

[64] Yiotis, A. G., Boudouvis, A. G., Stubos, A. K., Tsimpanogiannis, I. N., & Yortsos, Y. C., Effect of liquid films on the drying of porous media. AIChE Journal, 50(11), 2721-2737, (2004).

[65] Keshmiri, M., Troczynski, T., & Mohseni, M., Oxidation of gas phase trichloroethylene and toluene using composite sol–gel TiO2 photocatalytic coatings. Journal of hazardous materials, 128(2-3), 130-137, (2006).

[66] Kursawe, M., Hilarius, V., Pfaff, G., & Anselmann, R., Sol-gel Coating Processes. Modern Surface Technology, 205-220, (2006).

[67] Aymerich, M., Gómez-Varela, A. I., Álvarez, E., & Flores-Arias, M. T., Study of different sol-gel coatings to enhance the lifetime of PDMS devices: evaluation of their biocompatibility. Materials, 9(9), 728, (2016).

[68] Taşkın, D., Sol-Gel Metoduyla Hazırlanan Metaloksit Filmlerin Yapısal ve Elektriksel Karakterizasyonu (Doctoral dissertation, Marmara Universitesi (Turkey)), (2006).

[69] Sahu, N., Parija, B., & Panigrahi, S., Fundamental understanding and modeling of spin coating process: A review. Indian Journal of Physics, 83(4), 493-502, (2009).

[70] Tyona, M. D., A theoritical study on spin coating technique. Advances in materials Research, 2(4), 195, (2013).

[71] Shojaeiarani, J., Bajwa, D. S., Stark, N. M., Bergholz, T. M., & Kraft, A. L., Spin coating method improved the performance characteristics of films obtained from poly (lactic acid) and cellulose nanocrystals. Sustainable Materials and Technologies, 26, e00212, (2020).

[72] Vorotilov, K. A., Orlova, E. V., & Petrovsky, V. I., Sol-gel TiO2 films on silicon substrates. Thin Solid Films, 207(1-2), 180-184, (1991).

[73] Wang, Z., Helmersson, U., & Käll, P. O., Optical properties of anatase TiO2 thin films prepared by aqueous sol–gel process at low temperature. Thin Solid Films, 405(1-2), 50-54, (2002).

[74] Naceur, J. B., Gaidi, M., Bousbih, F., Mechiakh, R., & Chtourou, R., Annealing effects on microstructural and optical properties of nanostructured-TiO2 thin films prepared by sol–gel technique. Current Applied Physics, 12(2), 422-428.3, (2012).

[75] Wong, A., Daoud, W. A., Liang, H., & Szeto, Y. S., The effect of aging and precursor concentration on room-temperature synthesis of nanocrystalline anatase TiO2. Materials Letters, 117, 82-85, (2014).

[76] Hwang, K. J., Lee, J. W., Shim, W. G., Jang, H. D., Lee, S. I., & Yoo, S. J., Adsorption and photocatalysis of nanocrystalline TiO2 particles prepared by sol–gel method for methylene blue degradation. Advanced Powder Technology, 23(3), 414-418, (2012).

[77] Gürsoy, T. Sol-jel tekniği ile büyütülen TİO2 ince filmlerin yapısal ve optik özelliklerinin incelenmesi (Master's thesis, Fen Bilimleri Enstitüsü), (2019).

[78] Miki, T., Nishizawa, K., Suzuki, K., & Kato, K., Preparation of nanoporous TiO2 film with large surface area using aqueous sol with trehalose. Materials Letters, 58(22-23), 2751-2753, (2004).

[79] Malliga, P., Pandiarajan, J., Prithivikumaran, N., & Neyvasagam, K., Influence of film thickness on structural and optical properties of sol–gel spin coated TiO2 thin film. J. Appl. Phys, 6, 22-28, (2014).

[80] Cullity, B. D., & Stock, S. R., Elements of x-ray diffraction, (3rd ed.), Pearson New International Edition, United State of America, (2014).

[81] Raza, G., Titanium dioxide nanomaterials, synthesis, stability and mobility in natural and synthetic porous media (Doctoral dissertation, University of Birmingham), (2017).

[82] Ashraf, M., Akhtar, S. M. J., Khan, A. F., Ali, Z., & Qayyum, A., Effect of annealing on structural and optoelectronic properties of nanostructured ZnSe thin films. Journal of Alloys and Compounds, 509(5), 2414-2419, (2011).

[83] Li, G., Li, L., Boerio-Goates, J., & Woodfield, B. F., Grain-growth kinetics of rutile TiO2 nanocrystals under hydrothermal conditions. Journal of materials research, 18(11), 2664-2669, (2003).

[84] Zaidi, U. Z. M., Bushroa, A. R., Ghahnavyeh, R. R., & Mahmoodian, R., Crystallite size and microstrain: XRD line broadening analysis of AgSiN thin films. Pigment & Resin Technology, 48(6), 473-480, (2018).

[85] Özkavak, H. V., & UĞURLU, H. A., Coating TiO2 Film Using the Spin Method of AISI 304 Stainless Steel and Investigation of the Structural Properties. International Journal of Innovative Engineering Applications, 6(1), 97-102, (2022).

[86] Khot, A. C., Desai, N. D., Khot, K. V., Salunkhe, M. M., Chougule, M. A., Bhave, T. M., ... & Dongale, T. D., Bipolar resistive switching and memristive properties of hydrothermally synthesized TiO2 nanorod array: effect of growth temperature. Materials & Design, 151, 37-47, (2018).

[87] Shaik, K., & Cole, S., Comparative Study of Crystallite Size from XRD and TEM Results for Pure and V2O5 Doped CdO-FePO4 Composite Nanopowders. Physical Chemistry Research, 11(2), 241-251, (2023).

[88] Bae, J. Y., Kim, Y., Kim, H., Kim, Y., Jin, J., & Bae, B. S., Ultraviolet light stable and transparent sol–gel methyl siloxane hybrid material for UV light-emitting diode (UV LED) encapsulant. ACS applied materials & interfaces, 7(2), 1035-1039, (2015).

[89] Fox, G., The brewing industry and the opportunities for real-time quality analysis using infrared spectroscopy. Applied Sciences, 10(2), 616, (2020).

[90] Obeid, B. G., Hameed, A. S., & Alaaraji, H. H., Structural and optical properties of TiO2: MgO thin films preparing at 373K. Digest Journal of Nanomaterials and Biostructures, 12(8), (2017).

[91] Shinen, M. H., AlSaati, S. A. A., & Razooqi, F. Z., Preparation of high transmittance TiO2 thin films by sol-gel technique as antireflection coating. In Journal of physics: conference series (Vol. 1032, No. 1, p. 012018). IOP Publishing, (2018, May).